NUREG/CR-6511
ANL-96/17
Vol. 1

# Steam Generator Tube Integrity Program

## Semiannual Report
## August 1995 – March 1996

Prepared by
D. R. Diercks, S. Bakhtiari, O. K. Chopra, K. E. Kasza,
D. S. Kupperman, S. Majumdar, J. Y. Park, W. J. Shack

**Argonne National Laboratory**



**Prepared for**
**U.S. Nuclear Regulatory Commission**

## AVAILABILITY NOTICE

*Availability of Reference Materials Cited in NRC Publications*

Most documents cited in NRC publications will be available from one of the following sources:

1. The NRC Public Document Room, 2120 L Street, NW., Lower Level, Washington, DC 20555-0001

2. The Superintendent of Documents, U.S. Government Printing Office, P. O. Box 37082, Washington, DC 20402-9328

3. The National Technical Information Service, Springfield, VA 22161-0002

Although the listing that follows represents the majority of documents cited in NRC publications, it is not intended to be exhaustive.

Referenced documents available for inspection and copying for a fee from the NRC Public Document Room include NRC correspondence and internal NRC memoranda; NRC bulletins, circulars, information notices, inspection and investigation notices; licensee event reports; vendor reports and correspondence; Commission papers; and applicant and licensee documents and correspondence.

The following documents in the NUREG series are available for purchase from the Government Printing Office: formal NRC staff and contractor reports, NRC-sponsored conference proceedings, international agreement reports, grantee reports, and NRC booklets and brochures. Also available are regulatory guides, NRC regulations in the *Code of Federal Regulations*, and *Nuclear Regulatory Commission Issuances*.

Documents available from the National Technical Information Service include NUREG-series reports and technical reports prepared by other Federal agencies and reports prepared by the Atomic Energy Commission, forerunner agency to the Nuclear Regulatory Commission.

Documents available from public and special technical libraries include all open literature items, such as books, journal articles, and transactions. *Federal Register* notices, Federal and State legislation, and congressional reports can usually be obtained from these libraries.

Documents such as theses, dissertations, foreign reports and translations, and non-NRC conference proceedings are available for purchase from the organization sponsoring the publication cited.

Single copies of NRC draft reports are available free, to the extent of supply, upon written request to the Office of Administration, Distribution and Mail Services Section, U.S. Nuclear Regulatory Commission, Washington, DC 20555-0001.

Copies of industry codes and standards used in a substantive manner in the NRC regulatory process are maintained at the NRC Library, Two White Flint North, 11545 Rockville Pike, Rockville, MD 20852-2738, for use by the public. Codes and standards are usually copyrighted and may be purchased from the originating organization or, if they are American National Standards, from the American National Standards Institute, 1430 Broadway, New York, NY 10018-3308.

## DISCLAIMER NOTICE

NUREG/CR-6511
ANL-96/17
Vol. 1

# Steam Generator Tube Integrity Program

## Semiannual Report August 1995 – March 1996

Manuscript Completed: November 1996
Date Published: April 1997

Prepared by
D. R. Diercks, S. Bakhtiari, O. K. Chopra, K. E. Kasza,
D. S. Kupperman, S. Majumdar, J. Y. Park, W. J. Shack

Argonne National Laboratory
9700 South Cass Avenue
Argonne, IL 60439

J. Muscara, NRC Project Manager

**Prepared for**
**Division of Engineering Technology**
**Office of Nuclear Regulatory Research**
**U.S. Nuclear Regulatory Commission**
**Washington, DC 20555-0001**
**NRC Job Code W6487**

**Abstract**

This report summarizes work performed by Argonne National Laboratory on the Steam Generator Tube Integrity Program from the inception of that program in August 1995 through March 1996. The program is divided into five tasks, namely (1) Assessment of Inspection Reliability, (2) Research on ISI (in-service-inspection) Technology, (3) Research on Degradation Modes and Integrity, (4) Development of Methodology and Technical Requirements for Current and Emerging Regulatory Issues, and (5) Program Management. Under Task 1, progress is reported on the preparation of and evaluation of nondestructive evaluation (NDE) techniques for inspecting a mock-up steam generator for round-robin testing, the development of better ways to correlate burst pressure and leak rate with eddy current (EC) signals, the inspection of sleeved tubes, workshop and training activities, and the evaluation of emerging NDE technology. Under Task 2, results are reported on closed-form solutions and finite element electromagnetic modeling of EC probe response for various probe designs and flaw characteristics. Under Task 3, facilities are being designed and built for the production of cracked tubes under aggressive and near-prototypical conditions and for the testing of flawed and unflawed tubes under normal operating, accident, and severe accident conditions. In addition, crack behavior and stability are being modeled to provide guidance on test facility design, to develop an improved understanding of the expected rupture behavior of tubes with circumferential cracks, and to predict the behavior of flawed and unflawed tubes under severe accident conditions. Task 4 is concerned with the cracking and failure of tubes that have been repaired by sleeving, and with a review of literature on this subject.

## Contents

## Figures

## Tables

# Executive Summary

*Assessment of Inspection Reliability*

As part of the assessment of the in-service inspection (ISI) of steam generator (SG) tubes, a mock-up steam generator will be used for round robins (RR) tests and as a resource to assess new technology. The mock-up contains 400 tube openings, each with a 3.66-m (12-ft) length of tubing. Tubes will include a variety of defects and artifacts. The capabilities of a variety of eddy current (EC) and ultrasonic testing (UT) techniques to characterize the defects in the mock-up tubes are being evaluated. Twenty Alloy 600 tube specimens with a variety of flaws grown under laboratory conditions are being used for this evaluation. Estimates of the depth and length of the flaws, based on UT inspections using high frequency diffraction, Lamb wave, and amplitude drop methods, were performed by several experts in this area. Depth and length estimates were also made using eddy current techniques. Rotating-pancake-coil (RPC), multicoil-array, polarized-probe, and neural-network algorithms were used. Although results are preliminary, a clear trend is evident. The UT techniques appear to overestimate the depth of the crack in most cases and particularly so for shallow cracks. The estimates obtained by the neural-network analysis of EC data are better than those provided by most of the other techniques and significant improvements in accuracy can be expected when optimized training sets are used.

The twenty specimens contain longitudinal outer- and inner-surface cracks, circumferential outer- and inner-surface cracks, and intergranular attack (IGA). The preliminary estimates suggest that no one defect type appears easier to characterize than any other by either ultrasonic or neural-network analysis. It is somewhat easier to measure crack length than crack depth. Although length estimates obtained with EC probes are expected to be shorter than those obtained by UT techniques, because the threshold for detecting a crack is higher with EC methods, the preliminary data do not provide clear evidence for the validity of such a hypothesis.

The ultrasonic techniques provide better resolution than EC techniques and, as a result, cracks that may not appear to be segmented with EC analysis do appear as segmented on ultrasonic interrogation. Ultrasonic Lamb waves can be used to provide a good image of circumferential defects.

A Committee on Nuclear Regulatory Activities/Committee on the Safety of Nuclear Installations (CNRA/CSNI) Workshop on Steam Generator Tube Integrity in Nuclear Power Plants was held at Oak Brook, IL, October 30-November 2, 1995. One of the panel sessions addressed inspection issues. The consensus was that the most critical type flaw that must be characterized is SCC, that it is not related to a single degradation mode, and that the crack growth rate is the key factor in understanding the consequences of SCC in SG tubing. In the future, in order to better characterize the integrity of degraded tubing, personnel in a growing number of plants will clearly need to improve their ability to nondestructively detect and size cracks in SG tubing.

The issue of circumferential stress corrosion cracking (SCC) of SG tubes was reviewed. The present capabilities of EC and UT techniques to detect circumferential cracking were compared during this workshop. Eddy current testing with an RPC was considered to be a well-established method with a detection threshold of about 50% throughwall. While ultrasonic techniques may have the potential for higher spatial resolution and greater sensitivity, they are more likely to produce false positive calls. At present the techniques are complementary. Some cracks found by UT may not be found by EC testing because they are too shallow to be detected. Some cracks detected by EC testing may not be detected by UT because ultrasonic signals from roll transitions can be confusing.

Although there has been substantial progress in the development of techniques for inspection, improvements in the probability of detection (POD) and measurement of cracks are needed, along with improvements in the qualification of POD and measuring procedures. To obtain a POD with a high degree of confidence, 400 pulled tubes with defects are needed, including pulled tubes without significant nondestructive evaluation (NDE) signals. The inspection panel participants also pointed out that, while the present data provide a correlation between voltage and burst pressure, scatter in the data makes the 95% confidence limits on the correlation very broad. An improved empirical correlation would be very desirable. Improvements in signal analysis (e.g., application of neural-network algorithms) are being explored in this program to find a better method of correlating burst pressure and leak rate with EC data.

Many aspects of in-service inspection (ISI) that may affect inspection reliability are being reviewed. Neural-network technology has been applied to the analysis of EC data with good results, even with limited samples. It may be possible to improve neural networks so they are better than conventional pattern recognition techniques in the area of data analysis and interpretation. Inspection reliability could also be improved by signal analysis techniques that would simplify the interpretation of the data. It is possible that an image of the defects can be reconstructed from EC data but the reconstruction depends on the diffusion equation and one must rely on indirect algorithmic approaches to solve the inverse problem. The alternative to the inverse problem for EC techniques may be to use pattern recognition algorithms to interpret the signals.

Improvements in inspection reliability may also be achieved through the use of digital signal processing that may dramatically improve our capability to extract information from an EC probe. Digital filters could be used to solve problems that are now approached with multi-frequency techniques such as the elimination of signals from tube support plates.

*Research on ISI Technology*

The objective of this task is to evaluate advanced NDE and signal analysis techniques for reliable ISI of original and repaired SG tubes. Improved correlation between EC results and flaw morphology, leak rate and failure pressure will be examined. The implementation of degradation-specific management requires detailed knowledge about the specific nature and severity of flaws. Improved techniques (EC and others) are needed for more reliable detection and assessment of flaws. Furthermore, the robustness of EC measurement parameters and techniques must be evaluated with respect to their range of applicability.

Analytical modeling is being used to help understand the relationship between signal characteristics and the nature of the defect. Different electromagnetic (EM) modeling approaches that can simulate the EC probe response for NDE of SG tubing have been evaluated. The approaches consisted of closed-form analytical solutions, volume integral techniques, and finite element solutions. Although the finite element method (FEM) is the most computationally intensive technique, it is also the most flexible and the only one that can accurately model complex geometries. The current software being used at ANL is a commercial, general-purpose three-dimensional (3-D) FEM-based code that is a versatile research tool capable of precise modeling of the complex geometries that are often encountered in ISI of SG tubing. Sample calculations with both differential bobbin coil and absolute pancake coil (RPC) have been carried out to model two types of calibration standard defects, namely a flat-bottom hole and a circumferential outside-surface notch. Ultimately, the code will be used to model more complex crack-type defect geometries. The computer-aided-design-based (CAD) mesh-generating pre-processor of the software allows incorporation of various material property variations (e.g., presence of magnetite and copper deposits), as well as modeling of complex geometrical variations (e.g., defect-prone areas, such as baffle plates, and roll-expanded and crevice regions).

A series of FORTRAN programs, which were originally developed at Oak Ridge National laboratory (ORNL) and used for the design and analysis of EC SG problems of interest to the U.S. Nuclear Regulatory Commission (NRC), have also been modified to run on the platforms available at ANL. Separate computation and visualization software is currently utilized to process and display the outcomes of these programs. Because of the limited problem geometries that can be treated and the underlying assumptions in the formulation method, programs that are based on closed-form EM solutions can run with minimal computational resources. They can be used to simulate the impedance response to axisymmetric geometries for standard differential and absolute EC probes. These codes will be used to check the results of computationally intensive FEM solutions that can better simulate realistic flaw geometry and as a tool to analyze and determine EC probe and test parameters for general test case scenarios.

The research on improved EC inspection of steam generator tubes will focus primarily on the development of analytical and computational methods for the prediction of EC response as a function of probe design, flaw characteristics, and material properties, and on the development of signal analysis procedures for improved detection and characterization. The reliability and effectiveness of improved inspection techniques will be demonstrated through laboratory testing of the SG tube bundle mock-up and of SG tubes that contain various flaws. Final validation will utilize in-service-degraded SG tubing.

*Research on Degradation Modes and Integrity*

The objective of this task is to evaluate and experimentally validate models to predict potential degradation modes, progression rates, leak/rupture behavior, failure pressures, and leak rates for SG tubes and for repaired tubes under normal operating, accident, and severe accident conditions. Initial efforts have concentrated on the design and construction of experimental facilities for the production of flawed tubing and the rupture and leak-rate testing of flawed and unflawed tubing under a wide range of conditions. The facilities under design and construction are autoclave systems in which tubes will be

cracked under accelerated (chemically aggressive) conditions; a model boiler facility where tubes will be cracked under more nearly prototypic conditions; a blowdown facility in which tube-rupture and leak-rate tests will be conducted under simulated SG operating conditions; a high-temperature, severe-accident, tube-rupture facility; and a high-pressure tube-rupture and leak-rate test facility.

Two autoclave systems are being constructed for the production of cracked specimens for use in subsequent tube-rupture and leak-rate tests and for the evaluation of NDE equipment and techniques. Six tubular specimens will be simultaneously exposed at pressurized water reactor (PWR) SG operating temperatures to aggressive secondary-water chemistries at the outer surface. The specimens will be plugged at the bottom and pressurized from the top by means of an independent refreshed primary-water system to provide internal pressure loading. Individual valving of the six specimens will permit continuation of a given run after one or more of the specimens has developed a leaking crack. All of the components of the autoclave system have been ordered and delivered. Assembly of the first system is essentially complete, and initial check-out tests are about to begin.

A single-tube model boiler facility is being designed that can produce ODSCC cracks in tubes under near-prototypic secondary-side-water conditions. To avoid the cost and complexity associated with previous forced-circulation model boilers, ANL has settled on a simplified convective-flow design that utilizes a primary-side reflux boiler, a secondary-side convective-flow loop, and a simulated tubesheet crevice configuration. A first-cut design of the reflux boiler and the secondary-side vessel has been completed, and requests for bids on the major components have been issued to potential manufacturers. Work continues on modeling of the performance of the apparatus.

A tube-rupture and leak-rate blowdown test facility will be used to obtain data on burst pressures, failure modes, and leak rates of flawed tubing at temperatures up to 343°C (650°F), pressures of 21 MPa (3000 psi), and pressurized-water flow rates of up to 760 L/min (200 gal/min). The important features of the facility include a large 760-L (200-gal.) blowdown vessel water inventory to ensure high stable flow rate capability and to permit continued testing of initially stable leaking cracks; piping and valves of an appropriate size to minimize pressure drop in the supply line to the flawed tube and thereby permit high flow rates; the use of a downstream back-pressure regulator valve to control tube secondary-side pressure and thereby minimize nonprototypic two-phase flow from entering the tube; and computer feedback valve control to allow programmed ramps of the pressure differential across the tube. Flawed tubing for testing in this facility can come from three sources: (1) the severe chemistry autoclave cracking facilities, (2) the model boiler test facility, and (3) electro-discharge machining. The design of the facility is complete, and major components are being acquired. Modifications to the laboratory area for the installation of this equipment are underway, and an existing computer control room is being upgraded.

Modeling studies on crack stability and leak rate behavior have been conducted to aid the design of the Tube-Rupture and Leak-Rate Blowdown Test Facility described above. Analytical models were used to estimate critical crack sizes, leak before burst behavior, and expected leak rates for axial and circumferential cracks of various lengths and depths in

order to help assure that the facility has sufficient capacity and appropriate operating characteristics. These studies estimated the pressure increase and associated flow that is required to make a short, deep non-through wall cracks which will first break the remaining ligament and go through the wall grow in length. For example, a 12.7-mm (0.5-in.) crack with a/t=0.9 (90% through wall) will grow through wall and begin to leak at ≈1600 psi. As the pressure is increased from 11 to 30 MPa (1600 to 4400 psi), the crack will open more and leakage will increase, but the crack will not grow in length until the pressure reaches ≈30 MPa (4400 psi). At this pressure the crack can grow unstably in length, i.e., "burst." In order to make the tube "burst," the test system must be able to achieve a pressure of 30 MPa (4400 psi) with the crack leaking.

Shallower, longer cracks will actually "burst" without significant prior leakage because they will not break through and leak until the pressure is much higher than that required to cause a through wall crack of the same length to extend unstably. For example, a 1 in. crack with a/t = 0.5 will not leak until p ≈37 MPa (5400 psi). However, once the remaining ligament tears and the crack goes through wall, the pressure is well above that required to extend a through-wall 25-mm (1-in. crack), i.e., ≈18 MPa or 2600 psi). The maximum flow through the crack and maximum pressure that the tube can withstand without the crack becoming unstable and growing rapidly were also calculated as a function of crack length. Once the crack goes unstable, it is impossible to predict the leak area, and the resulting flow rates could be close to those for a double ended rupture (≈1720 and 2460 L/min [455 and 650 gpm] for 19.1 and 22.2-mm [0.750 and 0.875-in.] OD tubing, respectively). Cracks longer than ≈56 mm (2.2 in.) would be unstable under normal operating conditions, and the maximum flow rate through any stable crack will be ≈300 L/min (80 gpm) under single-phase flow.

Because the high-flow facility is limited to 3000 psi, a low temperature tube-rupture and leak-rate test facility is being constructed to perform tests at pressures up to 52 MPa (7,500 psi) and flow rates up to 45.4 L/min (12 gal/min). The system utilizes a high-pressure positive-displacement triplex pump to supply water at pressures up to 42 MPa (7,500 psi), and a fixed flow rate of 45.4 L/min (12 gal/min). This facility can be use to verify SG tube design margins for smaller flaws. It has sufficient flow capacity that most of the tests can be performed without the need to introduce a bladder to prevent leakage. The components for the system have been procured, but the facility will not be made operational under the high-flow test facility has been completed.

A high-temprature facility has been constructed to study the failure of flawed and unflawed tubes at the very high temperatures corresponding to severe accident conditions. The facility basically consists of a length of SG tube placed in a furnace, closed off at one end, and connected to a high-pressure nitrogen gas supply by suitable valving at the other end. During a test, the specimen is stabilized at a nominal SG operating temperature of 300°C (572°F) and a fixed internal pressure. The temperature is then ramped up at a predetermined rate until specimen failure occurs. Check-out tests have been completed, and the first of a series of tests on flawed and unflawed tubes with calculated temperature

histories for severe accident scenarios has been conducted. The scenario under investigation represent the thermal history associated by a total station blackout with a stuck-open SG secondary-side atmospheric dump valve, resulting in loss of feedwater and secondary-side depressurization. Two time/temperature histories, based upon severe accident analyses by INEL and EPRI, have been considered in the initial tests.

In addition to the test program analyses of the failure pressure of tubes under severe accident conditions (i.e., T>350°C) have been conducted. At these higher temperatures, plastic deformation is likely to be much more extensive than at normal reactor operating temperatures, and creep effects may no longer be negligible. The modeling efforts attempt to predict failure times and temperatures under the two time/temperature histories used in the experimental program.

Two different predictive models are being evaluated, namely the flow stress model and the creep rupture model. The flow stress model assumes that failure occurs when the applied hoop stress in the tube becomes equal to the flow stress of the material, which is typically taken to be the average of the yield and ultimate tensile strengths. For a tube containing a pre-existing flaw, the actual hoop stress at the flaw is equal to the nominal hoop stress multiplied by a stress multiplication factor, and three expressions for this multiplication factor are being evaluated. All three formulations of the flow stress models are found to predict the burst temperatures of unflawed tubes reasonably well for the INEL temperature ramp tests. The predicted failure temperatures for flawed tubes are conservative (i.e., less than the experimental temperatures) in all cases, but particularly so for the shorter and deeper cracks.

The creep rupture model assumes a linear summation of creep damage in terms of time under stress divided by the time to fail by creep rupture at that stress. These incremental damage fractions are integrated over the stress vs. time history for the tube, and failure is predicted when this integrated damage fraction is equal to unity. The stress magnification factors used for the flow stress analyses of throughwall and part–through cracks are also assumed to be applicable to the case of creep. The time to creep rupture used in the damage fraction calculations was determined using Larson-Miller parameter correlations for Alloy 600. The failure temperatures for the INEL temperature-ramp tests are still under-predicted, but they are much closer to the those observed in the experiments than those predicted by the flow stress models. In particular, they are quite close for the longer cracks.

The failure of tubes with circumferential cracks is also being examined. For circumferential cracks the effect of lateral constraint (e.g., by tube support plates) on failure pressure is significant. For the free-bending (unconstrained) case, tubes with 180° and 240° through-wall circumferential cracks were found to reach maximum pressures at a rotation of ≈8°. This is in agreement with the experimental observation that tubes appear to fail at a fixed rotation of the cracked section. Preliminary results for the constrained cases show that the maximum pressures are increased substantially. Models are available for the case of free– bending and for the case of complete constraint. A simplified beam bending model for the case of intermediate constraint is also being developed.

*Development of Methodology and Technical Requirements for Current and Emerging Regulatory Issues*

The objective of this task is to use the data, results, correlations and modeling that were assembled in work under the first three objectives to provide technical assessments and evaluations of current and emerging regulatory issues related to SG tube integrity. Included are items such as confirmatory research on existing and new models, evaluation of tube repair methods, and input and assessment of the new rule and regulatory guide on SG tube integrity.

Present activities under this task are concentrating on the compilation of data and evaluation of SG tube repair techniques and qualifications. The principal repair techniques under evaluation include sleeving and other methods of direct tube repair e.g., electroplating, weldment additions, and an autogeneous remelt process. The current effort is focused on collecting information on various sleeve designs and their qualification. Test methods to qualify the installation processes and to verify that the resistance of the sleeved tubes to SCC is acceptable are being evaluated. Process and material variables that may be relevant to qualification testing are being defined.

## Acknowledgments

The authors acknowledge the contributions of D. E. Busch, Y. Cai, J. E. Franklin, L. Knoblich, E. R. Koehl, C. F. Konicek, W. Lawrence, D. R. Perkins, W. Ruther, and C. W. Vulyak to the experimental work described in this report. This work is sponsored by the Office of Nuclear Regulatory Research, U.S. Nuclear Regulatory Commission, under FIN W6487; Project Manager Dr. J. Muscara.

The authors also thank R. Kurtz (PNNL), A. Diaz (PNNL), T. Gomm (INEL), C. Dodd, V. Cecco (Atomic Energy of Canada, Ltd.), M. Brook (ABB AMDATA) and J. Cox (Zetec) for their contributions to Task 1.

## Acronyms and Abbreviations

| | |
|---|---|
| ABB | ASEA Brown-Boveri |
| AECL | Atomic Energy of Canada, Ltd. |
| ANL | Argonne National Laboratory |
| APC | absolute pancake coil |
| ASME | American Society of Mechanical Engineers |
| AVB | antivibration bars |
| BC | bobbin coil |
| CAD | computer-aided design |
| CIDSCC | circumferential inner diameter stress corrosion crack/cracking |
| CSF | conjugate spectrum filters |
| CNRA | Committee on Nuclear Regulatory Activities |
| CODSCC | circumferential outer diameter stress corrosion crack/cracking |
| CSNI | Committee on the Safety of Nuclear Installations |
| DAS | data acquisition system |
| DBC | differential bobbin coil |
| DSF | defect sensitivity factor |
| EC | eddy current |
| ECT | eddy current testing |
| EDF | Electricité de France |
| EDM | electro-discharge machining |
| EM | electromagnetic |
| EPRI | Electric Power Research Institute |
| FEM | finite-element method |
| FM | flow meter |
| HEJ | hybrid expansion joints |
| ID | inner diameter |
| IE | integral equations |
| IGA | intergranular attack |
| INEL | Idaho National Engineering Laboratory |
| ISI | in-service inspection |
| LIDSCC | longitudinal inner-diameter stress corrosion crack/cracking |
| LMP | Larson-Miller parameter |
| LODSCC | longitudinal outer diameter stress corrosion crack/cracking |
| LWS | laser-welded sleeves |
| MM | moment method |
| MRPC | motorized rotating pancake coil |
| MS DOS | Microsoft™ disk operating system |
| MSLB | main steamline break |
| NDE | nondestructive evaluation |
| NRC | U.S. Nuclear Regulatory Commission |
| OD | outer diameter |
| ODSCC | outer diameter stress corrosion crack/cracking |
| ORNL | Oak Ridge National Laboratory |
| PC | (IBM) personal computer; pancake coil |
| PISC | Program for Inspection of Steel Components |

| | |
|---|---|
| PNNL | Pacific Northwest National Laboratory |
| POD | probability of detection |
| PWR | pressurized water reactor |
| PWSCC | primary-water stress corrosion crack/cracking |
| RPC | rotating pancake coil |
| RR | round robin |
| RFEC | remote-field eddy current |
| SCC | stress corrosion crack/cracking |
| SG | steam generator |
| SS | stainless steel |
| TOF | time of flight |
| TR | transmit/receive |
| TW | throughwall |
| UT | ultrasonic testing |

# 1 Introduction

The objective of this program is to provide the experimental data and predictive correlations and models that are needed to permit the U.S. Nuclear Regulatory Commission (NRC) to independently evaluate the integrity of steam generator (SG) tubes as plants age and degradation proceeds, new forms of degradation appear, and new defect specific management schemes are implemented. The areas addressed by the program include assessment of procedures and equipment used for in-service inspection (ISI) of SG tubes, and recommendations for criteria and requirements to improve the reliability and accuracy of ISI; validation and improvement of correlations and models that are used to evaluate integrity and leakage of degraded SG tubes; and validation and improvement of correlations and models that predict the generation and progression of degradation in SG tubes as a function of aging, including the effects of the operational environment such as temperature, dry-out and concentration conditions, stresses, and primary- and secondary-side water chemistry.

The studies in this program focus primarily on Alloy 600 SG tubing in the mill-annealed condition, because this is the tubing material that is (and will be) present in plants that have not replaced SGs and is more susceptible to cracking than replacement materials such as thermally treated Alloy 600 or 690. Although most SGs that use mill-annealed Alloy 600 will probably require eventual replacement, the behavior of this material will be of concern for many more years. Thermally-treated Alloy 600 and 690 will also be tested. Although these alloys are expected to be much less susceptible to degradation than mill-annealed Alloy 600, it is still necessary that we be able to predict their behaviors.

The bulk of the materials used in the program will be exposed to simulated operating conditions and environments during laboratory testing. Because some of the laboratory environmental conditions represent accelerated conditions, and because service degradation, tubing conditions, and in-service operating and inspection conditions cannot always be faithfully represented in laboratory conditions and specimens, this program will seek and use service-degraded tubing and perform in-situ inspections of generators removed from service for correlation with and validation of experimental data, integrity and degradation predictive models, and inspection capability. Comparisons will be made with the morphology and character of service-degraded flaws to help ensure that the flaws produced in the laboratory and used for studies on inspection reliability, burst, and leak testing will be as realistic as possible. The reliability of flaw detection and accuracy of flaw sizing data will also be assessed with typical ISI personnel, procedures, and equipment.

This program is divided into four technical tasks and one management task:

1. Assessment of Inspection Reliability

2. Research on ISI Technology

3. Research on Degradation Modes and Integrity

4. Development of Methodology and Technical Assessments for Current and Emerging Regulatory Issues

5. Program Management

This semiannual report, the first progress report for this program, describes activities since the inception of the program in August 1995.

# 2 Assessment of Inspection Reliability (D. S. Kupperman and S. Bakhtiari)

The objective of the inspection task is to evaluate and quantify the reliability of current and emerging inspection technology for current-day flaws [i.e., establish probability of detection, (POD)], correlate nondestructive evaluation (NDE) parameters with structural integrity, and establish the capability to size cracks. The reliability and accuracy of the techniques must be quantified so that plugging criteria and the consequences of degraded tubes that remain in service after inspection can be evaluated. Eddy current (EC) and other NDE techniques that are currently used for SG tube ISIs are being evaluated with respect to probability of flaw detection and accuracy of sizing. The consequences of degraded tubes that remain in service after inspections can then be evaluated. The methods and test parameters under investigation are those currently used for various forms (and locations) of degradation. The results of the NDE will be validated by inspection and destructive evaluation of service-degraded tubing.

This program will require an evaluation of results of a round-robin (RR) test that will be conducted by commercial ISI teams. The RR test will include both EC and ultrasonic test (UT) methods. Teams will report the flaw types, sizes, and locations, as well as other commonly used parameters such as voltage responses from the EC tests. Much of this testing will be performed on the SG tube bundle mock-up with laboratory-degraded tubes that is being developed at Pacific Northwest National Laboratory (PNNL). This mock-up will be moved to Argonne National Laboratory (ANL) in FY 96, where it will be set up for RR testing. The activities under this task will be coordinated with the RR testing being performed under the auspices of the Program for Inspections of Steel Components (PISC). Information on the methodology and flaws used, as well as data and results obtained during the PISC III RR testing of SG tubes will be obtained and compared with the results obtained in the RR testing carried out under this program. Coordination and insights will also be sought from the Performance Demonstration Program at the Electric Power Research Institute (EPRI) NDE Center. The mock-up will also serve as a resource for assessing new technology.

In addition to degraded tubing, it is also important to assess the effectiveness of ISI tubes that have been repaired (e.g., by sleeving). A matrix of repaired tube specimens, which concentrates on various sleeve repairs, is being designed to represent actual repairs conducted in the field. The matrix will be used to evaluate inspection methods.

## 2.1 Technical Progress

### 2.1.1 Mock-Up

The SG mock-up to be used for RR testing and as a resource for assessing new technology will contain 400 tube openings, each with a 3.66-m (12-ft) length of tubing. The mock-up will be partially assembled at PNNL, then shipped to ANL for final assembly. One possibility for an artificail defect in these tubes is a laser-cut slot. Although a laser-cut slot does not accurately represent a crack, it may be more representative of a crack than an electro-discharge machining (EDM) notch. Laser-cut slots are tapered and can have

entry widths as small as 10 μm. Bridging across the faces of the slot is also possible, making detection somewhat more difficult with a laser-cut slot than with an EDM notch of the same depth. Laser-cut slots 20% deep could be extremely difficult to detect and these slots could provide a detection and sizing challenge that lies in difficulty between detecting and measuring a field-induced crack and an EDM notch.

### 2.1.2 Evaluation of NDE Techniques for Characterizing Flaws in the Mock-Up

Eddy current and UT techniques are being evaluated as a means to characterize the defects in the mock-up tubes. Twenty Inconel 600 tubes with laboratory-grown cracks were provided by PNNL for blind testing. After the tubes were inspected with EC and UT techniques, they were metallographically analyzed to establish the actual depth, length, and profiles of the cracks. The analysis of the results will allow the best techniques to be used for characterizing the defects in the mock-up tubes.

The 20 tube specimens were prepared under laboratory conditions by the Westinghouse Science and Technology Center. The specimens exhibit longitudinal inner-surface stress corrosion cracks, longitudinal outer-surface stress corrosion cracks, circumferential inner-surface stress corrosion cracks, circumferential outer-surface stress corrosion cracks, and intergranular attack (IGA). Nine of the tubes show a roll transition. The Inconel 600 tubes are ≈0.30 m (12 in.) long, 22.2 mm (0.875 in.) in diameter with a wall thickness of 1.27 mm (0.050 in.). The degraded zone is nominally 25 mm (1 in.) long. The tubes were subjected to ultrasonic depth and length characterization by high-frequency diffraction, Lamb wave, and amplitude drop methods. Eddy current depth and length were estimated by using rotating pancake coil, (RPC), multi-coil arrays, a polarized probe, and a neural-network algorithm applied to the RPC data.

#### 2.1.2.1 Ultrasonic Evaluation at High Frequency

A. Diaz at PNNL and T. Gomm at the Idaho National Engineering Laboratory (INEL) collaborated to carry out ultrasonic inspections of the 20 tubes to determine the optimum method for inspecting tubes before they are integrated into the mock-up SG that will be used for RR studies and as a test bed for evaluating emerging technologies. The size, shape, and location of the flaws are required so that blind inspection results can be correctly interpreted. High-frequency, longitudinal, and shear waves in a focused, pulse echo mode were used with waves incident at 0 and 45° (for both axial and circumferentially oriented cracks). All of the PNNL/INEL inspections were carried out from the outside of the tube (some ultrasonic data acquired from the inside surface are also presented in this report). High-frequency backscatter and frequency analysis was used to characterize IGA. A, B, and C scans were used to characterize all of the cracks and the IGA. Time-of-flight (TOF) data were used to estimate depth when a crack tip echo was detectable, otherwise a 14-dB drop method with signal movement, was used to estimate depth.

Frequencies of 20-50 MHz were employed in an immersion tank. However, because of the attenuation in Inconel 600, the peak in the frequency spectrum is ≈30 MHz for propagation through the wall thickness and back (in pulse echo mode).

Two calibration tubes were used. The first tube contained two sets of outer-surface saw cuts. The first set included four axial cuts 0.25-1.02 mm (0.010-0.040 in.) deep and 5.08-9.78 mm (0.200-0.385 in.) long. The second set contained five circumferential cuts 0.127-1.016 mm (0.005-0.040 in.) deep and 2.16-6.86 mm (0.085-0.270 in.) long. A second tube contained outer-surface saw cuts (axial and circumferential) and EDM notches on the inner and outer surfaces. The saw cuts are 0.25-1.02 mm (0.010-0.040 in.) deep and 3.43-9.53 mm (0.135-0.375 in.) long. The EDM notches are nominally 0.51 mm (0.020 in.) deep and 6.35 mm (0.250 in.) long.

#### 2.1.2.2 Ultrasonic Evaluation with Lamb Waves

The 20 SG tube samples were also inspected by M. Brook at ABB AMDATA with an ultrasonic probe that propagated Lamb waves in the tube wall, which are unaffected by a roll transition. These waves propagate in a free tube wall and are capable of detecting inner or outer-surface circumferential cracks. Although axial cracks are not detectable with this probe unless circumferentially oriented branches are present, in principle, it is possible to make a Lamb wave probe that could detect axial cracks. The probe for the data reported in this report is used in a scan mode that covers a range of 140 mm (5.5 in.). In general, not enough information is present in the Lamb wave echo signal to determine the depth, but rough estimates can be made by measuring the echo amplitude. The length of the defect is accurately estimated by observing the drop in signal amplitude as the defect is scanned. IGA has been called correctly because the echo signals are generated over a large area of the tube.

Calibration was carried out with a tube that contained circumferential EDM notches with throughwall depths of 20, 40, and 60% and arc lengths of 20, 40, and 60°. The signal from the 20% TW, 60 degree arc notch was set to 80% Full Screen Height. The probe was moved axially 1.3 mm (0.05 in.) for every 360° scan. A, B, and C scans were generated. The probe was operated at a frequency of approximately 5 MHz. A PC-based Intraspect ultrasonic system was used to collect the data.

#### 2.1.2.3 Evaluation with an Eddy Current Array Probe

The 20 tubes were inspected with an EC C5/HD array probe by V. Cecco et al. at Atomic Energy of Canada, Ltd. (AECL). The probe consists of three parts. Two parts contain differential transmit-receive (TR) pancake coil arrays while the third contains a bobbin coil that was used simultaneously in differential and absolute modes. Each pancake array consisted of eight independent TR units. The coils in the two arrays are rotated relative to each other to completely cover the entire circumference. Thus, each unit "sees" an arc of 22.5°. The sensitivity to axial and circumferential cracks was comparable. Data could be displayed in Zetec Eddynet C-scan and clip-plot formats. The data from the absolute channels of the bobbin coil were useful in detecting long axial cracks. The amplitude from the bobbin coil was useful in distinguishing axial cracks from IGA. The tubes were also examined with a 24-probe array, each covering a 15° arc to see if more coils would lead to improvements. This data will be analyzed at a later date. The data presented in this report were collected with a Zetec MIZ-30 interfaced with a Hewlett Packard 700 series workstation. Data acquisition and analysis were carried out with Zetec

Eddynet software. A standard Zetec 4D probe driver with Zetec PM-1 motor controller was used to pull the probe through the tube at a constant speed of 0.30 m/s (12 in./s).

Calibration was carried out with a standard ASME tube, a tube supplied by PNNL that contained axial and circumferential outer-surface notches, and a Westinghouse-supplied calibration tube containing a 20% outer-surface axially symmetric EDM notch, a dent, and 1.6-mm (0.060-in.)-diam throughwall holes. Lack of calibration tubes with inner-surface notches and limited outer-surface notches severely restricted the ability to estimate the depth of the cracks. Data were collected as the probe was pulled back through the specimen and then through the calibration tubes. The frequencies used were 45, 90, 180, and 400 kHz. The dent was used to adjust the phase angle while the dent signal was oriented horizontally. The vertical component of the 20% outer-surface notch signal was set to 10 V. Frequency dependence of the Lissajous figure orientation and frequency dependence of the signal amplitude were used to distinguish outer-surface from inner-surface flaws and to determine whether the defect was deep or shallow. The expansion transition caused some problems with signal interpretation. If a flaw was detected with the array but not with the bobbin coil, it was called circumferential. If the flaw was detected by both array and bobbin coil, it was identified as axial or IGA.

#### 2.1.2.4 Neural-Network Analysis of Eddy Current Data

Using an array of 16 pancake coils, C. Dodd carried out a neural-network analysis of the EC data collected for the 20 tubes. The EC coils were ≈4.6 mm (0.180 in.) in diam. Data were acquired with the standard Zetec MIZ-30 acquire program. Manipulation of data was required to convert the neural net training with a single pancake coil to the individual coils of the array. Training of the neural net was carried out with tube standards and 23 samples with axial and circumferential outer-surface stress corrosion cracks and IGA that were metallographically sectioned. A complication in this effort was a lack of training data for inner-surface defects and only one training sample with a roll transition. Standards used contained 360° circumferential notches 20, 40, 60, and 80% throughwall. Lift off of 0.1 and 0.2 mm (0.004 and 0.008 in.) was also part of the calibration tube and was used to set the phase shift so the lift off signal is horizontal. The standard also contained a 100%-deep groove and axial notches.

#### 2.1.2.5 Experimental Results

Figure 1 shows preliminary estimated crack depth determined by high-frequency ultrasonic-wave examination and by a neural-network algorithm applied to EC data vs. the maximum crack depth determined by metallographic analysis of the tubes. Although these results are preliminary, they show a clear trend. The UT technique overestimates the depth of the crack in most cases and particularly for the case of shallow cracks. The main problem for the ultrasonic interrogation was the difficulty in detecting the echo from the crack tip that is used to obtain the depth estimate. The results from neural-network analysis of EC data are better and are particularly encouraging, because a proper training data set was not available for this analysis. Significant improvements in the correlation are

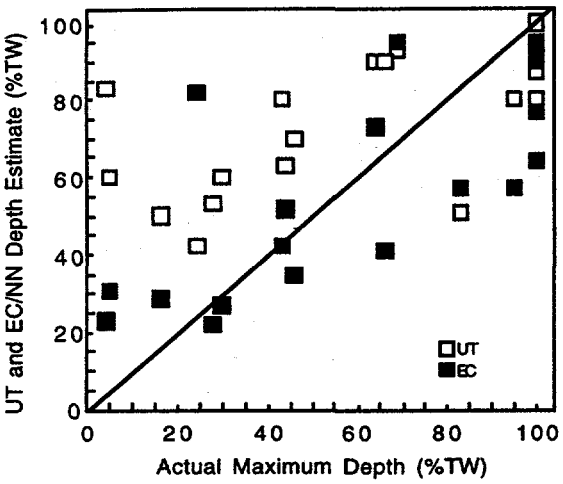


*Figure 1.*
*Preliminary comparison of the estimated depth (PNNL/INEL) using high frequency ultrasonic waves (open squares) and estimated depth from a neural network algorithm (C. Dodd) applied to EC data (black squares) versus the maximum depth of the crack from metallographic analysis (PNNL) of the set of 20 SG tube specimens.*

expected when optimized training sets are used with this neural-network algorithm. Despite the less-than-desirable UT results, the cracked tubes to be installed as part of the mock-up steam will be characterized by high-frequency ultrasonic waves, with improvements in the implementation of the technique where feasible as well as with eddy current neural network analysis.

UT vs. EC/neural-network results are shown in Fig. 2. The depth estimated by the UT technique is consistently greater than that predicted by the neural-network algorithm applied to the EC data.

To better understand the problems that are encountered while estimating depths, data from the 20 tubes have been analyzed in several ways. The data presented in Fig. 3 show the results of depth predictions for tubes with and without a roll transition. No dramatic difference in depth measuring capability can be observed when using the neural-network algorithm and EC data.

Some estimates of flaw depth were also made with an ultrasonic probe from the inner-surface of the tube (from PNNL report on ultrasonic examination). The results of estimating depth from the inner-surface are, on the average, noticeably lower than those from the outer-surface. This difference could be the result of differences in probe design but may also be the result of tube curvature effects. Waves incident on the tube inner wall are somewhat focused whereas waves incident on the outer-surface are spread out as they travel through the tube wall. Estimates of crack depth obtained by ultrasonic wave inspection on inner and outer-surfaces of 20 tubes are presented in Fig. 4, along with neural-network EC results.

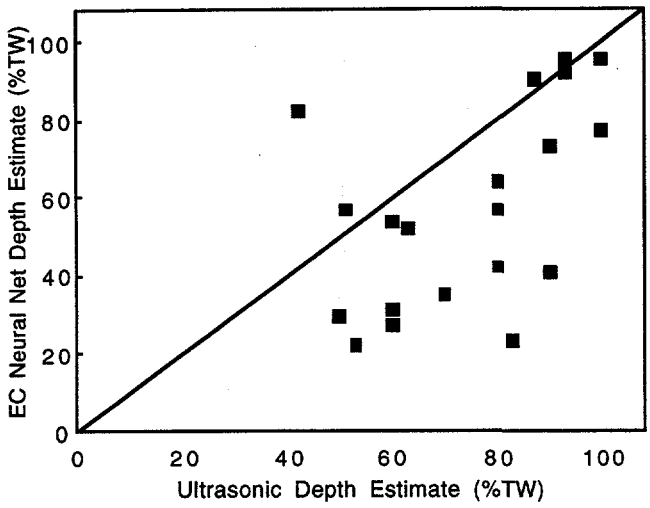


*Figure 2.*
*A comparison of flaw depth estimates from a high frequency ultrasonic wave technique (PNNL/INEL) and a neural network algorithm applied to the eddy current data (C. Dodd).*

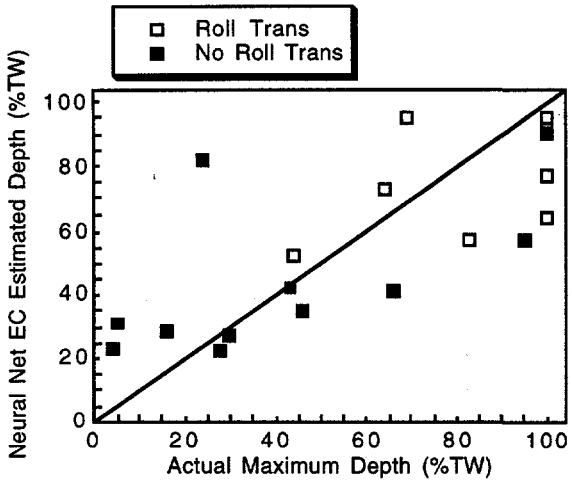


*Figure 3.*
*Comparison of the estimated depth applying the neural network algorithm to eddy current data (C. Dodd) for tubes with and without a roll transition.*

The results of applying a neural-network algorithm to EC data are presented as a function of flaw type in Fig. 5. Preliminary estimates from longitudinal outer-and inner-surface cracks, circumferential outer-and inner-surface cracks, and IGA are separated. No one defect appears significantly easier to characterize than any other though the correlation coefficient from a linear fit to data restricted to outer surface axial and circumferential cracks is a respectable 0.9. Similar data, obtained by high-frequency ultrasonic diffraction techniques, are shown in Fig. 6.

Crack length is somewhat easier to measure than crack depth. Figures 7-13 show preliminary crack length estimates for several of the tubes, with the primary emphasis on

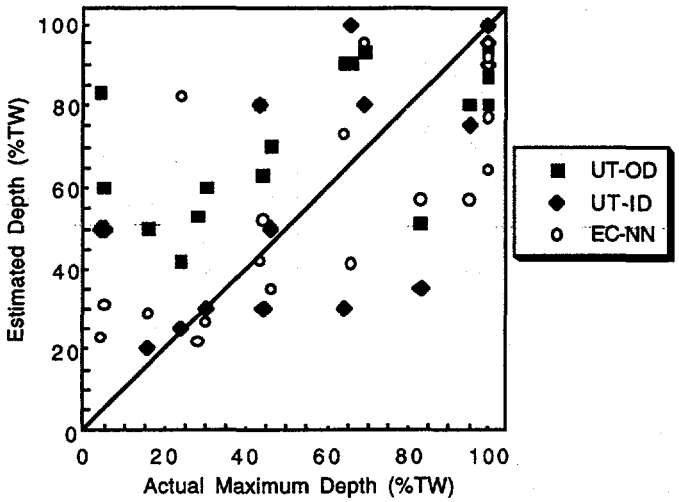


*Figure 4. Estimates of crack depth obtained by ultrasonic wave inspection of inner (Westinghouse/PNNL) and outer (PNNL/INEL) surfaces of 20 tubes along with preliminary neural-network EC results (C. Dodd) vs. actual maximum depth.*

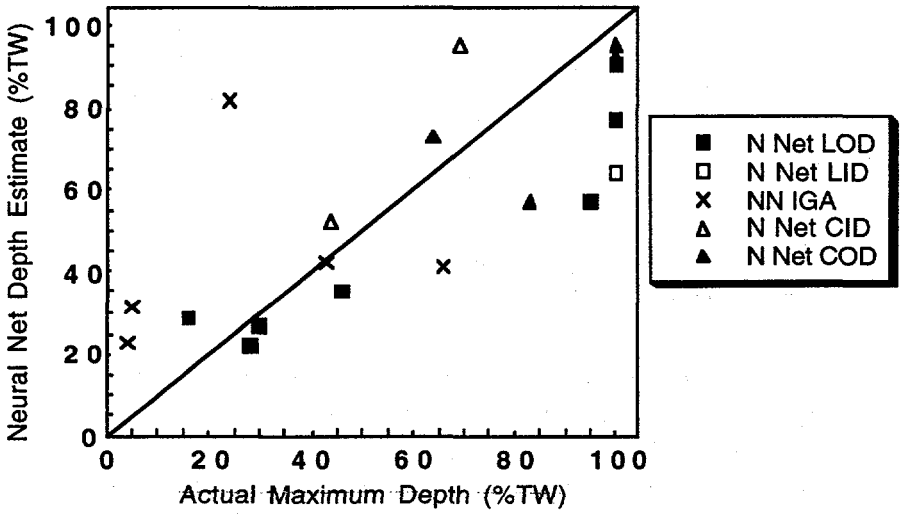


*Figure 5. The results of applying a neural network algorithm to eddy current data are presented as a function of longitudinal OD cracks, longitudinal ID cracks, circumferential OD cracks, circumferential ID cracks and IGA. No one defect appears easier to characterize than any other.*

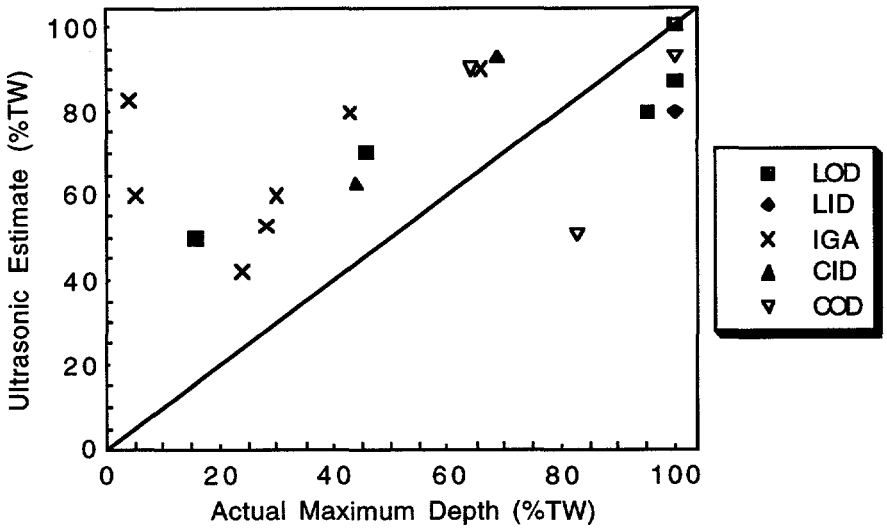


*Figure 6. Depth estimates (PNNL/INEL), using high frequency ultrasonic diffraction, for longitudinal OD cracks, longitudinal ID cracks, circumferential OD cracks, circumferential ID cracks and IGA. No one defect appears easier to characterize than any other.*

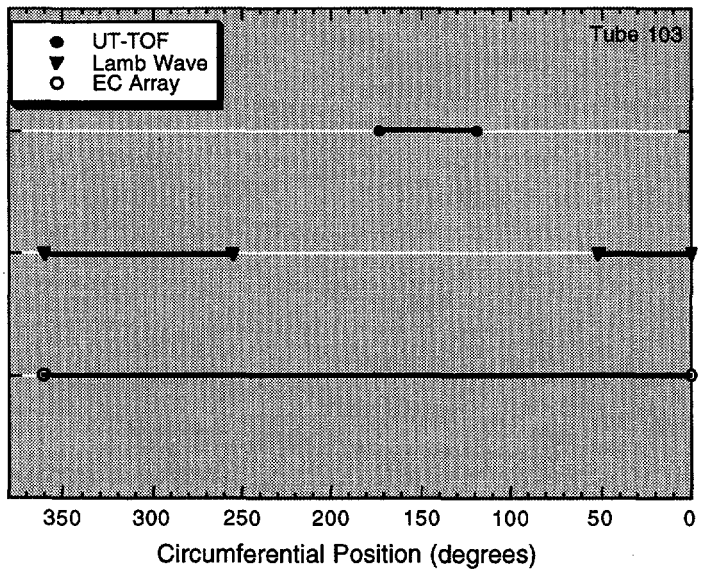


*Figure 7. Comparison of predicted length of circumferential ID crack in 22.2-mm (0.875-in.) diameter Inconel tube using high frequency ultrasonic wave (incident to the outer surface of the tube), Lamb wave (ABB AMDATA) and a C5/HD (AECL) eddy current array.*

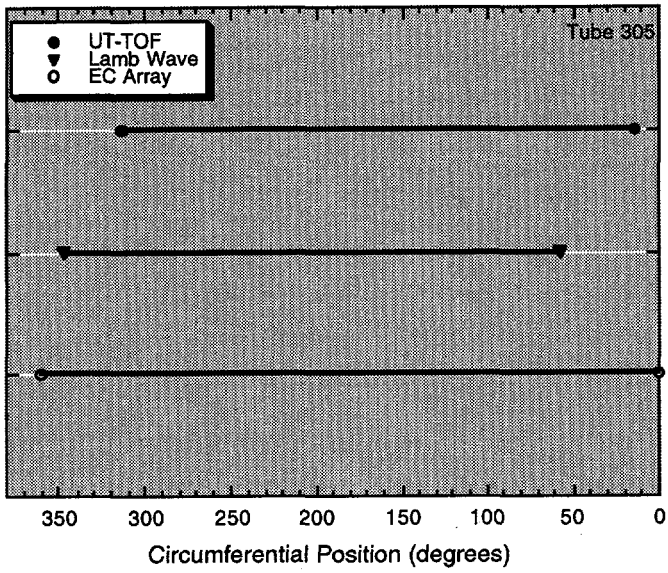


*Figure 8. Comparison of predicted length of circumferential ID crack in 22.2-mm (0.875-in.) diameter Inconel tube using high frequency ultrasonic wave (incident to the outer surface of the tube) (PNNL/INEL), Lamb wave (ABB) and a C5/HD eddy current array (AECL).*

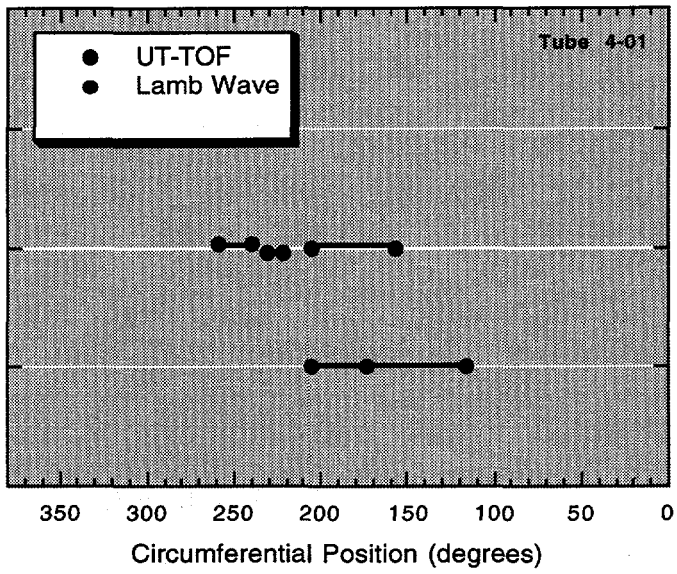


*Figure 9. Comparison of predicted length of circumferential OD crack in 22.2-mm (0.875-in.) diameter Inconel tube using high frequency ultrasonic wave (incident to the outer surface of the tube) (PNNL/INEL) and a Lamb wave (ABB). No eddy current array data is available for this tube. A symbol between the ends of the crack representation indicates a segmented structure.*

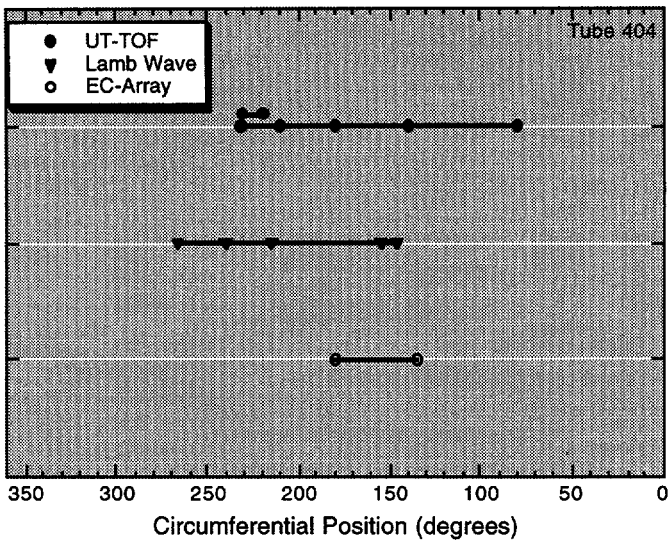


*Figure 10. Comparison of predicted length of circumferential ID crack in 22.2-mm (0.875-in.) diameter Inconel tube using high frequency ultrasonic wave (incident to the outer surface of the tube) (PNNL/INEL), Lamb wave (ABB), and a C5/HD eddy current array (AECL). Symbols between the ends of the crack representation indicates a somewhat segmented structure.*

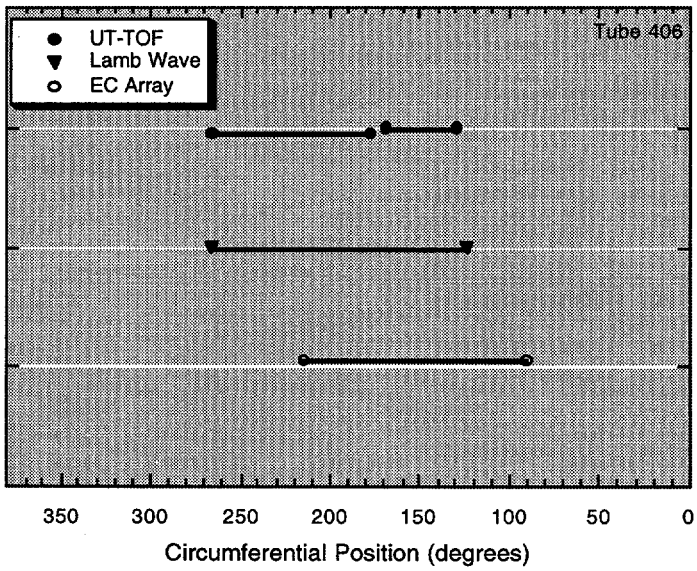


*Figure 11. Comparison of predicted length of circumferential ID crack in 22.2-mm (0.875-in.) diameter Inconel tube using high frequency ultrasonic wave (incident to the outer surface of the tube) (PNNL/INEL), Lamb wave (ABB) and a C5/HD eddy current array (AECL).*

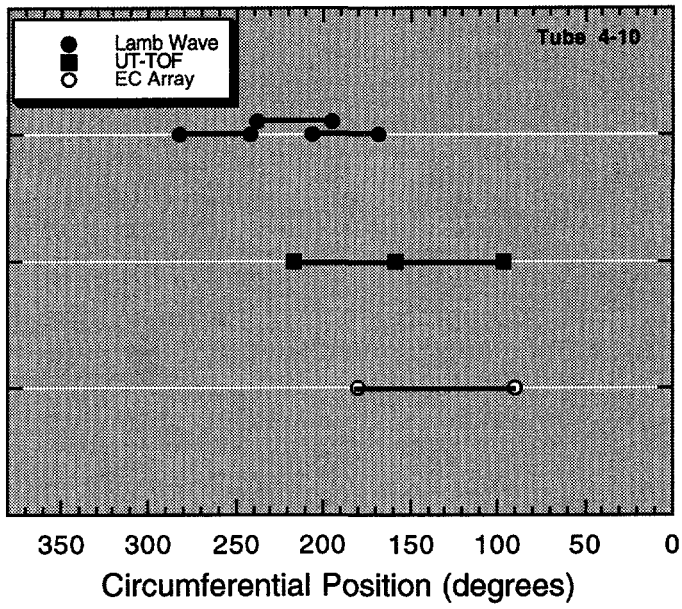


*Figure 12. Comparison of predicted length of circumferential ID crack in 22.2-mm (0.875-in.) diameter Inconel tube using high frequency ultrasonic wave (incident to the outer surface of the tube) (PNNL/INEL), Lamb wave (ABB) and a C5/HD eddy current array (AECL). Symbols between the ends of the crack representation indicates a segmented structure.*

circumferential cracks. The data were obtained by both ultrasonic TOF diffraction and amplitude drop (PNNL/INEL) and Lamb waves (ABB AMDATA) for circumferential cracks and EC probes (conventional array analysis/AECL, neural-network algorithm applied to data/Dodd and Plus Point/ANL/Zetec). Length estimates obtained with EC probes are expected to be shorter than those obtained with UT techniques, because the threshold for detecting a crack is higher with EC methods. The data presented do not necessarily support this expectation. The results obtained by UT techniques also exhibit better resolution, and as a result, cracks that may look segmented on ultrasonic interrogation may not be resolved individually with EC testing. The location of cracks may vary considerably with the technique used. When symbols are observed between the ends of a segment, the segment is said to have "structure," and the locations of the symbols coincide with the locations of signal peaks in the data.

Lamb waves were not especially useful for measuring crack depth. Ultrasonic inspection with Lamb waves appear to be useful for detection of circumferential cracks and length estimates. Lamb waves can also be used to detect axial cracks if they contain circumferential components and exhibit IGA. When used in a scanning mode, Lamb waves can provide a good image of a defect.

### 2.1.3 Determination of Leak Rate and Burst Pressure

Data that form the basis for the correlations between burst pressure and EC voltage and probability of leakage and voltage are limited. Substantial scatter is observed in tube burst pressure (more for pulled tubes than model boiler tubes) and leak-rate data when

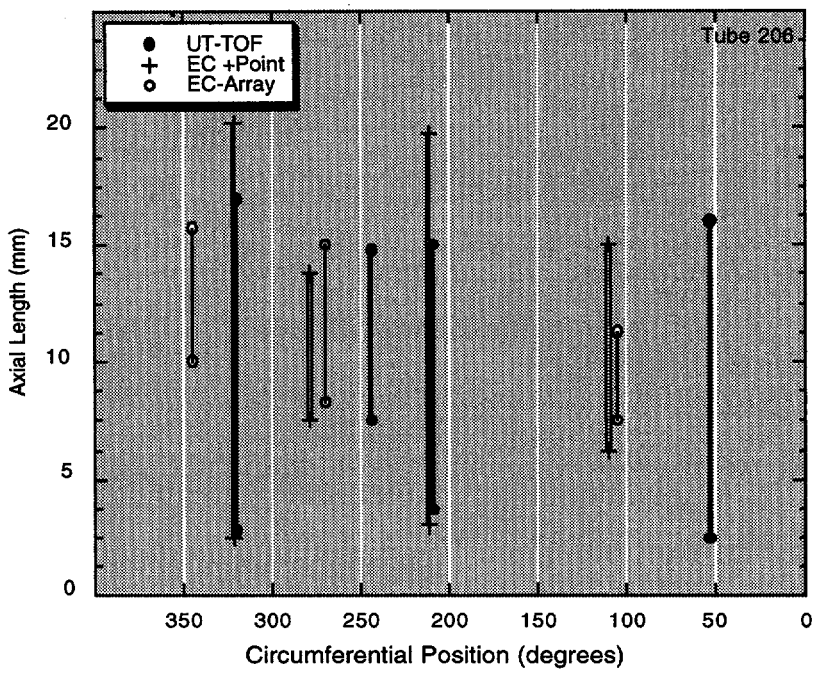


*Figure 13. Comparison of predicted length of axial OD crack in a 22.2-mm (0.875-in.) diameter Inconel tube using high frequency ultrasonic wave (incident to the outer surface of the tube) (PNNL/INEL), a Plus Point probe (Zetec/ANL), and a C5/HD eddy current array (AECL). Four cracks were resolved by the UT and Plus Point probes but only three by the eddy current array.*

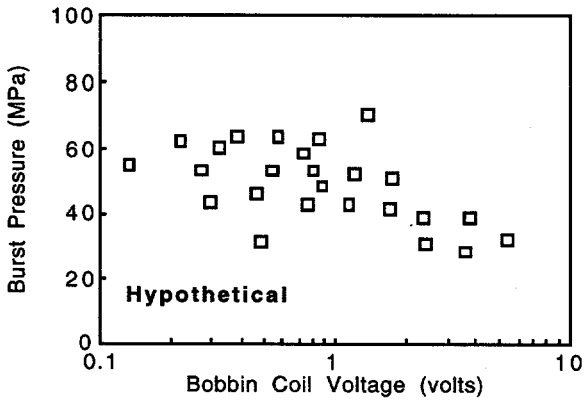


*Figure 14.*
*Hypothetical semi-log plot of burst pressure versus bobbin coil voltage for pulled tubes. The data presented have been extracted from Reference 1.*

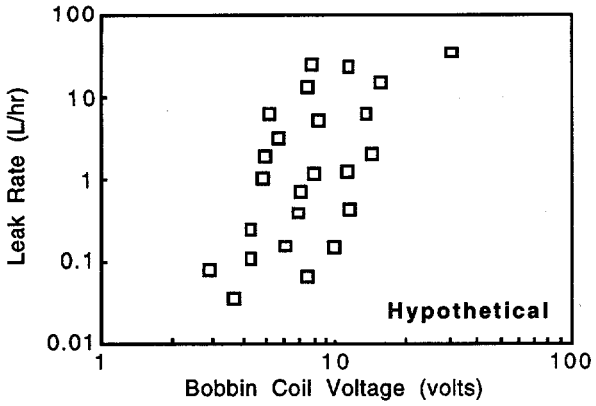


*Figure 15.*
*Hypothetical log–log plot showing leak rate vs. bobbin coil voltage for 19.1-mm (0.750 in.) pulled tubes and model boiler tests [ΔP= 16.1 MPa (2335 psi)]. The data presented have been extracted from Reference 1.*

correlated with EC voltage amplitude, as can be seen hypothetically in Fig. 14 and 15.[1] Correlations of leak rate with bobbin coil voltage (Fig. 15) show considerable scatter. Estimates of probability of leakage are <1% at 1 V for both 22.2-mm (0.875-in.)-and 19.1-mm (0.750-in.)-diameter tubes, 50% at 7 V for 22.2-mm (0.875-in.)-diam tubes, and 50% at 4 V for 19.1-mm (0.750-in.)-diam tubes. Monte Carlo techniques are one acceptable approach for accounting for the uncertainties implicit in these models.

Thus, the use of voltage amplitude to detect and measure flaws requires a conservative approach to data analysis and interpretation. Improvements in signal analysis (e.g., application of neural-network algorithms) are being explored in this program to find a better correlation between burst pressure and leak rate with EC signals.

### 2.1.4 Inspection of Sleeved Tubes

Two primary problems are associated with sleeved tubes: the large expansion and the distortion in signal from ferromagnetic material from welding procedures. Transmit-receive EC probes have an advantage over bobbin coils for inspection of sleeves.

Dobbeni et al. assessed the application of ISI technology to sleeved tubes.[2] Tubes were repaired with hybrid expansion joints in 1993 and 1994. Deep circumferential primary-water stress corrosion cracks (PWSCCs) were found in the parent material. Laser-welded sleeves were used in 1994. Cecco 3 (C3) and Plus Point probes were selected to detect circumferential and axial cracks, respectively, in sleeved tubes. Large permeability variations were found if the C3 probe was used without a magnetic bias. Magnetically biased probes are often used to reduce these variations. Based on C3 and Plus Point probe inspection data, tubes were pulled that showed axial and circumferential cracks in laser-welded sleeves (weld and hydraulic transitions) and circumferential cracks and wastage in hybrid expansion joints (parent tube and hydraulic transition). A false call was also present in the transition. This effort showed that a good correlation can be obtained between EC data and defects in sleeved tubes if the cracks are deep (>90% through-wall). Permeability variations create significant problems for analysis. The Plus Point probe provides good

imaging except in the weld area and experienced analysts are required to interpret the data for the C3 probe.

### 2.1.5 Program for Inspection of Steel Components III

Round-robin testing to evaluate techniques used to inspect SG tubing ended in 1993. The experimental evaluation of test procedure performance was carried out for a tubesheet, tube support plate, anti-vibration bars (AVB), and U bends. Approximately 100 defects were evaluated, consisting of limited stress corrosion cracking (SCC), including axial SCC and IGA, spark-eroded axial and circumferential narrow slots, pitting, and wastage. U.S. organizations involved with the RR testing were Allen Nuclear Tech, Conam, PNNL, Zetec, Westinghouse, and Oak Ridge National Laboratory (ORNL).

Although analysis of the RR has not yet been released, some teams performed consistently better than others. As a result, there is a need to determine what the teams that performed better did to obtain higher scores. The best results were associated with the UT techniques but not all defects were examined by UT and thus any claims of superiority of UT techniques must be qualified. In addition, speed and cost are other factors that must be considered when comparing EC and UT techniques. Nevertheless, detection of circumferential defects was relatively easy with UT. Combining EC with UT techniques did not seem to provide an overall advantage and there is no clear indication from this study that defects <40% deep can be detected. The correlation between the NDE signal and a defect is much better if the flaw is >40% deep. Another conclusion of this study is that there is a need to analyze each type of defect to establish the best NDE method for its detection.

Because the defects were not field induced, there is concern about how well the laboratory-grown cracks represent field cracks, particularly circumferential cracks. Furthermore the sample of defects consisted of 90 notches and only 7 cracks. There are questions about the argument that the POD for cracks and notches by EC is approximately the same and thus the use of notches is proper. The value of the results of this study is questionable because of the limited number of cracks and variations in inspection procedures.

## 2.2 Workshops and Training

A committee on Nuclear Regulatory Activities/Committee on the Safety of Nuclear Installations (CNRA/CSNI) Workshop on Steam Generator Tube Integrity in Nuclear Power Plants was held at Oak Brook, IL on October 30-November 2, 1995. One of the panel sessions addressed inspection issues. The potential subjects for discussion included standardization (calibration, probes, analysis), performance demonstration, measuring accuracy, flaw-specific POD, Program for Inspection of Steel Components (PISC) III, UT, plugging criteria, acceptance criteria, circumferential cracking, automated analysis, repair inspectability, feedback to integrity and risk analysis, limits of methods, scatter in data, approach to unexplained signals, computer modeling, inspection qualification, personnel training, and future actions. Planned presentations covered Cecco probes, PISC III, circumferential cracking and the Japanese experience. The following summarizes the issues that were discussed in some depth.

The issue of circumferential SCC of SG tubes was reviewed. The consensus was that the most critical flaw is SCC, that it is not related to a single problem, and that crack growth rate is the key factor in understanding the consequences of SCC in SG tubing. The current response to the detection of circumferential SCC of any size, in all involved countries except Belgium and Canada, is to plug the tube. However, in the future, a growing number of plants will clearly need to improve their ability to nondestructively detect and measure cracks in SG tubing.

The present effectiveness of EC and UT techniques to detect circumferential cracking were compared during this workshop. Eddy current testing with a MRPC is well established and has a detection threshold of ≈50% throughwall. Although ultrasonic techniques may have the potential for greater spatial resolution and sensitivity than EC techniques, they present problems with false positive calls. Currently, only Belgium uses UT for a base inspection and then only in combination with EC testing.

It is much more difficult to measure cracks than to detect them and only Belgium and Canada have methods that could be considered "qualified," however qualification procedures are being developed for some EC techniques in the USA. Even though it is much easier to measure the length than the depth of a crack, it is only possible to measure the part of the crack length that provides a signal above the minimum detection level, and, as a result, lengths could be easily underestimated. The use of EDM notches, acceptable as a screening tool for EC testing, is not representative of real cracks.

Differentiation of outer- from inner-surface cracks in the roll transition may be possible with phase information from an RPC (bobbin coil data is not adequate). From a collection of 70 pulled tubes with circumferential cracks, the capability of UT to detect 25% throughwall cracks was established (EDF study). Some cracks were found by UT and not by EC because of the depth. Some cracks were detected by EC and not by UT because the UT signals from the roll transition were confusing.

Although substantial progress have been made in the development of techniques for inspection, improvements in the probability of detection (POD) and measurement of cracks is needed, along with improvements in the qualification of POD and measuring procedures. Improving POD and measuring capabilities will require international collaboration and realistic "universal" samples. To obtain a POD with a high degree of confidence, 400 pulled tubes with defects are needed, including pulled tubes without significant NDE signals. Stress corrosion cracks should be present on the inner and outer-surfaces of the tubes, in both axial and circumferential orientations. Some cracks should be small because there is a need to detect cracks smaller than integrity requirements. Degraded-tube samples with artifacts are also important. While it is obviously important that pulled tubes be evaluated, evaluation of clean tubes with laboratory-grown cracks is also valuable, particularly for development work. Although good data are available on crack morphology of pulled tubes, comparable data are required on laboratory-grown cracks.

One consensus of the CNRA/CSRI group was that a widely accepted "robust" inspection method is possible through the use of multitechnique probes and corresponding advances in analysis and data handling routines. On the other hand, major weaknesses that must be

resolved are inherent in the voltage criteria, even though the criteria (for axial cracks) may be the best approach to selecting tubes to plug at this time. For example, a low voltage from a crack that could result in failure at low burst pressure is possible because, as cracks grow, ligaments connect and the crack becomes planar, a situation that can lead to tube failure. Furthermore, throughwall or nearly-throughwall cracks can fill with deposits and generate a low voltage signal. Although the present data suggest that correlating voltage to burst pressure is successful, the correlation may actually be poor. The current empirical correlations must be understood better. Data analysis must be improved and could lead to enhancements in our ability to capture critical aspects of a defect and provide a better rationale for the decision-making process, a process that is not based solely on empirical data.

The preparation of standards raises many difficult issues. For example, the fabrication of calibration tubes is difficult because EC responses from vendor-provided tubes that are supposed to be the same are variable. Comparison of signals from various countries is very complicated because of the use of differing frequencies, dependence of EC response on hole size, and because voltages are hard to compare. In the USA, a reference curve is prepared for each inspection. In France, parameters with more than flat bottom holes are used. In Canada, calibration is carried out on concentric grooves and 20-80% 1.6-mm (0.063-in.) diam holes. These differences are important and make comparison of voltages among countries difficult. To obtain a meaningful voltage comparison, it would be desirable to have the voltage output in each country mean the same thing.

The primary effort in the future will be directed toward improving in the detection of outer-surface cracks with EC probes (Plus Point, Cecco, etc.). For economic reasons there is a particular need for a single-pass probe (Cecco style). Some efforts in the future will focus on UT, but there are few if any current plans to use UT on an industry-wide scale.

U-bend cracks are now a concern at Ontario Hydro. Japan, already concerned with U-bend cracks, uses Plus Point probes for inspection. The Japanese are also developing a thin-film coil probe.

Table 1 presents the circumferential-crack inspection procedures that are used by research teams in nine countries.

Seminars and training classes on EC inspection of SG were held at ANL, December 4-8, 1995. These seminars and classes were a unique opportunity to learn about SG inspection technology and problems. The classes covered EC theory; probe design, including advantages and disadvantages; an overview of nuclear reactor SG basic design features; and probable tube damage mechanisms. Three work stations were set up for hands-on analysis of calibration and field data. MIZ-30 and EddyAcquire software was presented with hands-on training. An overview of data analysis concepts was presented with demonstration of and training in the use of Eddy95 data analysis system. The three workstations were used to review and analyze previously recorded EC data that showed bobbin coil and motorized RPC data and Plus Point technology applied to various field conditions. Some of the data acquired at Zetec from the 20 laboratory-cracked tubes were analyzed during this workshop. Advanced data analysis tools and concepts were also presented.

*Table 1. International comparison of circumferential crack inspection*

| Country | Technique | Detection Limit (minimum depth) | Sizing | Scope | Future Actions |
|---|---|---|---|---|---|
| USA | EPRI guidelines are employed. Use RPC (Plus Point, Pancake) and array probes (Cecco). | Limit is plant specific. Detection threshold is 40-50% through-wall, ID and OD. | No qualified sizing techniques expected until 1996. Current method for length is based on RPC. Phase and amplitude used for depth while Plus Point appears best for length. | Scopes are plant dependent. In general 20% of tubes are inspected. | Qualified sizing by EPRI guide-lines is expected. More tubes to be pulled for performance-based qualification. Alternate repair criteria and better probes and software needed. |
| France | RPC (absolute and differential) using EdF Procedures. Qualification based on pulled tubes. | The threshold is 50% throughwall for OD cracks.[a] | No depth sizing. OD circ. length not accurate. Only ID crack lengths are sized. (RPC accuracy is approximately ±30°). | Inspect 100% of 600MA tubes (hot leg) in roll trans. with RPC each year (OD). For 600TT tubes, inspect 100% sludge pile, and 25% at random. Nothing done for 690 tubes. | Qualifying UT equipment but no plans for industrial use. Improve OD circumferential crack detection (determination of size is not a primary objective). Automated analysis. |
| Japan | Detection with 8 x 1 probes. | 50% throughwall for ID cracks. | No data. | 100% at mechanical expansion using 8 x 1 (hot leg). | New probe for faster inspection (rotating field probe). Automated analysis and double manual analysis for future. |
| Finland | Bobbin coil for general inspection, with RPC on tube sheet. No crack-ing problems. | Not applicable | No sizing. | | Assess single-pass probe for detection. |

*Table 1. International comparison of circumferential crack inspection (cont'd.)*

| Country | Technique | Detection Limit (minimum depth) | Sizing | Scope | Future Actions |
|---|---|---|---|---|---|
| Canada | Cecco-3 is used for detection and sizing (amplitude based). Technique qualified on pulled tubes. Qualification based on lab samples. | 40-50% throughwall for OD cracks. | Use Cecco data from Bruce pulled tubes, estimate ±15% of throughwall depth, 5 mm length for OD cracks. | Inspection 100% with active known degradation. 20% for plausible degradation. Only small samples for I-800 SGs. | Auto analysis of CECCO probe data. Improved analysis using C-scan plots. Work on UT probe development and qualification. Validation program with lab/pulled tubes. |
| Germany | Bobbin coil and RPC but no cracks. | Not applicable | Not applicable | 10% every 4 years with BC, covering 100% of length. | No need |
| Belgium | RPC + UT and Plus Point used for inspections. Techniques qualified on EDM notches and pulled tubes. | 30-40% throughwall for OD cracks using EC + UT. | Estimation of degraded cross-sectional area from raw UT and TOF data. | 100% in plants with cracks (all hot leg tubes, some cold leg). | Continue to improve EC and UT technique. Continue to develop sleeve inspection technique. Assess new transmit/receive probes. |
| Spain | RPC with qualification on lab samples and pulled tubes. | 50% throughwall for OD cracks. | No sizing. | 100% of plants with cracks (hot leg) and 3% of others, except 0% for I-800 tubes. | Replace SGs that have circ. cracks. Use Plus Point and pancake RPC for detection. |
| Switzer-land | Use bobbin coil and RPC on crevice, tube sheet, etc. If nothing seen with bobbin coil then no RPC is used. No formal technique qualification required. | 50% throughwall. | Use reference notches, but change of length is most important for OD and ID cracks. Length criteria is 13 mm. | 3% of I-800 and I-690 tubes and 100% for I-600 tubes (hot leg). | Assess new multielement probes to be tried for fast screening. Need for better under-standing of growth rate and undefined signals. |

During the week of February 12, 1996 the NRC Steam Generator Tube Integrity Workshop was held in Charlotte, NC. The purpose of the meeting was to enhance cooperation and share information among NRR, RES and the Regions. NRR SG activities, regulatory policies, degradation mechanisms and inspection experiences were discussed. On the second day, the workshop was held at the EPRI NDE facility in Charlotte. A discussion of the EPRI SG Program was followed by a tour of the laboratories, which contain EC testing equipment, including probes and software. Demonstrations were presented with time for hands-on experience.

## 2.3 Emerging Technology

Many aspects of ISI technology can be improved. Some potential improvements are discussed below, including some that have already been implemented.

Faster EC data analysis is possible through fiber optic and satellite links. Raw EC data files can be transferred from an optical disc at a data acquisition location to a hard disc at the data analysis location via a fiber optic link, thus eliminating a delay of ≈4 h that would otherwise be experienced because of the need to physically transfer the optical disc to an off-site location for analysis. Digital satellite communication can also be used to connect off–site and on–site analysis. A transportable earth satellite station can be installed at a plant site while a permanent earth station can be established at the location where the analysis will take place. Cost savings and faster inspections can be realized with this communication option.[3]

Remote-field EC (RFEC) inspection employs low-frequency AC to inspect tubes from the inside. RFEC is a throughwall inspection technique. A solenoid coil generates the EC while detectors are axially displaced from the exciter by two or more tube diameters and may be oriented to measure any component of the flux density. The tube acts as a waveguide. The pickup coil senses mainly the indirect electromagnetic (EM) coupling. In contrast to conventional EC systems, in RFEC inspection, the field on the outside of the tube wall is much greater than the field on the inside. The field is mainly due to energy that is diffusing back inward from the outside. Defects cause the amplitude and phase of the signal to change. Impedance plane diagrams are used for signal analysis. In general, the angle of the defect trace on the monitor is used to characterize the anomaly, but amplitude is also used. Unlike the conventional impedance plane, the RFEC voltage plane is not restricted to the first quadrant. Points on the RFEC plot represent amplitude and phase of through-transmission signals. RFEC signals cause almost no phase change and are well separated from liftoff but separation of the different types of defects is relatively difficult. The technique might be useful for characterizing outer-surface defects.[4]

As indicated in this report, neural-networks have the potential for improvement over conventional pattern recognition techniques in the area of data analysis and interpretation. Neural-network technology has been applied to the analysis of EC data and is reported in this and other documents.[5] Good results have been achieved with limited samples and neural-networks show promise as a supplement to other data analysis schemes. The neural network processes and classifies raw data. While good results for defect detection have been achieved with four frequencies (100, 200, 400, 800 kHz) and a statistical least-squares method to fit the properties to the data is available, difficulties have been

encountered due to the presence of signals from tube supports, copper, and magnetite. The neural-network back-propagation method can better detect defects, such as ferrite or magnetite; however, the calculation time is much greater than that needed for the least-squares method.

It is possible that defects can be reconstructed from EC data but the reconstruction depends on the diffusion equation and one has to rely on indirect algorithmic approaches to solve the inverse problem.[6] Eddy current analysis is different from radiographic or ultrasonic techniques, where the reconstruction of defects is possible because the physical phenomena are governed by the wave equation. The time reversal nature of the wave equation permits the use of procedures such as holography and tomography for defect reconstruction. An alternative to solving the inverse problem for EC techniques is to use pattern recognition algorithms to interpret the signals. The variations in shape of the trajectories of the signal in the impedance plane are used in the pattern recognition schemes. Significant additional efforts are needed to optimize this method of signal analysis.

Other researchers have explored the possibility of using neural-networks to analyze EC data for systems other than SG tubing. Mann et al.[7] used neural-networks for the inversion of EC data to obtain flaw sizes. A back–projection algorithm was used in their work, with a uniform–field EC probe. The flaws used by Mann et al., consisted of five semi–elliptical EDM notches and two fatigue cracks in Ti–Al–4V. When a 1000–pair training set was used (representing ≈1% of the possible flaws) the correlation between predicted and actual depth was very good (within ±10%) and probably could be improved even more with a larger training set. In this study, the researchers suggest that the depth of a crack can be estimated reasonably well with neural-networks, even when the system is trained on EDM notches.

The application of a three–dimensional (3–D) EC EM modeling has been carried out for SG tubes.[8] A reasonable correlation between experimental and theoretically predicted results has been achieved. Finite element and boundary-element methods were applied to solve the EC problem. Experimental and calculated probe impedance trajectories for 100 and 400 kHz are presented for four 50% external slits with a width of 0.25 mm (0.010 in.), located 90° apart. The agreement between calculation and experiment (differential bobbin coil) is satisfactory. Because the computer time required to perform 3-D calculations is very long, simplified two–dimensional (2-D) analyses have been examined. Two– and 3-D analyses of EC signals from 50 and 100% throughwall cracks in SG tubes, with 100 and 400 kHz frequencies were compared with experimental measurements. The results are qualitatively similar, but, quantitatively, the 3–D analysis appears significantly better (2–D results were ≈1/2 of the experimental value). The problem with the 2–D analysis may be due to the lack of information about the volume of the crack. Other efforts to reconstruct 3–D images from EC signals (the inverse problem) are found in Refs. 7 and 8.

Advances in digital signal processing may dramatically improve our capability to extract information from an EC probe. It may be possible to use sophisticated digital filters to solve problems that are now approached by multi–frequency techniques, such as the elimination of signals from the tube support plates. Stepinski and Maszi[9] address the problem of detection and classification of material defects during an EC inspection. They

consider algorithms for detecting and characterizing flaws and propose a new type of filter for classifying EC data. The new 2-D conjugate spectrum filters (CSFs) are sensitive to both phase angle and shape of the EC response. They transform all of the EC patterns into straight lines and thereby simplify the decision-making process. If digitized EC data sampled at a frequency synchronized with the inspection speed is available, CSFs could be used with SG tubing.

Rose et al.[10] describe a method for inspecting SG tubing with guided ultrasonic waves. The advantage of this concept is the absence of a moving probe and 100% coverage of the tube. Launching of guided waves with sufficient energy to inspect a long length of tubing is very difficult and sensitive to ultrasonic frequency, but theoretical considerations have significantly helped to optimize probe design. The ultrasonic wave is injected at the top of the tubing and travels the length of the tube with little attenuation. Echoes that return to the transmitting probe indicate the presence of defects in the tube. Defects that are only 10% of the total cross-sectional area have been detected in tubes nearly 17m (55 ft) long. Tests have shown that guided waves can travel at least 49 m (160 ft). Though ultrasonic guided waves may be useful for inspection of SG tubing, satisfactory characterization of a detected flaw may not be possible for a fixed-probe configuration, because of the distortion of the ultrasonic wave as it propagates in the tube wall. The use of guided waves as part of a scanner, as described in this report, may be more effective for detecting circumferential cracks.

# 3 Research on ISI Technology (S. Bakhtiari and D. S. Kupperman)

The objective of this task is to evaluate advanced NDE and signal analysis techniques for reliable ISI of original and repaired SG tubes. Improved correlations between EC indications and flaw morphology, leak rate, and failure pressure will be developed. Eddy current ISI methods have not always proved reliable for detection, classification, and sizing of flaws, especially cracks. The implementation of degradation-specific management requires detailed knowledge about the specific nature and severity of flaws. Improved techniques (EC and others) are needed for more reliable inspection and interpretation of flaws. The reliability and accuracy of the techniques must be quantified so that plugging criteria and the consequences of leaving degraded tubes in service after inspection can be evaluated. Furthermore, the robustness of the voltage parameter and of other EC parameters and techniques must be evaluated with respect to their range of applicability.

The research on improved EC inspection of SG tubes will focus on four primary areas: (1) development of analytical methods for the prediction of EC response as a function of probe design, flaw characteristics, and material properties; (2) development of effective signal analysis procedures; (3) development of flaw imaging and display methods for simple and accurate flaw characterization; and (4) improved probe designs that may use directional arrays so that axial and circumferential defects can be examined simultaneously. The reliability and effectiveness of improved inspection techniques will be demonstrated through laboratory testing of SG tubes that contain various flaws and the SG tube bundle mock-up. Final validation will utilize in-service-degraded SG tubing.

## 3.1 Computational Electromagnetic Modeling

Because the interaction of the induced EC coil field with heterogeneous media is a complex phenomenon, it is vitally important to have a reasonably accurate a priori knowledge of the probe response to interpret the measured data and to optimize parameters for better probe design. One must distinguish between real defect signals and those due to the background signals, such as those due to tube support plates, probe wobble (liftoff), material inhomogeneities, thickness variations, etc. Reliable computational EM models are important to the researchers and practitioners in EC NDE applications.

In this work, three EM modeling approaches were initially evaluated in application to simulation of EC probe response for NDE of SG tubing. They consisted of closed-form integral solutions (by C. V. Dodd[13]), volume integral formulation (VIC-3D software by Sabbagh Associates), and finite element method (ELEKTRA interface module by Vector Fields). The closed-form solution (relaxation method) is based on Burrow's point defect theory, wherein the underlying assumption is that a point defect has an infinitesimal volume. Although calculations with this approach can be performed reasonably fast, the solutions are accurate only for small defects with uniform cross section. The solution accuracy degrades when larger, complex-shaped defects are modeled. VIC-3D uses a volume integral EM formulation in conjunction with a moment method numerical solution technique, which suggests a more computationally intensive calculation when compared with the previous method. The model is capable of taking into account more complex defect geometries for axisymmetric problems. The ELEKTRA package, which is currently

in use at ANL, is a general-purpose 3-D FEM-based computational code that may be used to treat steady state and transient field calculations. This software can be utilized as a research tool to design and analyze a wide range of EM-based systems. A brief description of these three modeling codes is given below.

FORTRAN programs that were originally developed at ORNL and used for the design and analysis of EC SG problems of interest to the NRC[13] were modified and made compatible with the platforms available at ANL. A listing of these programs, along with a brief description of their purpose, is provided in the appendix. To process and display the outcomes of these programs, computation and visualization software, MATLAB, is currently used at ANL. Because of their treatment of specific problem geometries and the underlying assumptions in the solution method, these programs can run with minimal computational resources. They can be used to simulate impedance responses to defects that are exhibited by four types of probes: pancake, reflection, circumferential boreside, and circumferential encircling. Both absolute and differential coils may be modeled for circumferential boreside and encircling probes. The defects can be treated as point defects, as point defects averaged over the depth of the actual defects, or as point defects averaged over the volume of the defects. In general, the solution accuracy is inversely proportional to defect size. For general test case scenarios, these codes will be used to check the results of computationally intensive FEM solutions that can better simulate realistic flaw geometry and as a tool for analysis and determination of EC probe response and test parameters.

VIC-3D software, developed by the Sabbagh associates with substantial support from EPRI, uses a volume-integral formulation to model EC probe response and computes flaw/field interactions in conjunction with a moment method solution technique. The objective of such integral equation methods is to cast the solution for the unknown current density, which is induced on the scatterer, in the form of an integral equation where the unknown induced current density is part of the integrand. The integral equation is then solved for the unknown induced current density by numerical techniques such as the moment method. VIC-3D can model absolute and differential probes (with or without ferrite cores), simulate layered materials with planar and tubular geometries, model cracks and flaws due to manufacturing defects, corrosion pitting, or other destructive processes. A general axisymmetric model allows the description of tubes with tube supports, rolled-expansion transition zones, or welded sleeves. The model also allows consideration of linear ferromagnetic materials. The flaw library includes holes, axially oriented thin cracks, user-defined flaws, such as IGA, and various axisymmetric artifacts. Typical simulation of EC probe response to a crack would consist of specifying probe coil dimensions and number of turns, modeling of test material by specifying intrinsic EM properties, specifying flaw conductivity and dimensions, and, finally, specifying the operating frequency and scan positions. The results can be presented in both tabular and graphic form, 2- and 3-D plots, strip charts, and impedance-plane formats, which simulates the display of an NDE instrument. This software is available for PC (MS DOS), as well as for workstation environments such as Sun OS, HP-UX, UNIX, etc.

The ELEKTRA software module from Vector Fields uses a discrete finite element model to solve the partial differential equations that govern the behavior of a system and includes the EM finite element pre- and postprocessor OPERA-3D. Using the

preprocessor, a mesh is formed that is discretized into elements. A 2-D grid is created initially and swept through space to create a 3-D model. The sweep operation includes facilities for rotation, projection and translation. The mesh primitive blocks are assigned orientations and material characteristics. Upon enforcement of the appropriate boundary conditions, the resulting input is fed into the analysis module. The 3-D time-varying field equations are subsequently solved. The time variation can either be transient or steady state. In addition, the effects due to motion can be computed. The problem space is defined such that total and reduced magnetic scalar potentials are used in nonconducting media which reduces the solution costs and corrects the cancellation errors associated with the simple reduced potential approach. In conducting media, magnetic vector and electric scalar potentials are used, which are directly coupled with the potentials in the exterior medium. The post processing environment provides facilities to display the results of the analysis in a number of ways including, 3-D model viewing from any angle, graphs, histograms, contour maps of the solutions, contour components of the results on any surface, calculation of fields, forces and energy, and user-defined functions. Although a PC version of this software is available, the full version for 3-D analysis and display, necessary to model and analyze nonplanar EC field distributions, is primarily intended to run on platforms ranging from workstations to mini and mainframe computers.

Modeling EM NDE sensors poses some specific challenges for 3-D FEM formulations. The desired solutions (e.g., change in the EC coil's primary magnetic field due to a small defect in a tube) are often variations that are three to four orders of magnitude smaller than the calculated total fields. To accurately model a scanning probe, a number of initial trials are often required to achieve an acceptable convergence as well as computationally efficient solutions. In general, details of the impedance locus are of interest which require accurate impedance calculations. This suggests finely discretized regions under the coil may have to be moved for each new coil position. Several iterations of the mesh design are usually required to obtain a satisfactory mesh for the first coil position, from which the others can then be derived. 3-D FEM-based models could be the only alternative to achieve reasonably accurate solutions for EC NDE problems with complex model geometries and awkward defect boundaries.

## 3.2 Sample Calculations

### 3.2.1 Closed-Form Solutions

Using the closed form solution method, sample calculations were performed for a differential bobbin coil and an absolute pancake coil. The calculations are generic, i.e., the parameters used for the simulation such as coil diameter, height, number of turns, and current density, do not represent any particular industry standard probe. The results here are given either in terms of the defect sensitivity factor (DSF) for an array of point defects at various axial and radial positions within the tube wall, modeled as a flat layer for the pancake coil simulations, or in terms of the probe impedance variation for a fixed defect as a function of coil position. An impedance-plane representation of the result, which resembles a typical measurement instrument display, is also given for each case. For all cases, the tube OD was 19.1 mm (0.750 in.) with a tube wall thickness of 1.27 mm (0.050 in.). A resistivity value of $\rho$ = 100 $\mu\Omega$-cm was used for the tube material which represents alloy (Inconel) 600. The upper and lower frequency limits of f = 100 kHz and f = 500 kHz

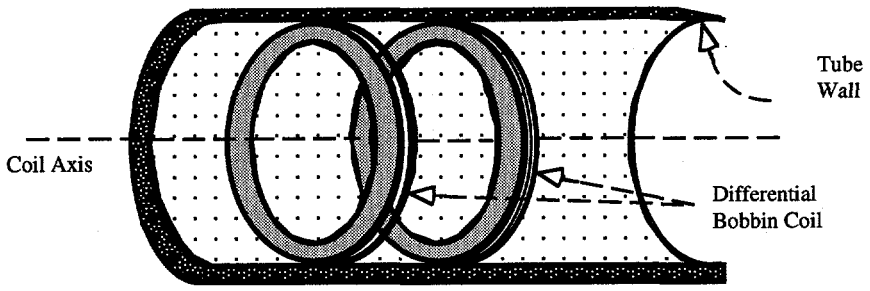


*Figure 16. Geometry of differential bobbin probe inside a tube.*

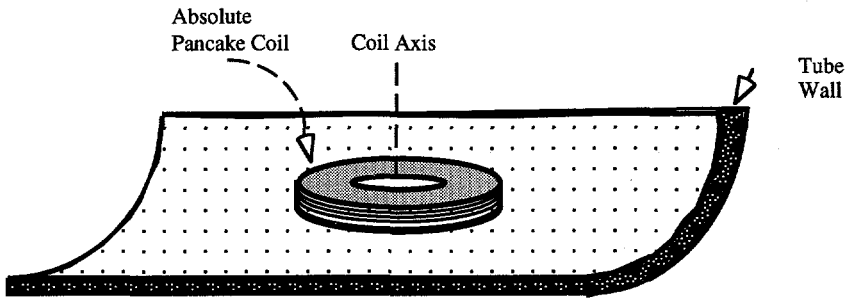


*Figure 17. Geometry of absolute pancake probe inside a tube.*

that were used in these calculations are typical for inspection with standard probes. An arbitrary liftoff distance (the coil to tube inner-wall separation) of $L_1$ = 0.25 mm was assumed for this case.

Figures 16 and 17 depict the EC inspection geometries being considered. Figures 18a and b show cross-sectional views of the coils and tube, along with the model parameters. Figures 19 and 20 show the amplitude and phase variation of DSF for an array of point defects located at various axial and radial positions within the tube wall that was obtained with a bobbin coil operating at a frequency of 100 and 500 kHz, respectively. Comparison of the two figures clearly indicates the fact that lower frequencies allow for greater depth of penetration. Nevertheless, better sensitivity is achieved at higher frequencies, if the signal loss due to skin depth attenuation does not completely eliminate the defect indication. For the same coil size, the greater depth of penetration achieved at lower frequencies generally implies less resolution and lack of measurement sensitivity to small variations.

Figures 21 and 22 show the variation in probe resistance and reactance, as well as an impedance-plane plot of the same parameters for flat-bottom holes with depths of 20, 40, and 100% throughwall. Again, the results indicate better depth of penetration at the lower frequency. Examination of phase variation from the impedance-plane figures also shows

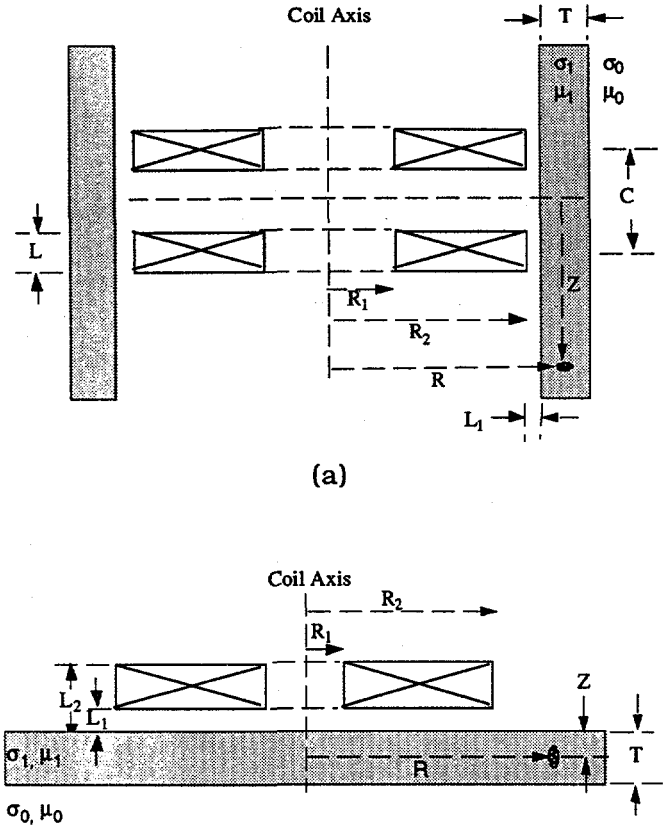


*Figure 18. Problem geometry of (a) differential bobbin coil, and (b) pancake coil for SG tube inspection.*

the lack of sensitivity at lower frequencies. This can be observed from smaller rotation angle (i.e., phase variation) of the impedance-plane signal trajectory at the lower frequency that could result in less accurate defect depth estimation in practical ISI applications.

Figures 23-26 are the simulation results for a pancake coil. Here, a small pancake coil with inner radius $R_1$ = 1.27 mm (0.05 in.) and outer radius $R_2$ = 3.18 mm (0.125 in.) was modeled. The other simulation parameters were the same as in the previous test case with the bobbin coil probe. The effect of frequency is similar to that observed for the bobbin coil. When compared with the bobbin coil, the results indicate a smaller penetration depth for the pancake coil, i.e., the depth of penetration is dependent not only on the operating frequency but also on the coil geometry.

### 3.2.2 Finite Element Method

Sample calculations are presented that pertain to EM modeling of EC probes for inspection of SG tubes with the FEM-based code. A model of an SG tube was initially

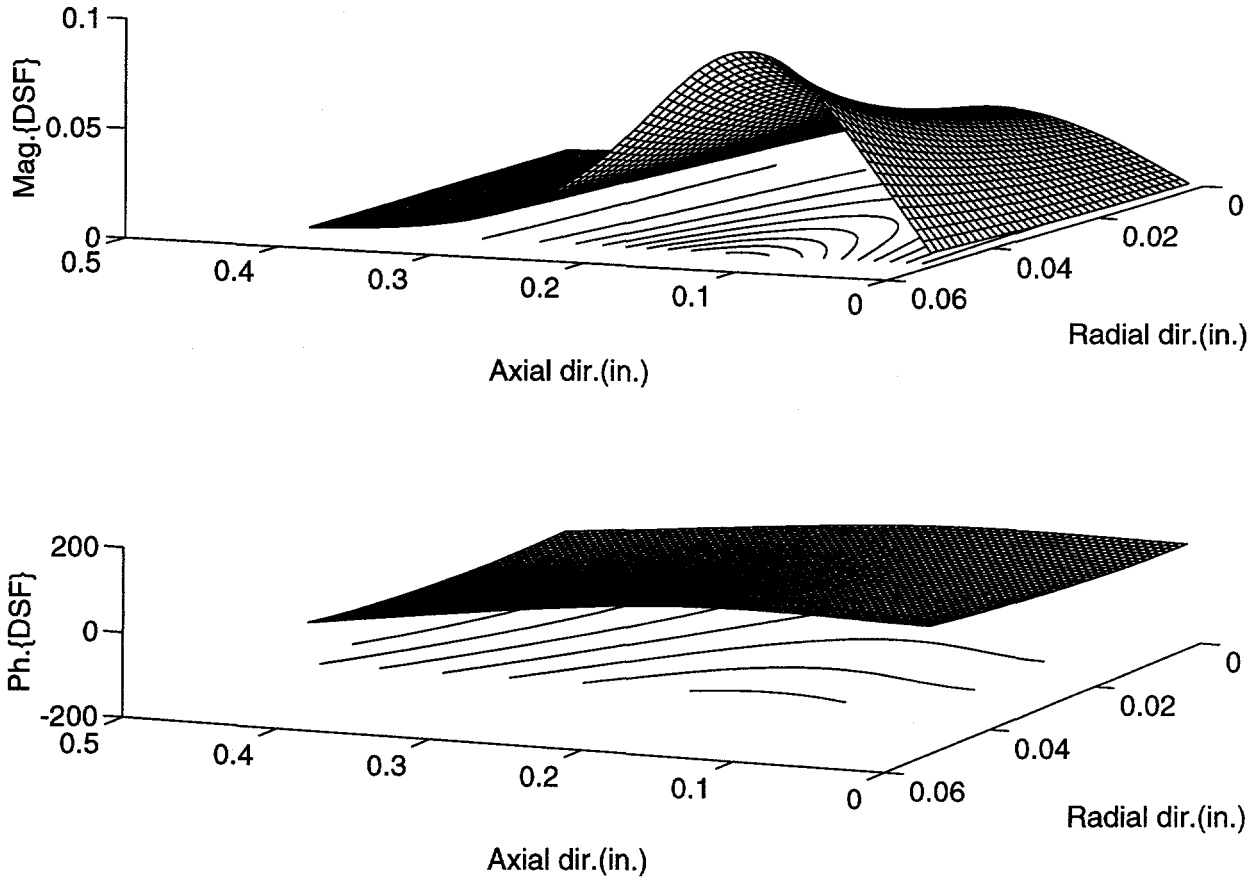


*Figure 19. (a) Magnitude and (b) phase of defect sensitivity factor for differential bobbin coil inside Inconel 600 tubing for an array of point defects at various axial and radial positions.* f = *100 kHz, wall thickness = 1.27 mm.*

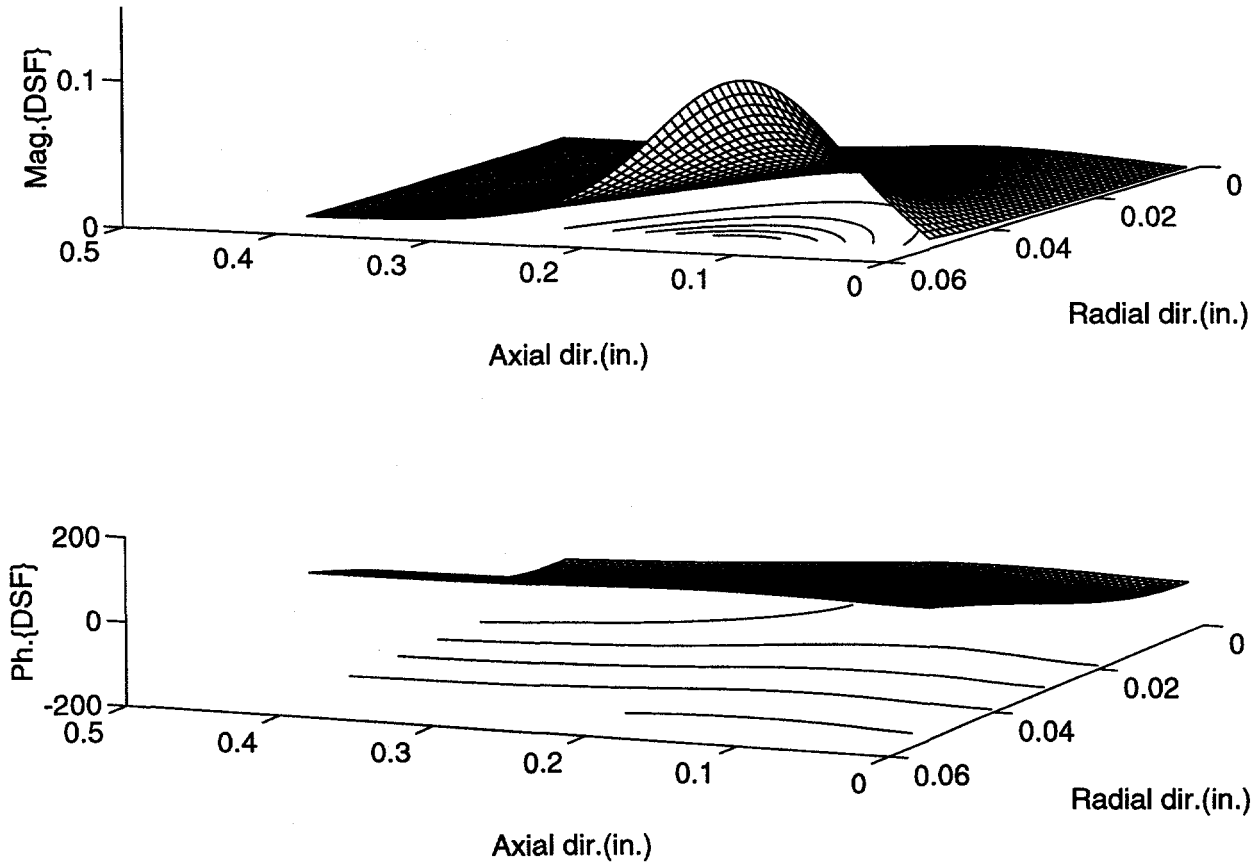


*Figure 20. (a) Magnitude and (b) phase of defect sensitivity factor for differential bobbin coil inside Inconel 600 tubing for an array of point defects at various axial and radial positions.* f = *500 kHz, wall thickness = 1.27 mm.*

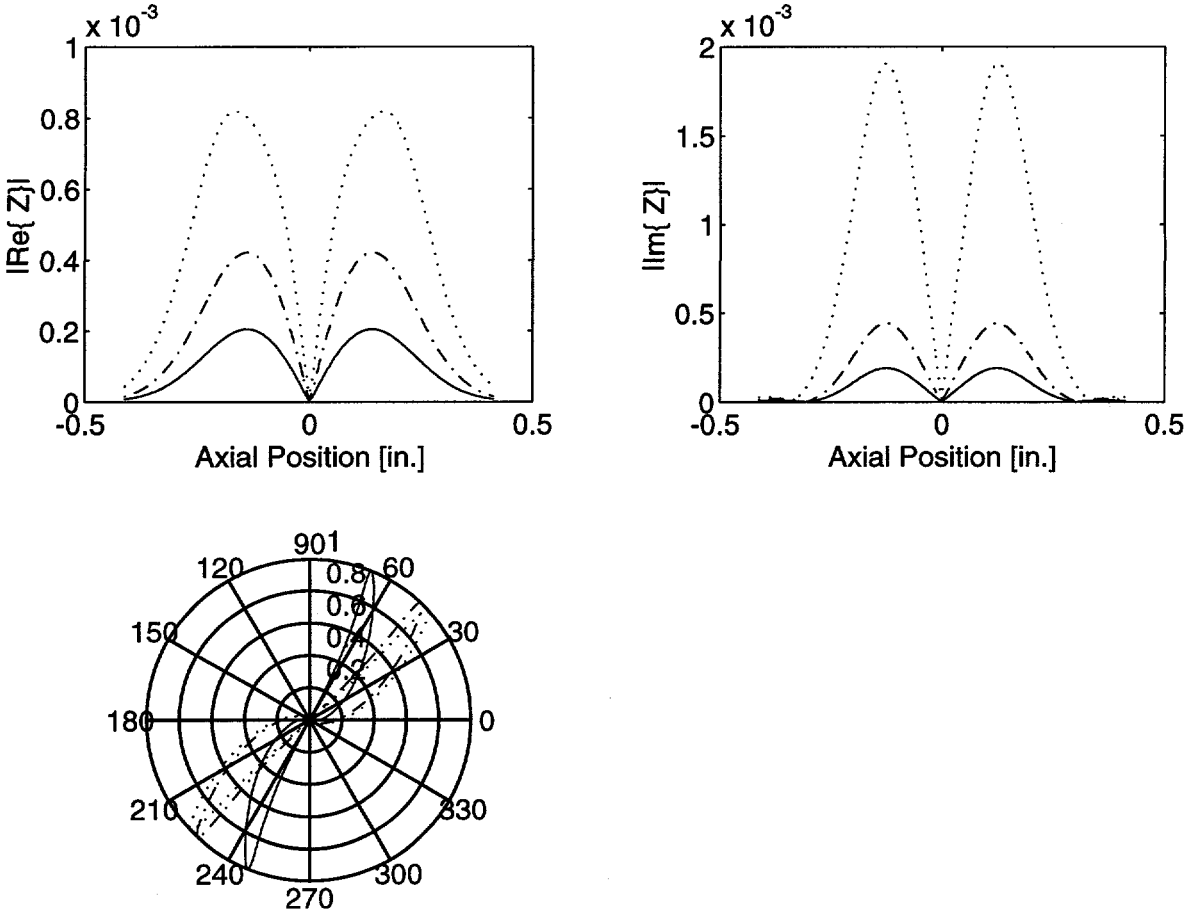


*Figure 21. Magnitude of real and imaginary parts of impedance variation vs. axial distance, along with impedance-plane plot for differential bobbin coil inside Inconel 600 tubing with wall thickness = 1.27 mm at* f = *100 kHz. Defects consisted of 20% [-], 40% [-.], and 100% [.] OD flat-bottom holes.*

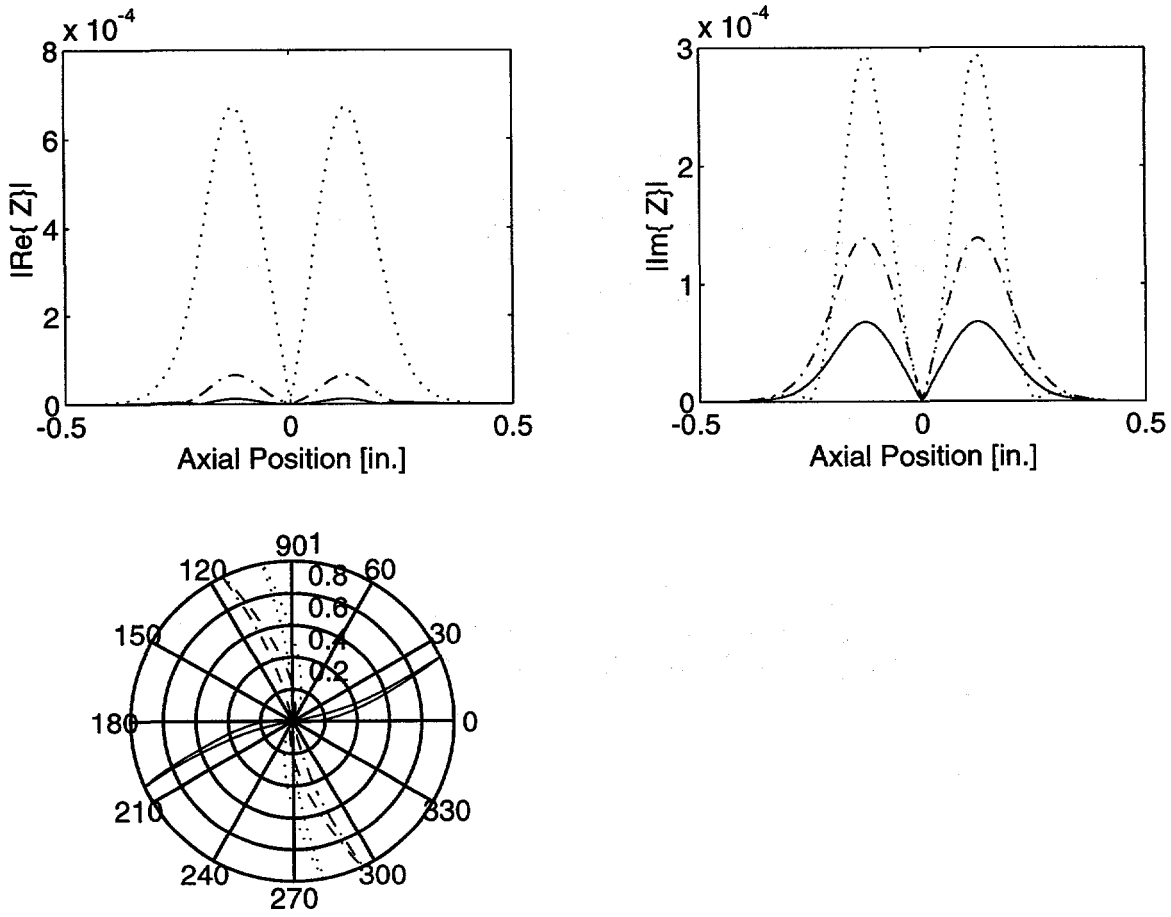


*Figure 22. Normalized impedance-plane plot for differential bobbin coil inside Inconel 600 tubing material with wall thickness = 1.27 mm and at f = 500 kHz. Defects consisted of 20% [-], 40% [-.], and 100% [.] OD holes.*

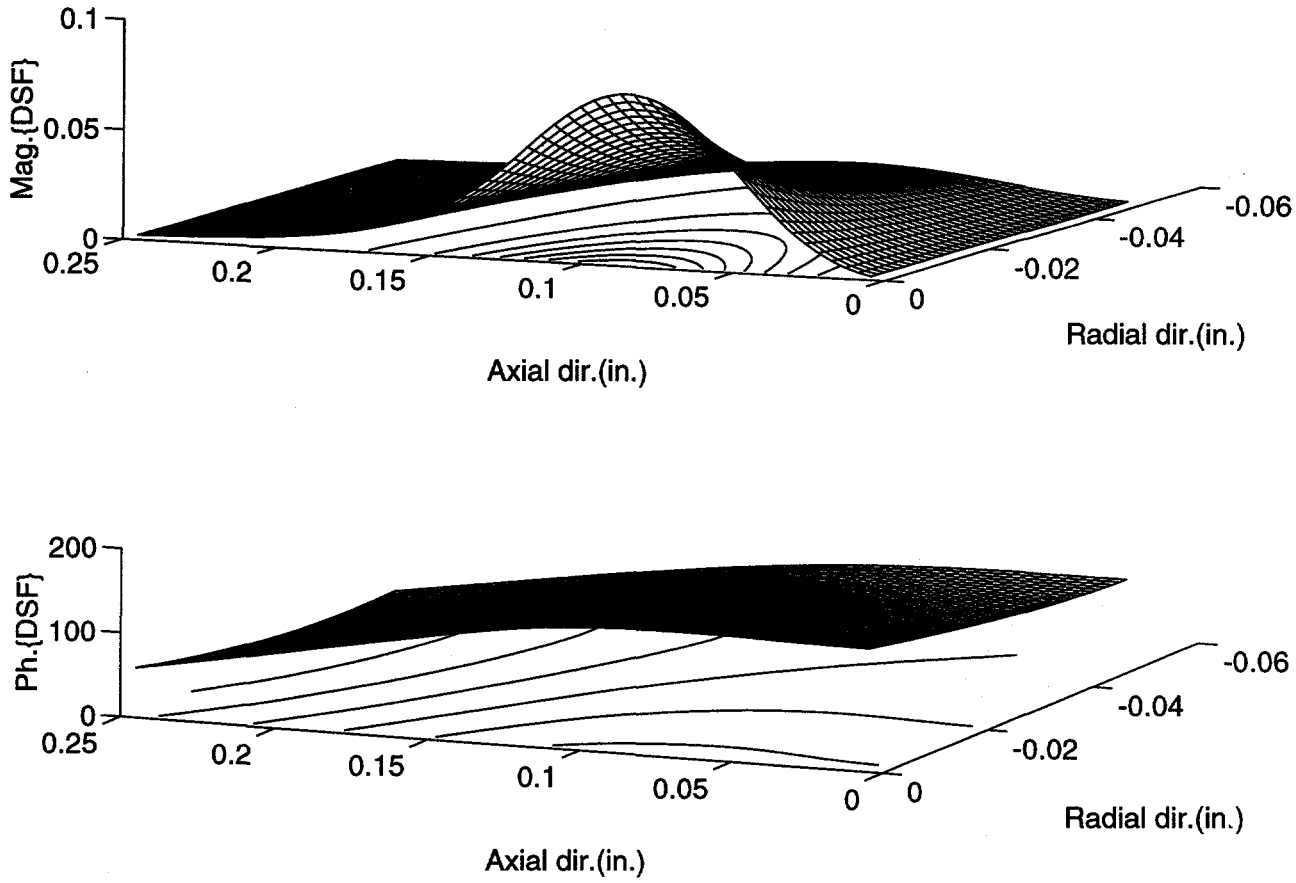


*Figure 23. (a) Magnitude and (b) phase of defect sensitivity factor for absolute pancake coil on Inconel 600 tubing for an array of point defects at various axial and radial positions.* f = *100 kHz, wall thickness = 1.27 mm.*

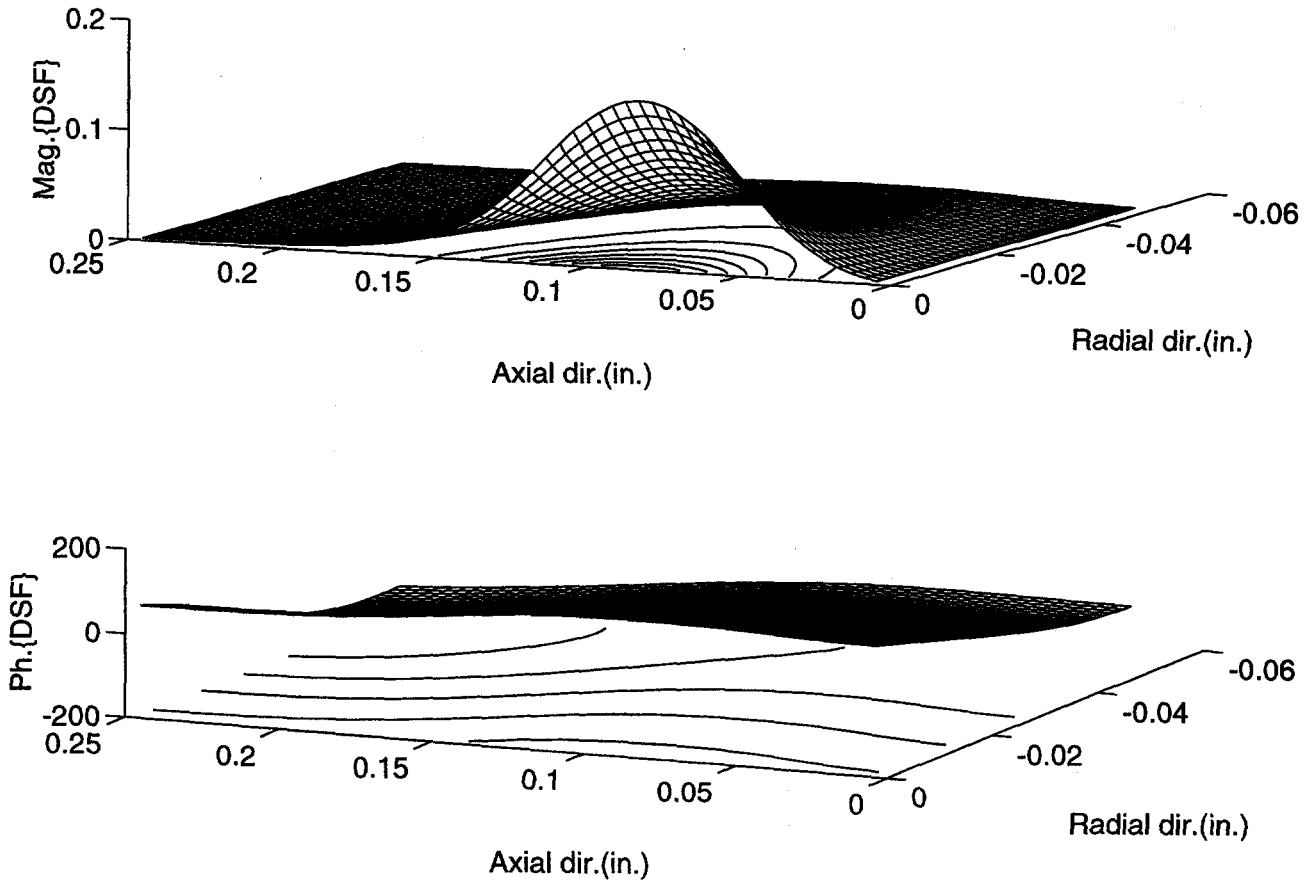


*Figure 24. (a) Magnitude and (b) phase of defect sensitivity factor for absolute pancake coil on Inconel 600 tubing for an array of point defects at various axial and radial positions.* f = *500 kHz, wall thickness = 1.27 mm.*

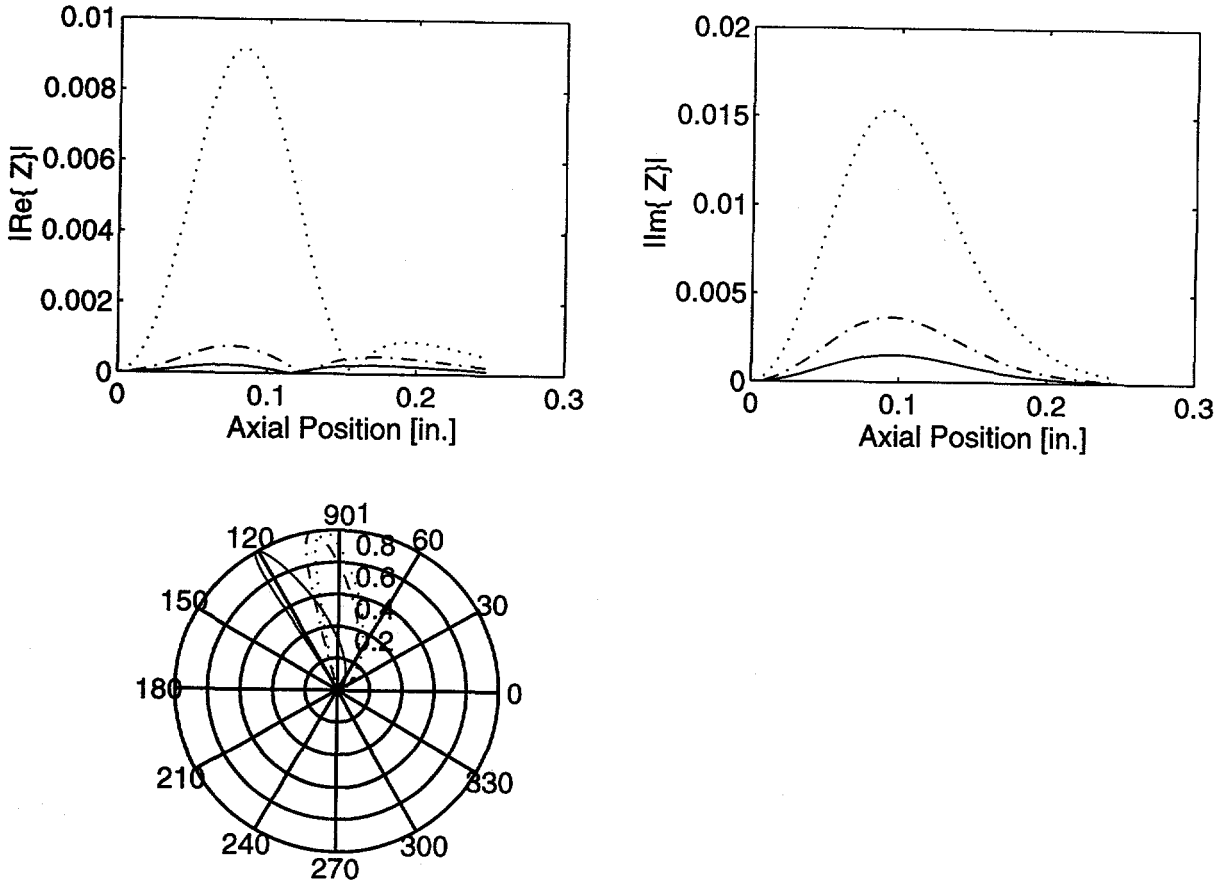


*Figure 25. Magnitude of real and imaginary parts of impedance variation vs. axial distance along with impedance-plane plot for the absolute pancake coil at* f = *100 kHz. Defects consisted of 20% [-], 40% [-.], and 100% [.] OD holes.*

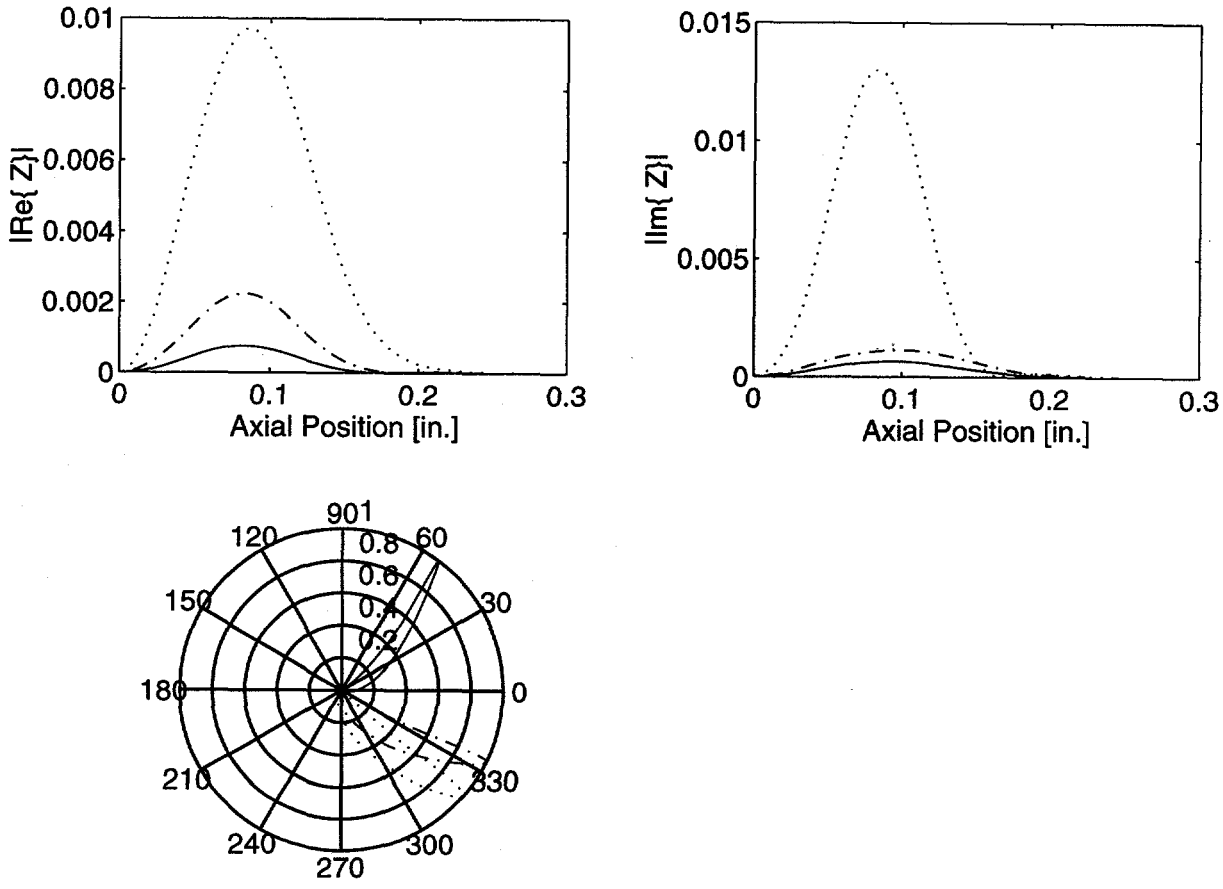


*Figure 26. Magnitude of real and imaginary parts of impedance variation vs. axial distance along with the impedance-plane plot for the absolute pancake coil at* f = *500 kHz. Defects consisted of 20% [-], 40% [-.], and 100% [.] OD holes.*

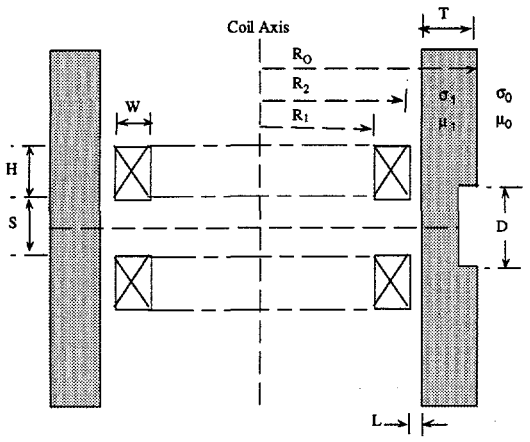


*Figure 27.*
*Cross-sectional geometry of a differential bobbin coil inside a tube.*

constructed to examine the solution accuracy. Representative test case scenarios are presented that, with a differential bobbin coil and an absolute pancake coil, simulate the field perturbation due to the presence of an OD flat-bottom hole (i.e., typical calibration defect) and a circumferential notch. The variation of the EC probe complex impedance was subsequently determined in the postprocessing stage through energy and power calculations. These cases were chosen to allow both the determination of the accuracy of FEM results through convergence tests on the solutions and the possibility to verify the results by comparing with previously discussed closed form solutions which are limited to axisymmetric problem geometries and defects of specific cross-section (e.g. spherical and cylindrical volumes). In the future, the FEM code will ultimately be used to model more complex defect geometries such as fatigue cracks, SCC, and IGA. The FEM's elaborate mesh-generating pre-processor will also allow incorporation of various nonuniform material property variations such as presence of magnetite and copper deposits, as well as modeling of defect-prone areas such as baffle plates, and roll-expanded regions.

Next, a test case is presented that simulates a tube with an OD calibration defect at three frequencies of f = 100, 250 ($f_{90}$), and 400 kHz. These represent typical frequencies that are used for multifrequency ISI of standard SG tubing with wall thickness of ≈1.27 mm (0.050 in.). Figure 27 shows a cross-sectional view of the coil and tube for the test case considered here. The probe used was a differential bobbin coil, with the coil width reduced to half of its height. Reduction of the coil height-to-width ratio is often used in practice to create a more uniform coil field distribution over the test sample, and, as a result, achieve better sensitivity. According to Fig. 27, the tube diameter was $2R_0$ = 19.1 mm (0.750 in.), with a tube wall thickness of T = 1.27 mm (0.050 in.). The radius of the embedded defect D/2 was 1 mm (0.04 in.), which represents a 40% OD throughwall hole. A resistivity value of $\rho$ = 100 $\mu\Omega$-cm was used for the tube material, which represents Inconel 600. Each medium is defined with a conductivity $\sigma$ and permeability $\mu$. Nonmagnetic media (i.e., relative permeability $\mu_r$ = 1) was assumed for all of the involved materials. Here, a differential bobbin coil with inner radius $R_1$ = 7.35 mm (0.289 in.), outer radius $R_2$ = 7.95 mm (0.313 in.), width W = h/2 = 1.2 mm (0.048 in.), and coil spacing of S = 1.27 mm (0.050 in.) was used. The coil represents 50 turns carrying a current density of 0.175 A/mm$^2$. An arbitrary liftoff distance of $L_1$ = 0.3 mm was assumed for the coil-to-tube inner-wall separation. Because of the symmetry of the problem, only half of the geometry was modeled.

Figure 28 is a plot of the magnitude of magnetic flux density $\bar{B}$ along the tube/coil axis for the three frequencies that were used. As expected, the highest peak value of $|\bar{B}|$ occurs at the lowest frequency of 100 kHz. Figure 29 depicts the tube's model geometry, along with the distribution of the current density $|\bar{J}|$ at f = 400 kHz. The probe center is at z = 1.235 mm (0.049 in.) along the tube axis so that one of the differential coils is positioned under the defect. The current distribution on the outer surface of the tube shows the distortion of the path of circumferentially induced currents that are forced to go around the defect. Because of the inverse relationship between frequency and depth of penetration, the results indicate the fact that, at this highest frequency, the fields are more confined to the inner surface of the tube and attenuate rapidly in the radial direction. Furthermore, comparison of the results with the earlier test cases also show that the highest probe resolution in the axial direction is achieved at the shortest wavelength. Figure 30 is a plot of the calculated real and imaginary parts of the coil's complex impedance as a function of position along the tube axis for three test frequencies. The results indicate that, for the geometry modeled here, the variation of coil impedance (i.e., probe sensitivity) increases with frequency. This was expected because for the tube wall thickness used in the model, the skin depth attenuation even at the highest test frequency would still allow detection of a 40% OD artifact.

Next, two representative test cases are presented that show the calculated current distribution for a 22.2-mm (0.875 in.) -diameter tube in the presence of a 40% OD circumferential (360°) notch, for both the bobbin coil and the pancake coil. To test different probe sensitivities, an oversized axisymmetric defect was initially considered. The effect of probe parameters, such as frequency and dimensional variations, and defect characteristics such as depth, length, width, and orientation, will eventually be studied to gain insight into the nature of field interactions for various probe/tube geometries. For the second test case presented here, the coil dimensions represent those of a P90 probe. For this initial calculation, a flat coil is considered. This flat-coil configuration is different from that of the actual P90 coil design, which has a curvature made to fit the tube inner surface. Modification of the model geometry from a flat coil to a cylindrically shaped coil is currently underway and will be presented in future reports. This coil geometry was originally selected based on the criteria that would provide an optimum compromise between resolution, when used as RPC, and circumferential coverage, when used in an array configuration.

Two test cases are presented next that simulate a tube with a circumferential OD notch. These preliminary results are given in terms of the surface current distribution and the current distribution along the tube wall at an excitation frequency of f = 180 kHz for both a differential bobbin coil and an absolute pancake coil. Figures 31a and b depict cross-sectional views of the two coils inside the tube. All linear material medium within the problem space are defined with a conductivity $\sigma$ and permeability $\mu$. Once more, a resistivity value of $\rho$ = 100 $\mu\Omega$-cm was used for the tube material which represents alloy 600. According to these figures, the tube diameter $2R_0$ was 22.2 mm (0.875 in.), with a tube wall thickness of T = 1.27 mm (0.050 in.). The width of the embedded wedge-shaped defect is $W_d$ = 0.5 mm (0.020 in.) on the outer surface of the tube and tapers down to zero at a 40% depth from the outer surface. As shown in Fig. 31a, a differential bobbin coil with inner radius $R_1$ = 7.35 mm (0.289 in.) and outer radius $R_2$ = 7.95 mm (0.313 in.) was used for the first test case, with H = 2W = 1.2 mm (0.047 in.), and coil spacing of S =

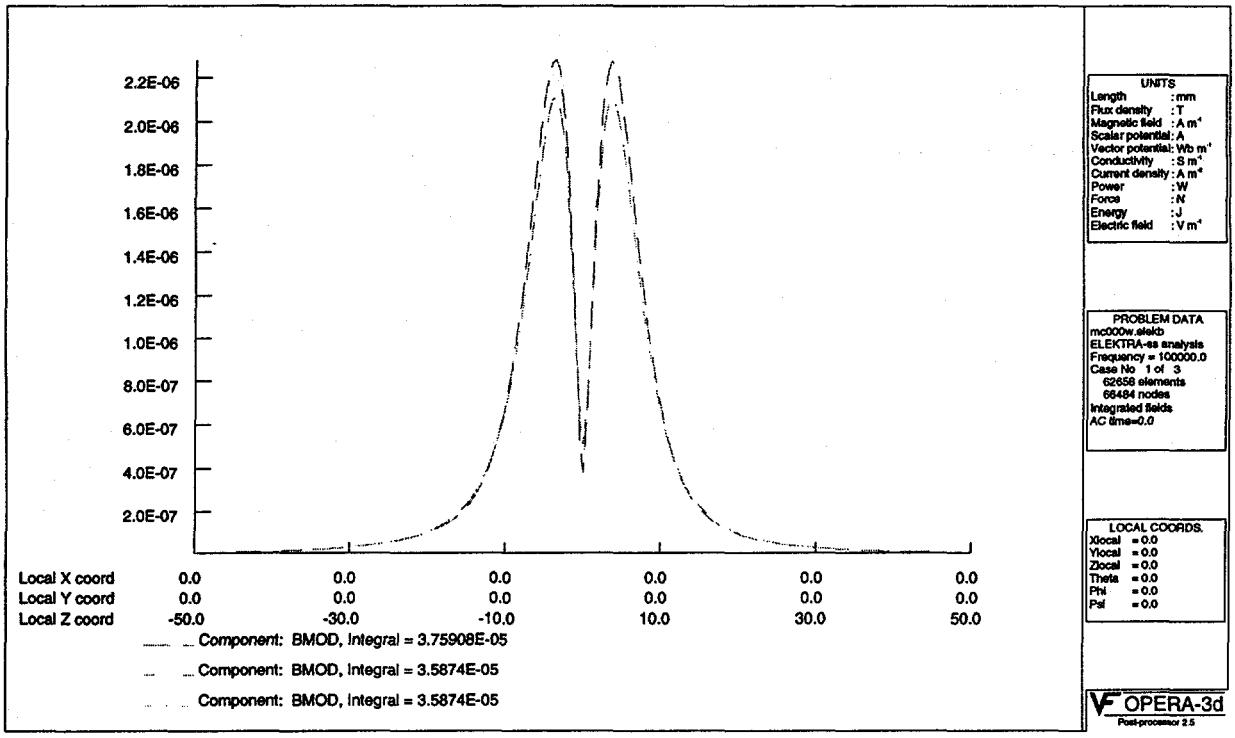


*Figure 28. Plot of $|\bar{B}|$ along the tube axis for differential bobbin coil at f = 100, 250, and 400 kHz.*

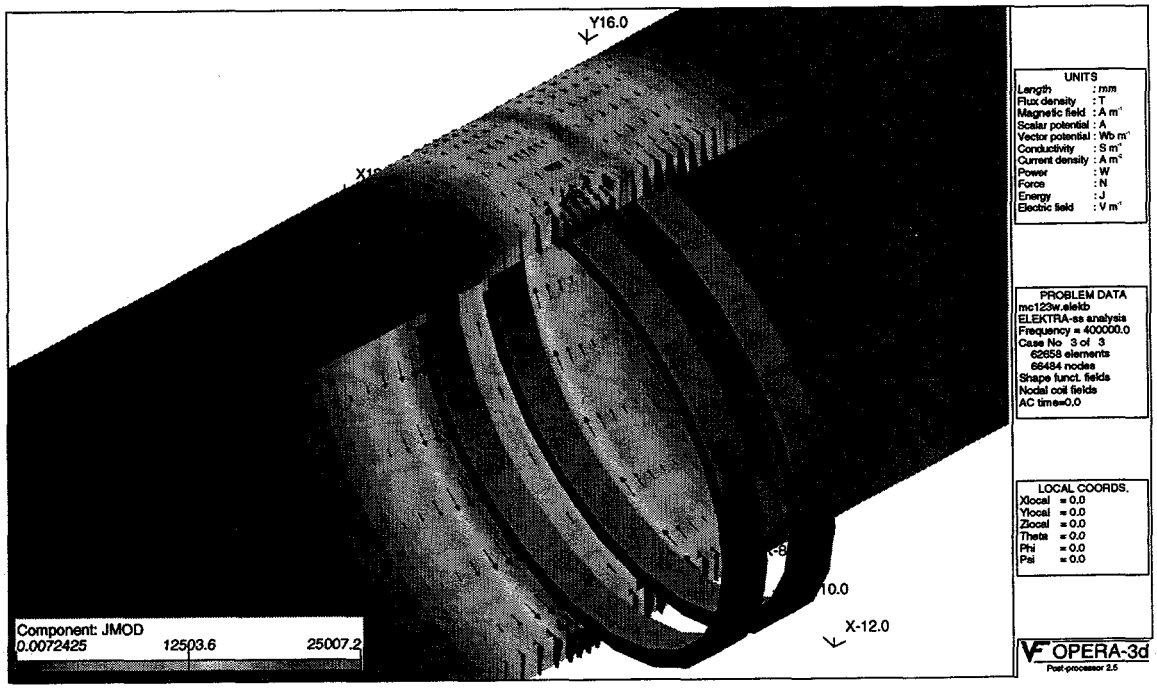


*Figure 29. Current density distribution $|\bar{J}|$ at f = 400 kHz for differential bobbin coil over a 40% OD defect (hole).*

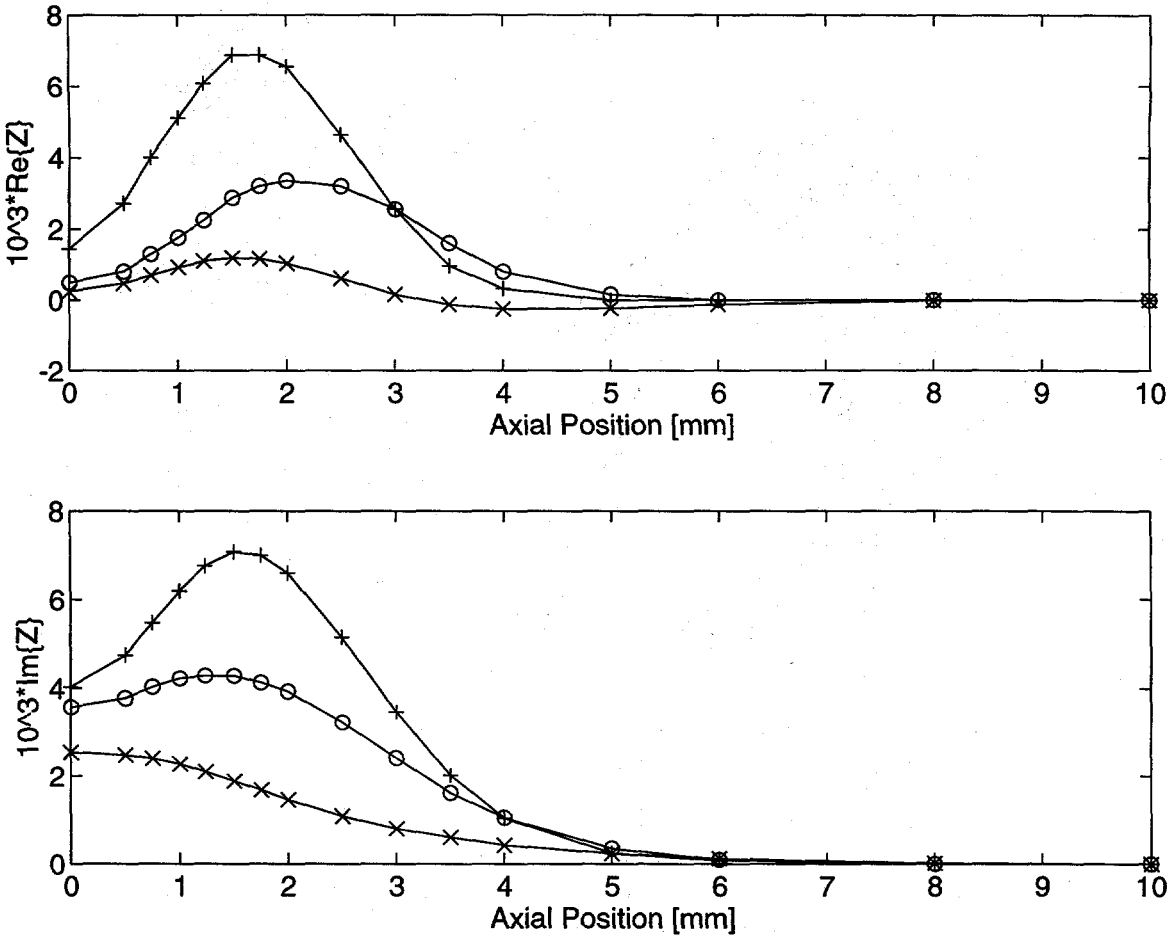


*Figure 30. Plots of variation in real and imaginary parts of impedance vs. axial distance at f = 100 [x], 250 [o], and 400 [+] kHz.*

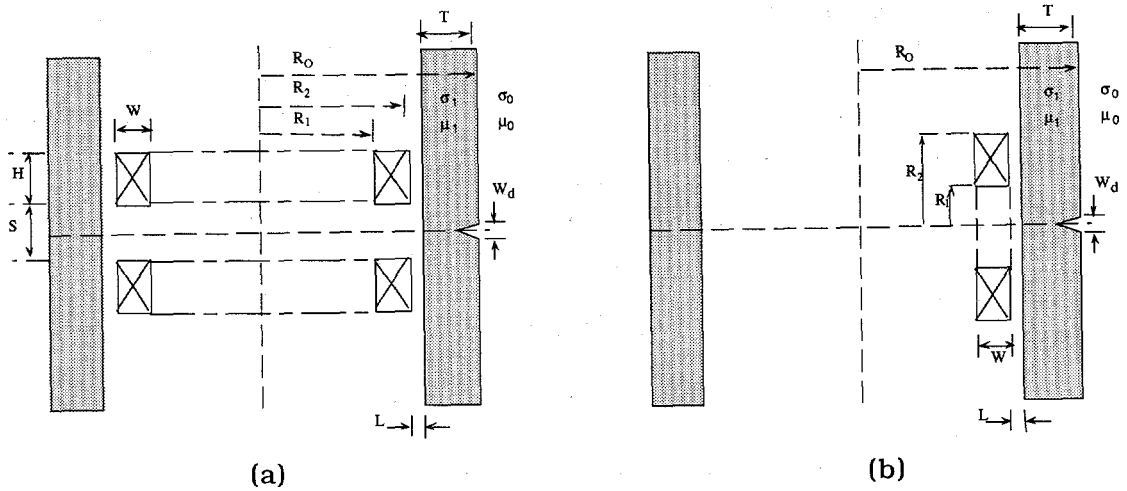


*Figure 31. Cross-sectional geometry of (a) differential bobbin coil and (b) absolute pancake coil inside a tube with a circumferential OD notch.*

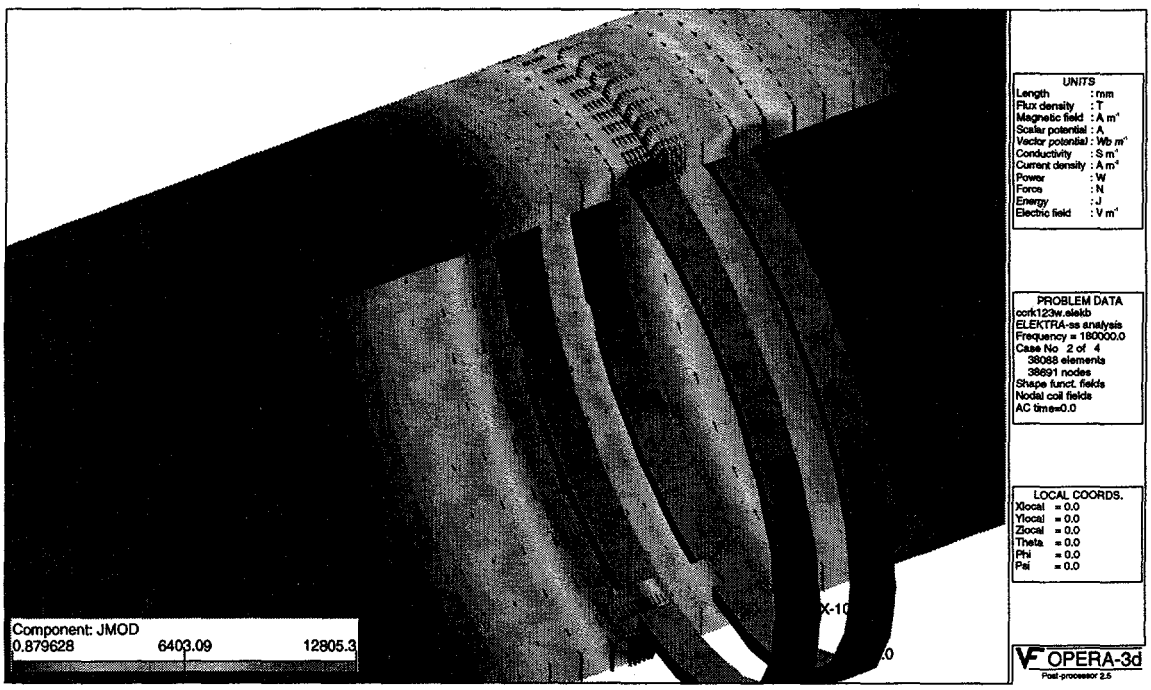


*Figure 32. Current density distribution at f = 180 kHz for differential bobbin coil over a 40% OD circumferential defect (notch).*

1.27 mm (0.050 in.). For the pancake probe of Fig. 31b, the coil ID was 3.05 mm (0.12 in.) and the coil OD was 6.10 mm (0.24 in.) (i.e. $R_2 = 2R_1 = 3.05$ mm). The coil length is H = 0.010 in. (0.254 mm) and the lift-off distance is L ≈ 0.4 mm (0.016 in.). Once more, due to symmetry of the problem, only half of the geometry is modeled in both cases.

Figure 32 depicts the model geometry of the tube along with the distribution of the current density at f = 180 kHz. The probe center is at z = 1.235 mm (0.049 in.) along the tube axis so that one of the coils of the differential probe is positioned under the defect. The current distribution on the outer surface of the tube shows minimal distortion along the path of circumferentially induced currents, which run parallel to the defect. The preliminary results from the calculation of coil impedance for this case also attest to this fact. Once more, because of the inverse relationship between frequency and depth of penetration, the results also indicate that at this frequency the fields are more confined to the tube's inner surface and attenuate rapidly in the radial direction. As expected, analysis of the initial test case results indicate the lack of bobbin coil sensitivity to a circumferential defect that runs parallel to the direction of induced current flow. This is due to the fact that the coil's primary magnetic field is maximally perturbed when the defect path runs perpendicular to the direction of induced EC flow.

Figure 33 shows the current distribution for the case of the pancake coil geometry shown in Fig. 31b. Here, the induced currents flow in a circular path that is parallel to the coil winding. Ideally, this coil configuration should be sensitive to defects of any orientation. Because the diameter of the P90 coil is relatively large, it is expected that use of a flat coil in a cylindrically shaped tube geometry will reduce the probe sensitivity. This is so because a small liftoff distance between the outer edge of the coil and tube's inner surface results in a relatively large gap at the center of the coil. This limitation can be

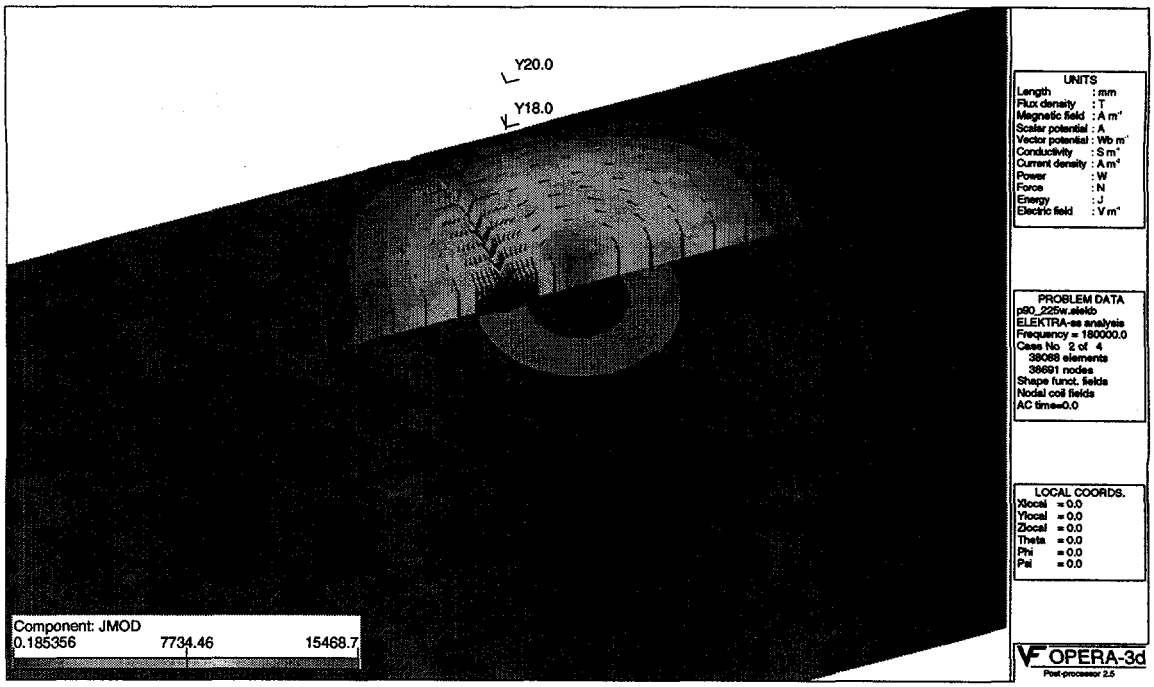


*Figure 33. Current density distribution at* f = *180 kHz for absolute pancake coil over a 40% OD circumferential defect (notch).*

alleviated in two ways, either by reducing the coil diameter or shaping the coil into a cylindrical or spherical surface parallel to the tube inner surface, leading to a uniform field distribution over the sensing area of the coil. This modification would further allow to increase the fill factor (reduction in liftoff), which should result in better coupling of the coil field and in turn greater measurement sensitivity.

# 4 Research on Degradation Modes and Integrity (D. R. Diercks, K. E. Kasza, S. Majumdar, J. Y. Park, and W. J. Shack)

The objective of this task is to evaluate and experimentally validate models to predict potential degradation modes, progression rates, leak/rupture behavior, failure pressures, and leak rates for SG tubes and for repaired tubes under normal operating, accident, and severe accident conditions.

Deterministic and probabilistic models for predicting leak rates from degraded tubes under normal operating and accident conditions in SGs have been formulated and used in previous investigations. These models have often been generated from limited data and/or data and correlations from laboratory work where the flaw morphology and tube conditions did not necessarily represent inservice conditions representative of current-day degradation modes. The work performed under this task will update and validate these models and correlations or, if required, produce new correlations for flaw types of current interest.

Previous investigations have also focused on normal operating conditions and design basis accidents. Questions have arisen about failure pressures and leak rates from degraded tubes subjected to severe accident conditions. Material flow (creep) and crack opening may be greater under the higher temperature conditions than under normal operating temperatures, and the leak rates may be higher, while failure pressure may be lower.

Initiation of environmentally assisted cracking, crack growth rates, and crack arrest and reinitiation are not well predictable or quantified for current-day cracks in operating SG tubes. Crack initiation times, crack growth rates, and changes in morphologies can be quite variable. Furthermore, the factors that influence the nature of crevices and crevice corrosion cracking are not well understood. To evaluate the continued integrity of currently unaffected and of degraded SG tubes left in service, a better and quantitative understanding of the above phenomena and of their variability is needed.

Efforts under Task 3 during the initial phase of the program have concentrated on the design and construction of experimental facilities for the production of flawed tubing, and the rupture and leak-rate testing of flawed and unflawed tubing under a wide range of conditions. The facilities under design and construction include an autoclave system for producing cracks in tubes under accelerated (chemically aggressive) conditions, a model boiler facility to produce cracks in tubes under more nearly prototypic conditions, a blowdown facility for conducting tube rupture and leak-rate tests under simulated SG operating conditions, a high-temperature severe accident tube rupture facility, and a high-pressure tube-rupture and leak-rate test facility. The capabilities of the latter three test facilities are summarized in Table 2. In addition, effort has been devoted to the analysis and modeling of flaw stability for various flaw geometries and loading conditions.

*Table 2. Summary of capabilities of SG tube rupture and leak rate test facilities under design and construction*

| Facility | Maximum Pressure (MPa) | Maximum Temp. (°C) | Maximum Flow Rate (L/min) | Pressurizing Medium |
|---|---|---|---|---|
| Blowdown Facility | 21 | 320 | 760 | water/ steam |
| High-Temperature (Severe Accident) Facility | ≈28 | 1000 | - | $N_2$ |
| High-Pressure Facility | 52 | R.T.[a] | 46 | water |

[a]R.T. = room temperature

## 4.1 Autoclave Tube Cracking Facility

Because cracked tubing from operating or retired SGs is difficult and expensive to obtain and the availability of such tubing is limited, it is necessary to produce prototypic cracks in tubes as a part of this program. These tubes will be used for subsequent tube-rupture and leak-rate tests and for the evaluation of NDE equipment and techniques. Under the present program, two facilities are being designed to produce cracked tubes. The first of these, the autoclave facility described here, will be used to produce cracks under accelerated aggressive conditions. The second facility, the model boiler described in Section 4.2, will be used to produce cracks under more prototypic conditions that simulate those in an SG.

### 4.1.1 Description of Autoclave Facility

Two autoclave systems for the production of cracked specimens are being constructed. The design of these systems, which is based on a previously described concept,[14] is shown in Fig. 34. Six tubular specimens, each ≈0.30 m (12 in.) long, in a hexagonal array, will be simultaneously exposed at pressurized water reactor (PWR) SG operating temperatures (or slightly higher to accelerate cracking) to aggressive secondary-water chemistries at the outer surface under slowly refreshed (≈1 $cm^3$/min) flow conditions. The specimens will be plugged at the bottom and pressurized from the top by an independent refreshed primary-water system to provide internal pressure loading. Individual valving of the six specimens will permit continuation of a given run after one or more of the specimens has developed a leaking crack. Present plans call for the use of high-purity water on the primary side, but it may be possible to modify the chemistry of this water to induce PWSCC failures on the inner surface.

The key component in these systems is an 8-L Hastelloy C-276 autoclave that is used to contain the specimens and the aggressive solutions that are used to induce cracking. Present plans call for the use of secondary-water solutions that contain as much as ≈60% NaOH plus CuO, Cu, and other additions that are known to induce stress corrosion cracking in Alloy 600. Hastelloy C-276 was selected as the construction material for the autoclave because of its high resistance to SCC. Other components in the facility that

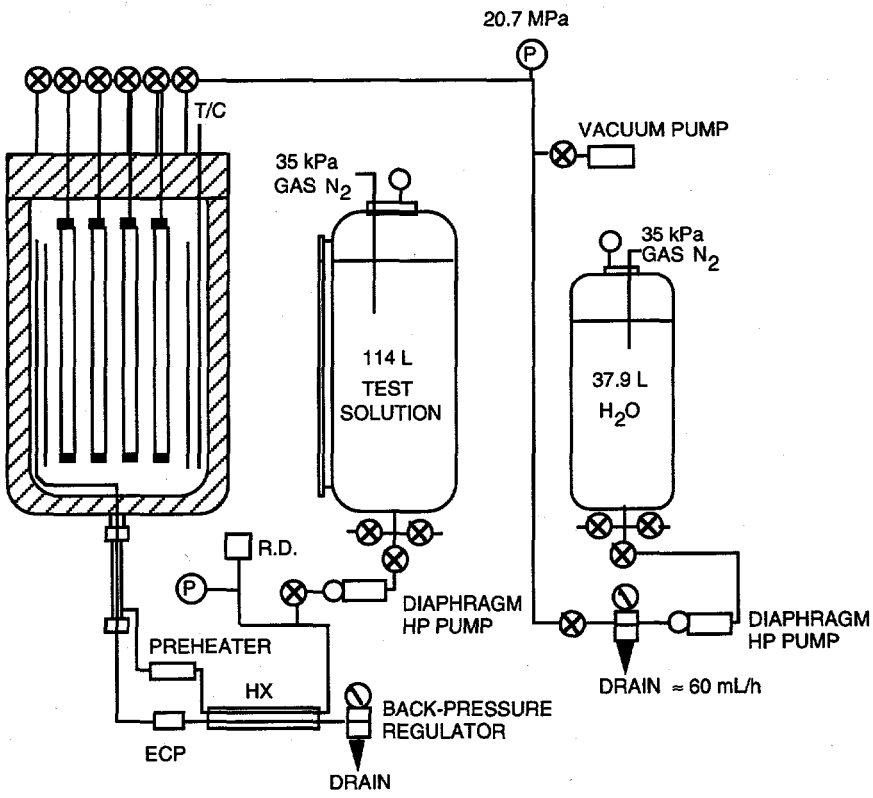


*Figure 34. Schematic diagram of autoclave test specimen cracking facility.*

operate in contact with the aggressive secondary water chemistry will be fabricated of Hastelloy C-276 or stainless steel (SS), depending on temperature.

During operation, deionized deaerated primary water stored in a 38-L (10-gal.) tank under nitrogen cover gas will be used to pressurize the closed-end tube specimens with a high-pressure [≈21 MPa (3000 psi)] diaphragm pump. The water will be refreshed at a rate of ≈1 cc/min. On the secondary side of the specimens, the aggressive secondary solution will be slowly pumped through the autoclave at 8.3 MPa (1200 psi) by a similar pump after preheating to ≈300°C (570°F). The pressure differential across the specimen wall has been selected to correspond to ≈60% of its yield strength. Shrinkable Teflon™ tubing will be used to mask those portions of the specimens where SCC is not desired. A throughwall crack in a given tube is indicated by depressurization of the primary side, and the leaking tube can be valved off to permit continuation of the run to crack the remaining tubes.

The autoclave is rated for a maximum pressure of 13.1 MPa (1900 psi) at 350°C (662°F) and will be ASME Code stamped. The pressure in the autoclave will be controlled with a back-pressure regulator, and a rupture disk will be installed for additional protection. All of the components of the autoclave system have been ordered and delivered. Assembly of the first system is essentially complete, and initial checkout tests are about to begin.

## 4.2 Model Boiler Tube Cracking Facility

A single-tube model boiler facility is being designed that will be used to produce outer-surface stress corrosion cracks in tubes under near-prototypical secondary-side water conditions. Both crevice and secondary-side freespan cracks will be produced for subsequent tube-rupture and leak-rate testing and NDE. The apparatus is a simplified version of more conventional multitube boiler concepts that have been used in the past.

Model boilers that have previously been used to study corrosion-induced SG tube degradation have typically utilized a clustered array of seven tubes mounted in a massive block of metal to simulate a tubesheet, with appropriate prototypical crevices between the tube and the tubesheet. Prototypical heat fluxes immediately above the tubesheet are in the range of 160,000-320,000 $W/m^2$ (50,000-100,000 $Btu/hr\text{-}ft^2$), temperatures are on the order of 300°C (570°F), and the primary- and secondary-side pressures are typically ≈2250 and ≈7 MPa (1000 psi), respectively. These operating conditions, together with the need for pumped primary and secondary flow loops in the classical model boiler design, necessitate large, complex facilities that are very costly to build and operate. In addition, these model boilers are not very flexible for use in exploring important parameter effects. In view of these limitations, at ANL we decided to use a simplified single-tube convective-flow design that eliminates the need for forced-flow primary and secondary loops and provides reduced construction and operating cost and increased flexibility for simulating a wide range of relevant operating conditions.

Some important features of the ANL boiler are: a primary-side reflux boiler to create heat transfer across the tube wall, a secondary-side natural convective flow loop with condenser to maintain constant boiling conditions on the outside of the tube, a tubesheet/crevice simulator that employs electrical pin heaters to simulate surrounding tubes, and computer control and data acquisition that permits unattended operation.

### 4.2.1 Equipment Features

A schematic diagram of the ANL model boiler concept is shown in Fig. 35. The primary objective of this apparatus is to produce prototypical boiling conditions on the secondary side of the SG tube in the crevice region between the tube and the tubesheet. Both tube and tubesheet are made of prototypical materials, and prototypical temperature, pressures, and heat fluxes are present in the crevice region. The secondary-side water chemistry can be adjusted to correspond to typical PWR conditions or to more aggressive conditions to accelerate tube degradation and permit the study of water chemistry parameter effects. The facility is not designed for the study of PWSCC.

Primary-side heating is provided by a reflux boiler heated by a 5 kW heater. This boiler generates steam, which flows up the inside of the tube and condenses on its inner surface, thereby transferring heat to the tube wall. Typical conditions on the primary side of the tube are anticipated to be saturated steam at 338°C (640°F) and a corresponding pressure of 14.2 MPa (2060 psi). However, temperatures up to 360°C (680°F) and corresponding saturated-steam pressures up to 18.7 MPa (2710 psi) are possible by varying the heat input to the reflux boiler. As stated previously, the system is not designed

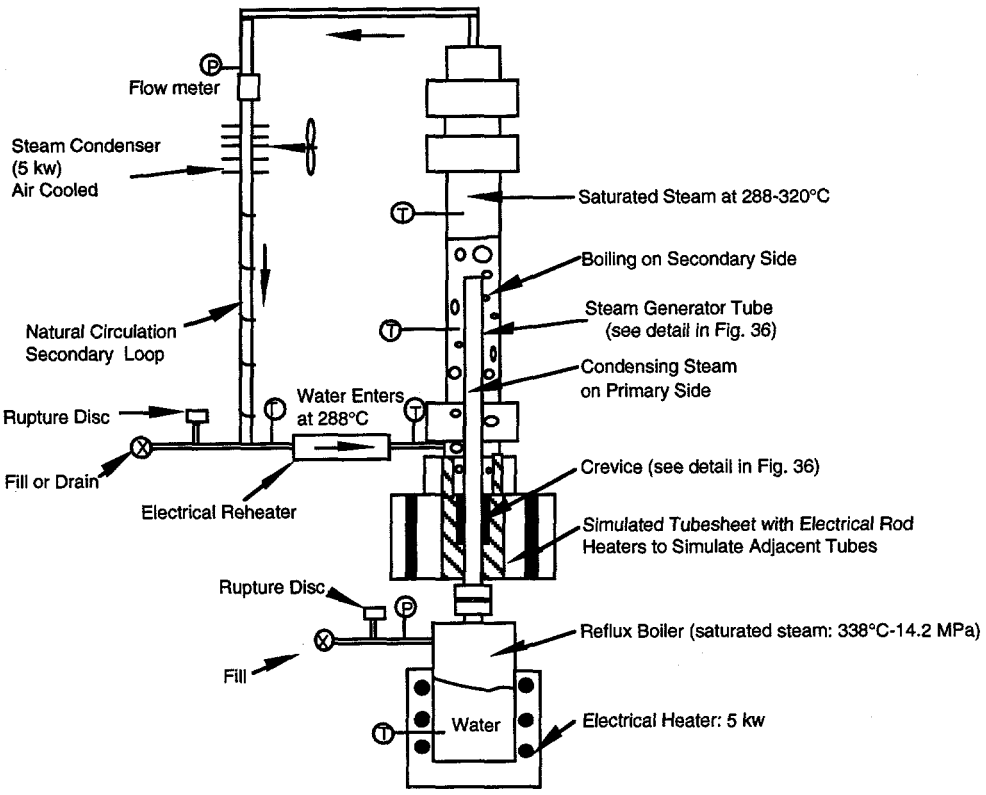


*Figure 35. Schematic diagram of model boiler test facility. for primary-side corrosion studies. The heat transfer through the tube wall and into the secondary side of the boiler will cause boiling at the nominal prototype secondary-side temperature of 285-320°C (545-608°F) and the associated saturation pressure. As described below, the tube and simulated tubesheet are designed with simulated crevices to produce localized boiling and concentration effects similar to those present in an actual SG.*

The secondary side of the apparatus forms a natural circulation loop, driven by the heat input at the SG tube and the heat removal by a steam condenser outside the boiler (see Fig. 35). Downstream of the condenser, an electrical reheater raises the water temperature to 288°C (550°F) just before it reenters the secondary side of the boiler. The temperatures and pressures on both the primary and secondary sides of the model boiler can be varied by controlling the electrical heater of the primary-side reflux boiler, the electrical reheater on the secondary side, and the amount of heat removed at the steam condenser. A primary-to-secondary-side heat transfer model has been developed for the apparatus tube region. As shown in Fig. 35, this model simulates the coupled falling-film condensation heat transfer that occurs within the tube from the reflux-boiler-generated steam, the heat conduction through the tube wall, and the boiling that occurs on the outside of the tube as a function of the primary and secondary thermalhydraulic conditions. It has been demonstrated that, by controlling the primary reflux boiler and the secondary condenser, a wide range of crevice region heat transfer conditions can be achieved, including prototypical tube wall temperatures. Work continues on refining the facility performance prediction model. The secondary side convection loop model is being coupled with the tube region heat transfer model to allow modeling of the entire facility.

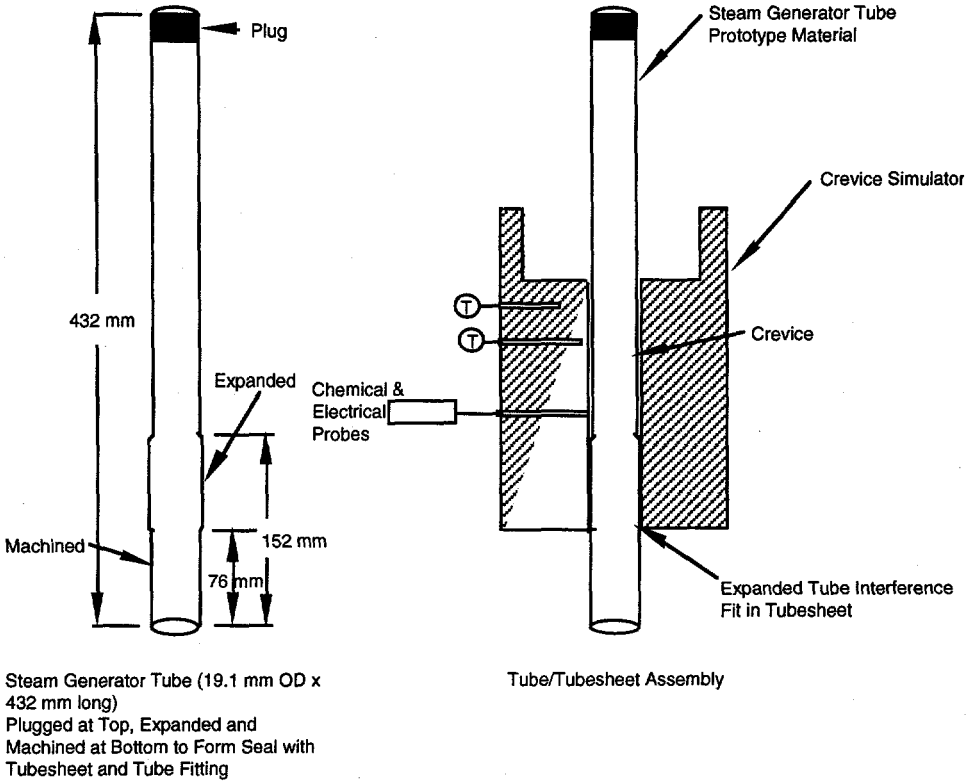


*Figure 36. Details of the tube/tube support plate region of the model boiler.*

This model will be used to establish the final design features of the model boiler and will also provide guidance for developing a test plan, operating the facility, and interpreting corrosion data.

The tube boiler housing and reflux boiler will be constructed of welded Schedule 160 Type 316 SS pipe components. The SG tube will be held in place with a Swagelock fitting, thereby permitting its easy removal and transfer to other testing facilities. The secondary-side natural circulation loop will use thick-wall 19.1-mm (0.750-in.) diam tubing to minimize flow losses and maximize natural circulation flow. Other components, such as the simulated tubesheet and the reflux boiler, are also joined with Swagelock fittings to facilitate assembly and disassembly, thereby enhancing the ease of alteration for parameter studies.

Details of the SG tube/tubesheet geometry and interface are shown in Fig. 36. Tubes 0.43 m (17 in.) long and either 19.1 or 22.2 mm (0.750 or 0.875 in.) in diam can be tested in this apparatus. The tubes will be plugged on the top end and expanded over the lower 0.15 m (6 in.), with subsequent turning of the OD on the bottom 3 in. to achieve a fit with a standard Swagelock fitting. The expanded portion of the tube will be interference fit into the lower portion of the tubesheet by cooling the tube and heating the tubesheet. The tubesheet will be made of prototypical carbon steel material, and the upper portion will be bored out over a portion of its length to a diameter that is appropriate to achieve the desired crevice geometry when the tube is mounted. The length of the tube that extends above the top of the tubesheet is nominally 0.18 m (7 in.). Although not shown in Fig. 36,

tube/tube support plate crevice corrosion can also be studied by using a ringmounted around the tube above the tubesheet to simulate the tube support plate. The annular gap between the tube and the ring can be adjusted to achieve prototypical conditions.

Surrounding the tubesheet is a cylindrical metal ring (of the same material as the tubesheet), in which electrical rod heaters are embedded to simulate adjacent tubes in an actual SG. This guard heater ring is designed to improve control over thermal conditions in the tubesheet crevice, thereby enhancing the prototypicality of the system and permitting improved studies of crevice conditions.

The tube/tubesheet crevice conditions are monitored through penetrations in the tubesheet simulator block. Embedded thermocouples will be used to monitor the temperature distribution in the tubesheet and crevice. Other penetrations may be used to obtain information on crevice water chemistry. It may also be possible to develop a fiber optics viewing system for the crevice region to view actual boiling characteristics during chemical concentration and the early stages of deposit buildup. The boiling information could be recorded with an existing 12,000 picture per second video to provide unique information on the thermalhydraulic mechanisms that influence crevice corrosion.

### 4.2.2 Facility Status

A first-cut design of the reflux boiler and the secondary side vessel has been completed, and component specification and source vendor lists have been developed for the facility hardware. Requests for bids on the major components have been issued to potential manufacturers, and discussions with responding bidders are underway. Work continues on refining the apparatus performance prediction model.

## 4.3 Tube-Rupture and Leak-Rate Blowdown Test Facility

The ANL tube-rupture and leak-rate blowdown test facility will be used to obtain data on burst pressures, failure modes, and leak rates of flawed tubing at temperatures up to 343°C (650°F), pressures of 21 MPa (3000 psi), and pressurized-water flow rates up to 760 L/min (200 gal/min). In designing this facility, available information on the design and performance of previous facilities was reviewed. The ANL facility incorporates several features that are necessary to obtain more prototypical data under stable, controlled conditions. In overview, the important features of the facility are a large blowdown vessel water inventory to ensure high, stable flow rate capability and permit continued testing of initially stable leaking cracks; piping and valves of a size appropriate to minimize pressure drop in the supply line to a flawed tube and thereby permit high flow rates; the use of a downstream back-pressure regulator valve to control tube secondary-side pressure, thereby minimizing nonprototypical two-phase flow from entering the tube; and a computer feedback valve control to allow programmed ramps of the pressure differential across the tube.

A schematic diagram of the facility is shown in Fig. 37. The pressurized and heated blowdown vessel is of a size that will hold ≈760 L (200 gal) of water and thereby provide adequate water inventory for ramping the pressure differential P1-P2 and testing tube specimens that contain preexisting throughwall flaws. The tube specimen is housed in the

test module containment vessel. The pressure differential rampup is produced through a back-pressure regulator valve (V6) located downstream from the test module containment vessel. The blowdown vessel is maintained at a constant pressure P3 up to 3000 psi during a test by use of regulated nitrogen cover gas pressurization from a 41-MPa (6000-psi) tank farm. The differential pressure P1-P2 across the specimen wall is ramped up in a series of quasi-steady plateau increases through feedback control of Valve V6, which controls pressure P2. The option also exists for linear ramping of P1-P2 at differing rates to simulate more prototypical tube loadings. During the rampup of P1-P2, information on flow rate Q, the pressure differential P1-P2, and possibly the jet leak behavior at the flaw (as viewed through the ultra-high-speed 12,000 frames per second video) will be recorded as a function of time.

The rampup of the differential pressure P1-P2 will be terminated when the tube crack becomes unstable (i.e., the tube ruptures, causing a dramatic increase in Q) or the water level in the blowdown vessel becomes too low. For large throughwall flaws, the rupture pressure will be considerably <21 MPa (3000 psi) and high flow rates will be required. Under these conditions, short-duration differential pressure plateaus (P1-P2) of 10 s or less will be used, and crack flow rates on the order of 760 L/min (200 gal/min) are achievable and measurable, with the water inventory stored in the blowdown vessel. For short throughwall cracks with considerably lower flow rates but higher rupture pressures, the time available for ramping will be considerably longer.

Flawed tubing for testing in this facility can come from three ANL sources: (1) the severe chemistry autoclave cracking facilities, (2) the model boiler test facility, and (3) EDM. Flexibility in moving tubes between the various facilities is achieved by mounting the tubes with identical Swagelock fittings. The tubes tested in the present facility can range from several inches in length to ≈1 m (40 in.), which is the length of the test module vessel. The test module will also allow study of the influence of tube support characteristics on rupture pressure through the use of support stings fitted on the inside of the module to simulate support plate constraints on flawed tubes.

### 4.3.1 Equipment Features

The blowdown vessel (Fig. 38) is 0.61 m (2 ft.) in diam and 3.7 m (12 ft.) long and the test module vessel (Fig. 39) is 0.20 m (8 in.) in diam and 1 m (40 in.) long. Both vessels are constructed of welded Type 316 SS and will be ASME Section VIII, Div. 1 Code stamped for 21 MPa (3000 psi) at 343°C (650°F). Each tank has over-pressurization protection vented to an outside muffler. The 3030-L (800-gal) water storage and conditioning tank will be exposed to only low-pressure service near room temperature and is made of Type 304 SS.

The piping that connects the blowdown vessel to the test module is 50.8-mm (2-in.) Schedule 160, flanged Type 316 SS, to minimize pressure drop under 760-L/min (200-gal/min) flow conditions. Valves V3, V4, and V6 in the main flow path that connects the blowdown and test module vessels are also of a size adequate to pass the 760-L/min (200-gal/min) flow with acceptable pressure drop. Piping downstream of the test module is

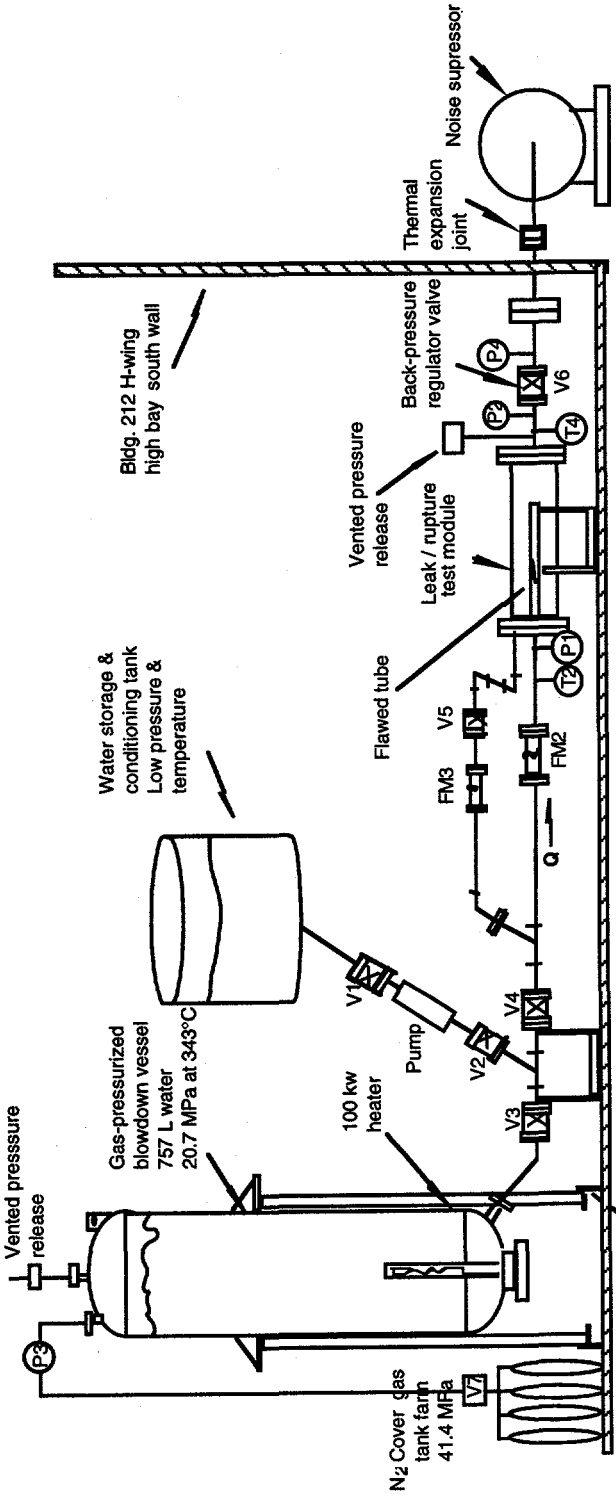


*Figure 37. Schematic diagram of tube-rupture and leak-rate blowdown facility.*

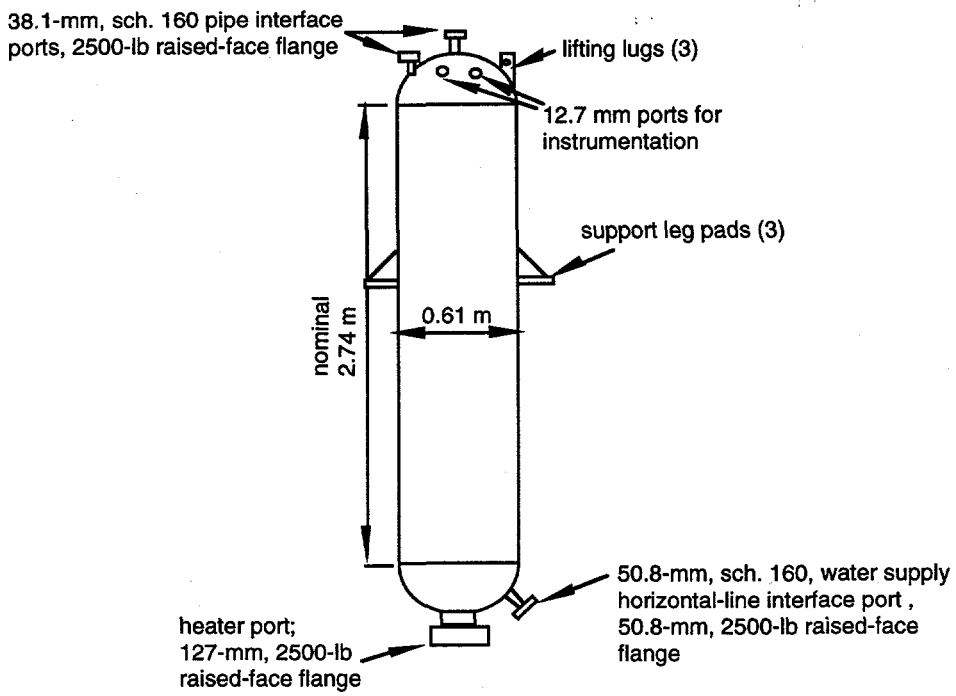


*Figure 38. Blowdown vessel for tube-rupture and leak-rate blowdown facility.*

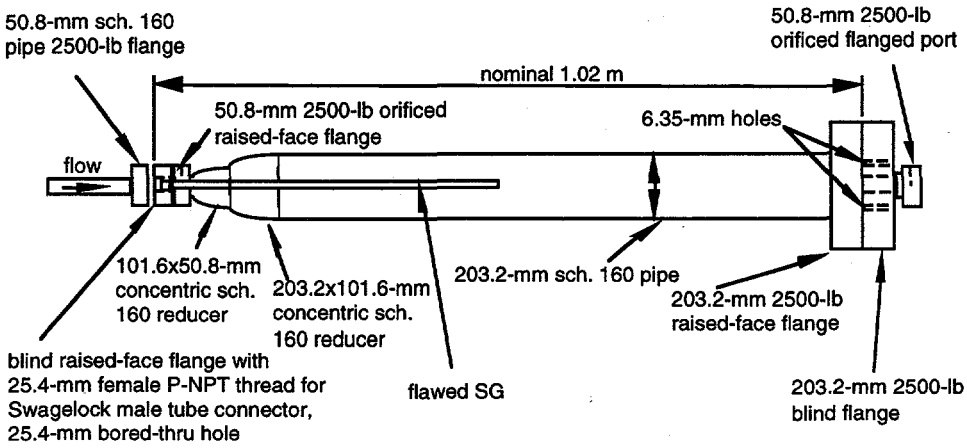


*Figure 39. Specimen test module for tube-rupture and leak-rate blowdown facility.*

likewise of a size large enough to minimize back pressure on the test module so that Valve V6 exerts the dominant controlling back pressure. Downstream of Valve V6, the piping size is increased to 0.25 m (10 in.) to improve valve control and for interfacing with the inlet of the noise suppresser.

The back-pressure regulator Valve V6, located downstream of the flawed-tube test module, is used to control and vary the pressure differential across a flawed tube that is being tested. At the start of a test, the pressure differential P1-P2 across the tube wall is zero; it is then ramped up with time in a stepwise fashion under control of Valve V6 to a

maximum of 21 MPa (3000 psi), which is the constant cover gas pressure maintained on the water in the blowdown vessel. Specimens with throughwall flaws may leak at the earliest stages of the pressure rampup, and a nearly closed Valve V6 will cause P2 to nearly equal P1. However, for cases where the flawed tube does not begin to leak until P1-P2 reaches much larger values, water from the pressurized blowdown tank is routed into the test module through a small line under control of Valve V5 at 4-8 L/min (1-2 gal/min) for preheating of the test assembly. Valve V6 operates at this flow to regulate P2 or the differential pressure P1-P2. When the flawed tube begins to leak in response to increasing P1-P2, Valve V6 maintains the desired control of pressure P2. When the tube leak becomes several times larger than the bleed flow from the blowdown vessel, the bleed flow can be turned off with Valve V5. The facility also allows us the option to use gas pressurization of the test module in place of the blowdown vessel bleed to achieve pressurization prior to tube leak. However, this option does not result in conditioning of components.

The back-pressure regulator Valve V6 will operate under changing fluid conditions during a test and has been selected for controllability under these varying conditions. During the initial stages of the rampup of P1-P2, Pressure P2 in the test module will be above the saturation pressure that corresponds to the water temperature supplied by the blowdown vessel, and the flawed tube will leak pressurized water into the test module. However, when Valve V6 reduces P2 below the saturation pressure, the water leaking from the crack will flash to steam, and Valve V6 will be controlling a steam flow. The facility is designed to accommodate tube leak rates as high as 760 L/min (200 gal/min) of water, which corresponds to 12.6 kg/s (100,000 lb/h) of steam. The size of Valve V6 is adequate to pass this steam flow without choking. During typical testing of a flawed tube, the progressive increase of P1-P2 will cause the crack to gradually open and result in higher flow rates. Some tubes will also reach a point of unstable crack behavior; the tube will rupture and cause a rapid increase in flow rate. The facility is designed to yield information on Q and P1-P2 for all of these leak regimes, provided Q $\leq$12.62 L/h (200 gal/min), P1-P2 $\leq$21 MPa (3000 psi), and the blowdown vessel has not been emptied.

A turbine flow meter FM2 is located just upstream of the test module to monitor the leak rate Q of the flawed tube as a function of P1-P2. However, we feel that two methods of flow measurement must be available in this harsh operating environment to have a backup and cross check on this vital piece of information. Hence, the facility will incorporate provisions for continuous weighing of the water content of the blowdown vessel as a function of time during the ramping of P1-P2 by including load cells in each of the three support legs of the vessel. The data will provide a second flow rate measurement and a check on turbine flow meter calibration. The accuracy of the flow rate determined from the weight-change measurements is potentially greater than that from the turbine flow meter.

All pressure, temperature, flow rate, heater electrical power supplies (for the blowdown vessel and trace heaters on various components), and control valve actuation signals will provide analog readouts at a master control panel that is shielded from the pressurized components of the facility (see Fig. 40). The shielding consists of stacked concrete slabs on three sides of the blowdown and test chamber vessels and associated piping. When the test system is at temperature and pressure, personnel will not be

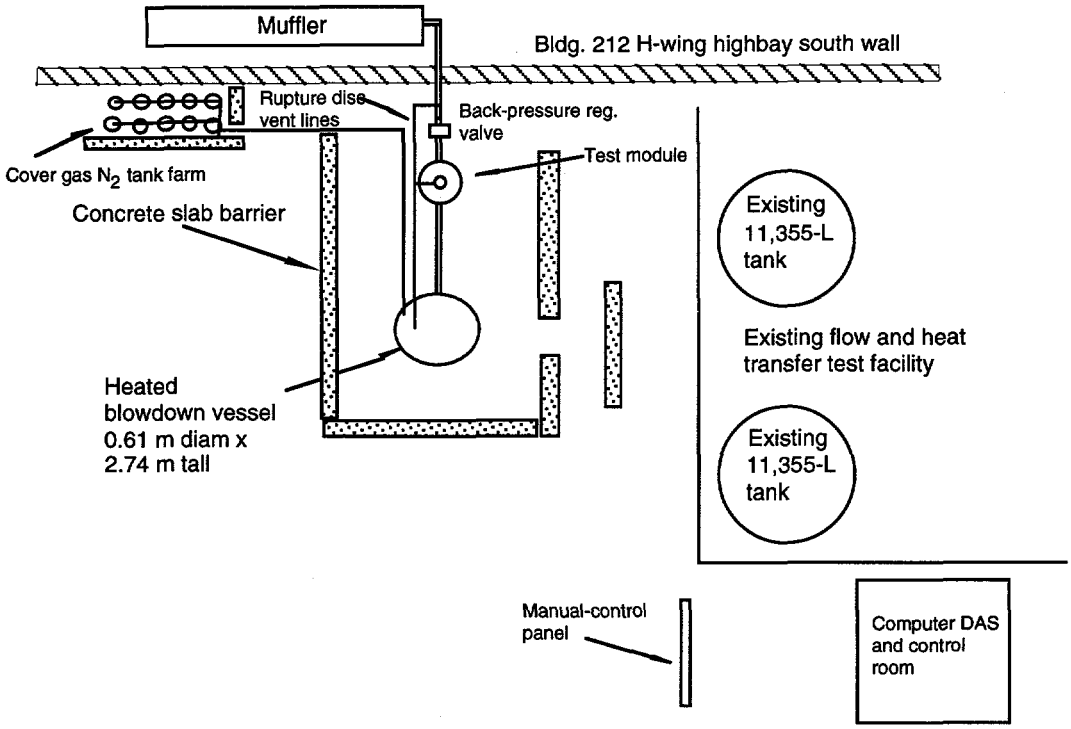


*Figure 40. Tube-rupture and leak-rate blowdown test facility floor layout.*

permitted inside this barrier. All measurement and control signals will be logged into a computerized data acquisition and control system located in an existing air-conditioned control room.

Another important component of the blowdown facility is the muffled noise suppresser located outside of the south wall of the laboratory space (Fig. 40). It is designed to handle the maximum anticipated 12.6 kg/s (100,000 lb/h) steam flow from the test module; as well as possible tank overpressurization steam releases. The unit is 0.91 m (3 ft) in diam and 5.2 m (17 ft) long and is capable of 45-dB noise reduction. To accommodate the outside location of the muffler, a wall penetration for a 0.25-m (10-in.) diam steam hookup pipe and a concrete base mat will be provided. Because the back-pressure regulator Valve V6 and the leaking flawed tube in the test module are also noise sources for a range of the test conditions, they possibly will also require noise suppression. The valve manufacturer has estimated that Valve V6, under certain conditions, could generate noise at the 110-dB level.

Because of the batch testing mode associated with recharging the blowdown vessel and the elevated temperatures, thermal shock of the facility components is a design consideration. Thermal shock will be minimized by carefully controlling the heatup rate for the blowdown vessel and by using electrical heat tape wrap and insulation on all piping and components downstream of the blowdown vessel. The slow bleed of heated water from the blowdown vessel prior to the start of the rampup of pressure differential across the flawed tube will also facilitate thermal conditioning of downstream components.

Thermal expansion of components along the main flow path is accommodated by rigidly anchoring the piping at Valves V3 and V4 and allowing the components to move unconstrained in the axial direction by use of a thermal expansion joint. This joint is located at the other end of the flow path, in front of the noise suppressor, in the low-pressure zone.

### 4.3.2 General Facility Operation

The general philosophy of facility operation will be to utilize manual control when bringing the facility to initial steady-state conditions for the beginning of a test, and computer control for actual testing. During the setup period, readings of all instrumentation and the status of controlled hardware will be displayed on a control panel located outside of the blast barrier. All hardware will be controllable from the control panel. During the setup period, the computer will also log all instrumentation data and record controlled hardware configurations. This will include display of real-time plots of critical safety data and important thermalhydraulic conditions for tracking the approach to steady state. The facility computer is a Power Macintosh 8500 that utilizes National Instruments Labview Software and data acquisition and control boards.

System setup under manual control includes configuring the facility for a particular test, attaining steady-state conditions associated with time zero of that test, and verifying that the computer software is properly configured for the transient portion of the test. Once these conditions are attained, as verified by the facility operator, the test will be switched to computer control, and the transient portion of the test will be automatically initiated under computer control after a short stabilization period to eliminate any switching transients. Once under computer control, a test can terminate in several ways. The first of these is normal termination, in which the flawed tube progresses through stages of increasing leakage and finally to crack instability and tube rupture, with a corresponding rapid increase in leak rate. However, a test may require termination before specimen rupture because the blowdown vessel is low on water, the back-pressure regulator valve fails to stabilize as it is changed under computer control, or the desired ramping of the pressure differential across the cracked tube cannot be achieved for any reason. Finally, the operator can manually terminate the test at any time because of safety concerns or any other reason.

The following describes, in detail, a facility operation scenario.

Setup stage (manual control)

1. Approximately 760 L (200 gal) of room-temperature, conditioned, deionized water are pumped from the 3030-L (800-gal) storage tank to the blowdown vessel to charge it while Valves V1, V2, and V3 are open. Valves V4 and V5 are closed.

2. Valves V1, V2, and V3 are closed.

3. Heat-wrap tapes on all downstream piping and components are turned on to bring the structures to the desired operating temperature.

4. The pressure of the blowdown vessel cover gas is set to a value slightly above the saturation pressure associated with the desired tank water temperature to prevent boiling during heatup (a pressure P3 of 11.4 MPa [1650 psi] would be adequate if the desired water temperature is 315°C [598°F]).

5. The blowdown vessel electrical heater is turned on and the water is brought to temperature at a rate sufficiently low to minimize thermal stressing of the vessel.

6. When the blowdown vessel has stabilized at the desired operating temperature, the heater is turned off and the pressure of the cover gas is raised to the desired operating value, not to exceed 21 MPa (3000 psi).

7. The back-pressure regulator Valve V6 is fully closed.

8. Valve V5 in the blowdown tank bleed line is opened slightly.

9. Valve V3 is opened full and then V4 is slowly opened full.

10. The flow through the bleed line is set at 4-8 L/min (1-2 gal/min) as it is monitored by flow meter FM3. This may require a slight opening of Valve V6 to facilitate conditioning of downstream components and to provide flow on which Valve V6 can operate. With this valve configuration, the differential pressure P1-P2 should be near zero.

11. The system is held in this configuration for several minutes to achieve equilibration.

12. The computer data acquisition system (DAS) is readied to acquire flow rate Q, P1-P2, and other measured quantities vs. time.

Transient stage (computer control)

13. The back-pressure regulator Valve V6 is put under either computer control or under control of the vendor-supplied valve control module after ensuring that the initial state of the valve is set in accordance with Step 7 or 10.

14. Valve V6 is activated for transient control and P1-P2 is ramped up stepwise to increase the pressure differential across the flawed tube and possibly cause the flaw to progressively open and rupture.

15. The test is terminated when a tube ruptures or the water level in the blowdown tank becomes too low.

16. All water control valves are shut, the trace heaters are turned off, and the blowdown-vessel cover gas pressure is reduced to just above the saturation pressure of the remaining water to allow for slow cooldown of the vessel.

### 4.3.3 Program Status

The design of the blowdown facility has been completed and all major components have been identified. Formal requests for bids have been issued to manufacturers for the major high-cost components, purchase orders have been issued for most of the remaining items, and some components have been delivered. Modifications to the laboratory area are underway, i.e., the required electrical service, blowdown vessel floor load dispersion plates, and the concrete pads and wall penetrations for the outside muffler are being installed. An existing computer control room is also being upgraded.

## 4.4 High-Temperature (Severe Accident) Test Facility

The tube-rupture and leak-rate blowdown test facility described in detail above will be used to determine the rupture behavior and leak rates of flawed tubes under more or less prototypic SG operating conditions [$T \leq 343°C$ (650°F), $p \leq 21$ MPa (3000 psi)]. However, the rupture pressures of flawed and unflawed tubes at very high temperatures under severe accident conditions are also of interest.

Several hypothetical core-melt-accident scenarios could lead to high-temperature coolant boiloff and the potential for tube rupture at very high temperatures. Of these, the station blackout scenario with failed auxiliary feedwater and loss of secondary side integrity, presents one of the most severe challenges to the SG tubes. Under this scenario, the tubes would be exposed to superheated steam from the core in combination with high pressure gradients across the tube wall, and multiple tube failure, particularly of tubes that contain preexisting flaws, must be considered. A high-temperature facility to determine the burst pressures of unflawed and flawed tubes at very high temperatures has, therefore, been constructed as part of the present program.

### 4.4.1 Facility Description

A schematic drawing of the high-temperature severe accident test facility is shown in Fig. 41. In simplest terms, it consists of a length of SG tube placed in a furnace, closed off at one end, and connected to a high-pressure nitrogen gas bottle through suitable valving at the other end. During a test, the specimen is stabilized at a nominal SG operating temperature of 300°C (572°F) and a fixed internal pressure, and the temperature is then ramped up at a predetermined rate until specimen failure occurs.

Constant pressure is maintained during the test by a back-pressure regulator, and the pressure is monitored by a pressure transducer. A constant-leak valve is installed after the back-pressure regulator as an alternate means of gas pressure control in combination with the pressure regulator on the gas cylinder. A high-flow cut-off valve is also installed in the gas line to automatically cut off the flow of nitrogen under high-flow tube-failure conditions. This prevents emptying of the gas bottle upon specimen failure in unattended long-term tests. Temperature control of the furnace and specimen is accomplished with a programmable temperature controller, and both the pressure and temperature outputs are recorded.

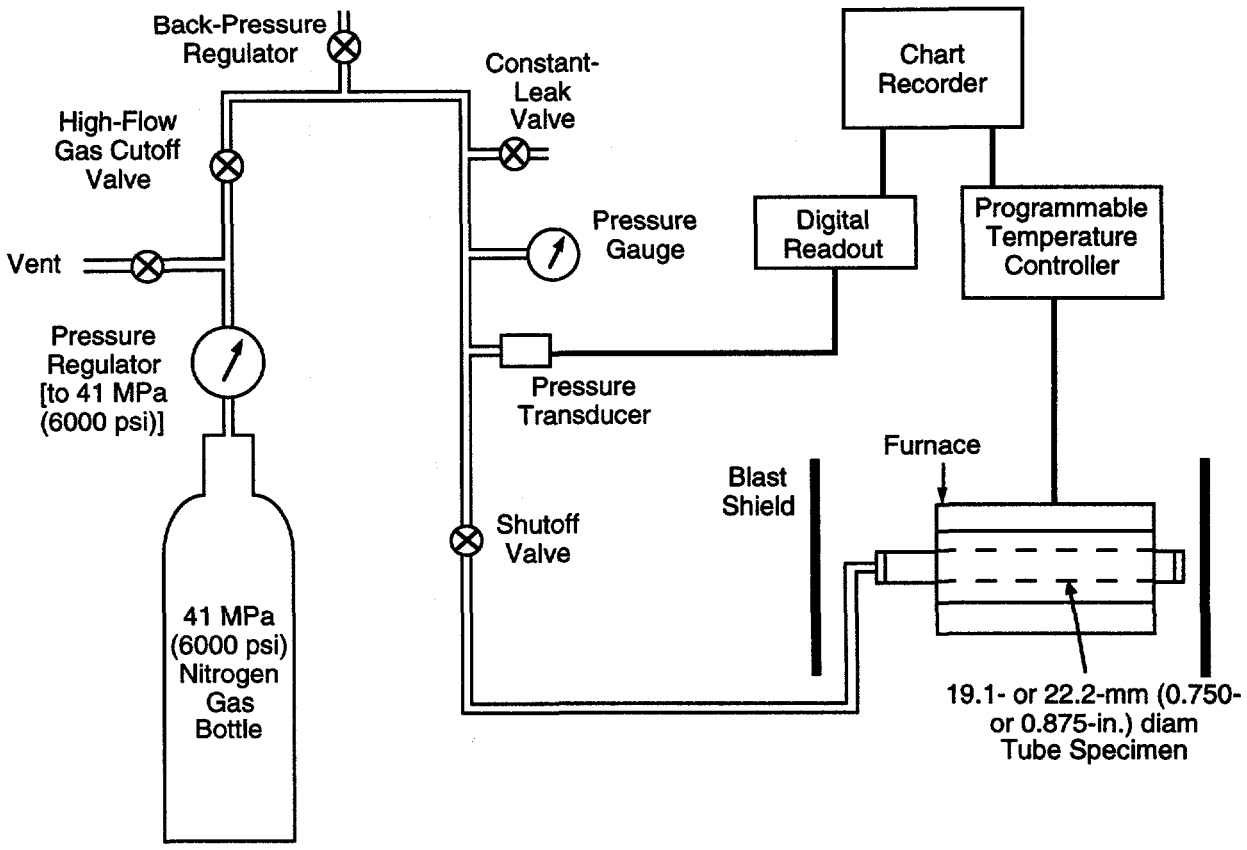


*Figure 41. Schematic diagram of high-temperature (severe accident) tube-rupture facility.*

The test specimen is ≈0.45 m (18 in.) long and the furnace is ≈0.33 m (13 in.) long with a uniform temperature zone ≈80 mm (3 in.) long near the center. Welded end plugs close each end of the specimen, and these end plugs are located outside the furnace during testing to avoid failure at the welds. A tapped hole in one end plug permits connection to the gas pressurization system, and a solid mandrel inside the specimen displaces most of the pressurized gas volume to reduce the stored energy. The specimen furnace is fitted with heavy metal plate blast shields at each end to contain any projectiles produced during a tube failure, and the furnace is also fitted with a heavy-wall SS tube to prevent projectile damage to the furnace elements.

### 4.4.2 Planned Test Program

A detailed analysis of the behavior of the Surry nuclear power plant has been carried out by INEL for several hypothetical core melt scenarios. One of the scenarios analyzed is a total station blackout with a stuck-open SG secondary-side atmospheric dump valve, which results in loss of feedwater and secondary-side depressurization.[11] In this analysis, the temperature histories were calculated with the SCDAP/RELAP5 code for several critical components, including the pressurizer surge line nozzle and the SG tubes at the inlet location. Plots of the calculated temperatures for the tubes are shown in Fig. 42, with tube inlet temperature histories shown for the case of complete coolant mixing and for no mixing. Data are needed to characterize tube rupture behavior under these severe

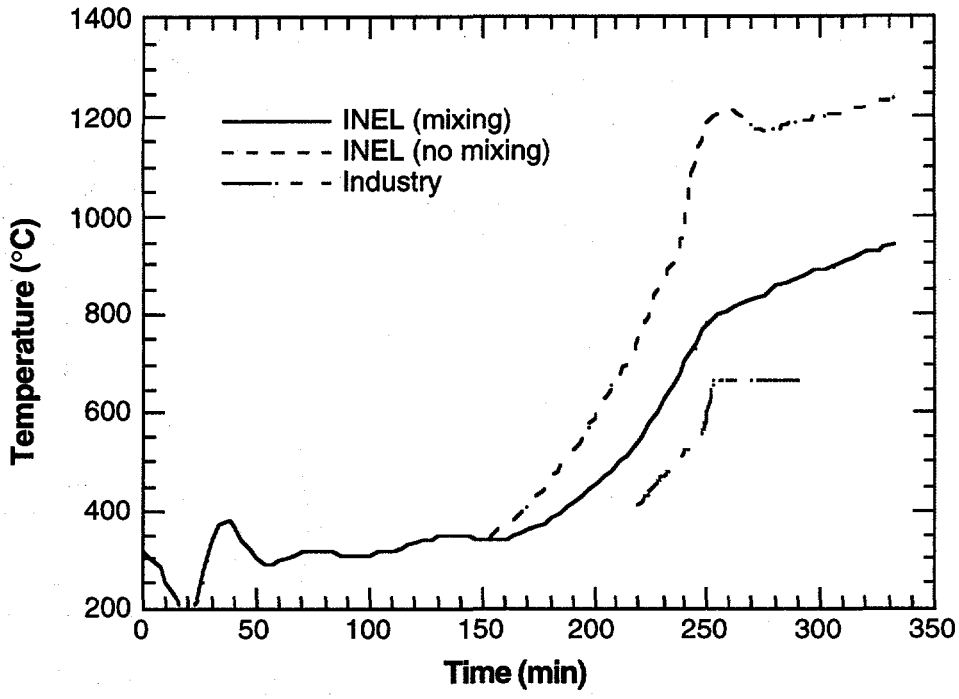


*Figure 42. Calculated steam generator tube inlet temperatures for hypothesized station blackout core melt conditions, with loss of feedwater and secondary-side depressurization.*

accident conditions and to determine if the rupture temperatures and pressures can be analytically predicted. Most analysts now feel that the complete mixing case provides the better approximation of actual tube temperatures, and the severe accident tube rupture tests being conducted at ANL use this mixing case "INEL ramp" (solid curve in Fig. 42) as one of temperature histories

Similar analyses were performed under industry sponsorship for a generalized "Zion-like" PWR with the MAAP 4.0.2 computer code.[12] Again, the analyses assumed station blackout conditions with loss of primary feedwater and secondary-side depressurization. These analyses, which calculated the temperature history for the hottest tubes (near the tubesheet on the inlet side), are also shown in Fig. 42. The peak temperature was calculated to be ≈667°C (1230°F) for an assumed primary-to-secondary leak rate of 380 L/min (100 gal/min). The predicted peak tube temperature varied somewhat with leak rate, from 662°C (1224°F) for a zero leak rate to 687°C for a leak rate of 760 L/min. (200 gal/min). The analysis predicted rupture of the SG hot-leg nozzle ≈6 minutes after the SG tubes reached peak temperature; the temperature history in the absence of nozzle failure after this point was not calculated.

Constant-pressure tube-rupture tests on unflawed and flawed SG tubes will be conducted according to the INEL "mixing" and the "industry" ramps (Fig. 42). The details of these planned tests are shown in Table 3. As indicated, triplicate tests will be run

*Table 3. Severe accident tube rupture test matrix. Three tests will be run for each set of conditions.*

| Temperature[a] | Pressure (psi) | Flawed/Unflawed a/t[b] | Flawed/Unflawed length, mm (in.) | Estimated duration |
|---|---|---|---|---|
| INEL ramp | 2350 | Unflawed | | < 3 h |
| INEL ramp | 2350 | 0.25 | 50.8 (2.00) | < 3 h |
| INEL ramp | 2350 | 0.5 | 50.8 (2.00 | < 3 h |
| INEL ramp | 2350 | 0.65 | 25.4 (1.00) | < 3 h |
| INEL ramp | 2350 | 0.8 | 6.35 (0.25) | < 3 h |
| Industry ramp | 2350 | Unflawed | | < 3 h |
| Industry ramp | 2350 | 0.25 | 50.8 (2.00) | < 3 h |
| Industry ramp | 2350 | 0.5 | 50.8 (2.00) | < 3 h |
| Industry ramp | 2350 | 0.65 | 25.4 (1.00) | < 3 h |
| Industry ramp | 2350 | 0.8 | 6.35 (0.25) | < 3 h |
| 600 | 2350 | 0.25 | 50.8 (2.00) | <4 days |
| 600 | 2350 | 0.5 | 50.8 (2.00) | <4 days |
| 600 | 2350 | 0.75 | 25.4 (1.00) | <4 days |
| 600 | 2350 | 0.9 | 6.35 (0.25) | <4 days |
| 700 | 2350 | 0.25 | 50.8 (2.00) | <5 h |
| 700 | 2350 | 0.5 | 50.8 (2.00) | <5 h |
| 700 | 2350 | 0.75 | 25.4 (1.00) | <5 h |
| 700 | 2350 | 0.9 | 6.35 (0.25) | <5 h |
| 600 | 2350 | Unflawed | | <7 days |
| 600 | 3000 | Unflawed | | <1 days |
| 700 | 1250 | Unflawed | | <5 days |
| 700 | 2350 | Unflawed | | <1 days |
| 700 | 3000 | Unflawed | | <1 days |
| 650 | 2350 | Unflawed | | <5 days |
| 750 | 1250 | Unflawed | | <1 days |
| 750 | 2350 | Unflawed | | <5 h |

[a] The INEL ramp is shown in Fig. 43 and the industry ramp in Fig. 44. The remaining temperatures are expressed in °C.

[b] a/t = flaw depth/tube wall thickness.

under all of the conditions indicated; two of these tests will be on 22.2-mm (7/8-in.)-OD tubing and the third on 19.1-mm (3/4-in.)-OD tubing. The axial flaws will be introduced at the outer surface by electro-discharge machining; flaw lengths will vary from 6.4 to 50.8 mm (0.25 to 2 in.) and depths from 25 to 90% of the wall thickness. The isothermal tests outlined in the lower half of the matrix shown in Table 3 will be conducted as needed to provide additional data that are required for the model used to analytically predict the rupture times for the temperature ramp tests.

### 4.4.3 Program Status

The design and construction of the high-temperature severe accident test facility have been completed, and temperature measurements have been conducted on an instrumented dummy specimen to determine the temperature profiles along the length and through the thickness of the specimen. Under isothermal conditions at 700°C (1400°F), the temperature along the length of the specimen was found to vary ≈6°C over a 50-mm (2-in.)-long central portion that corresponds to the maximum flaw length to be tested. During a 400°C/h (720°F/h) constant temperature ramp, the temperature gradient through the thickness was ≈8°C (14°F), with the temperature of the inner surface being lower as expected.

A preliminary checkout test was then conducted on 19.2-mm (0.750-in.)-dia. Alloy 600 tubing with a wall thickness of 1.09 mm (0.043 in.). The test specimen contained a 50.8 mm (2-in.)-long axial flaw with a width of ≈0.20 mm (0.008 in.) and a depth of one-half the wall thickness. In this test, the temperature was stabilized at 700°C (1400°F) with no internal pressure, and the pressure was then increased to 17.2 MPa (2500 psi) over a 5-min interval. The specimen failed by rupture at the machined flaw after 120 min under pressure. During the test, the pressure stability over time was ±0.02 MPa (3 psi) and temperature stability was within ±1°C (1.8°F).

The first test under a simulated INEL temperature ramp (Fig. 42, "mixing" conditions) was then conducted. In this test, an unflawed 19.1-mm (0.750-in.)-OD tube was stabilized at 300°C (572°F) and then pressurized to 16.2 MPa (2350 psi). Following this, the temperature was ramped to 800°C (1472°F) at a rate of 450°C/h (810°F/h), at which point the ramp rate was decreased to 120°C/h (216°F/h). The specimen failed by ductile rupture near the center at 823°C (1513°F). The rupture was axial and occurred over a length of ≈51 mm (2 in).

A second INEL ramp test was carried out on a 19.1-mm (0.750-in.)-OD tube. This time, the tube contained a 50.8 mm (2-in.)-long half-throughwall machined axial flaw. This specimen failed at 783°C (1441°F), again by rupture at the flaw.

Following these tests, the temperature ramp during the tests was modified to more closely simulate the calculated INEL ramp. The three-step ramp sequence shown in Fig. 43 was, therefore, developed. In this sequence, the temperature is first stabilized at 300°C (572°F). It is then ramped to 550°C (288°C) at a rate of 3.75°C/min (6.75°F/min), followed by ramping to 800°C (1472°F) at 7.50°C/min (13.5°F/min), and then to specimen failure at a rate of 1.75°C/min (3.15°F/min). As indicated in Fig. 43, this ramp provides as good simulation of the actual INEL ramp, particularly for temperatures above 400°C (750°F), at which measurable creep damage may occur.

The industry ramp tests listed in Table 3 will be conducted by following the calculated temperature history reported in reference 12. Figure 44 shows a plot of this temperature history and the simulation to be used in the ANL tests. The ANL simulation consists of stabilizing the specimen at 300°C (572°F), as for the INEL simulation, ramping to 564°C (1047°F) at a rate of 5.37°C/min (9.67°F/min), then to 582°C (1080°F) at 10.6°C/min (19/.1°F/min), to 630°C (1166°F) at 28.24°C/min (50.83°F/min), and to 667°C (1233°F) at

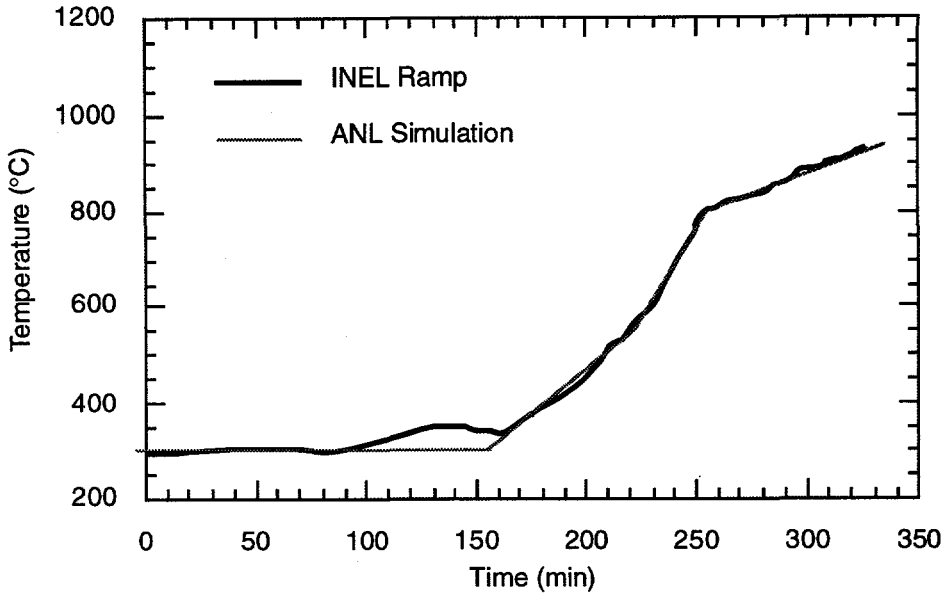


*Figure 43. Comparison of INEL-calculated severe accident temperature ramp with simulation used in ANL severe accident tube-rupture tests.*

14.80°C/min (26.64°F/min). The calculated temperature history indicates a dropoff in temperature after ≈223 min, corresponding to a predicted rupture of the SG hot leg nozzle. Because the present tests are concerned only with the behavior of the tubes, this event will be ignored and the temperature will be held at 667°C (1233°F). For some of the planned tests, failure is not expected in reasonable times at 667°C (1233°F), and we plan to ramp to failure at a rate of 2°C/min (3.6°F/min) after a 2-h hold time at 667°C (1233°F). In addition, the rapid ramp rates of 28.24°C/min (50.83°F/min) between 582 and 630°C (1080 and 1166°F) and 14.80°C/min (26.64°F/min) between 630 and 667°C (1166 and 1233°F) may be impossible because of the high power required to achieve these heating rates. As a practical matter, the actual heating rate used over these temperature intervals will probably, instead, be the maximum rate possible for the facility.

After modifying the INEL temperature ramp to be used in the tests, additional temperature profile tests were conducted on a dummy specimen following the modified INEL temperature ramp. Adjustments were made in the programming of the temperature controller to optimize the temperature response of the specimen, and minor modifications were made to thermocouple placement and specimen positioning in the furnace. As a result, the temperature of the specimen followed the desired temperature ramp very closely, and the temperature gradient over the central 51 mm (2 in.) of the specimen was reduced to ≈4°C (7°F). The temperature gradient through the specimen thickness was ≈6°C (11°F) during the 7.50°C/min (13.5°F/min) ramp rate, and less for the slower rates. The facility is now ready for completion of the testing program outlined in the upper portion of Table 3.

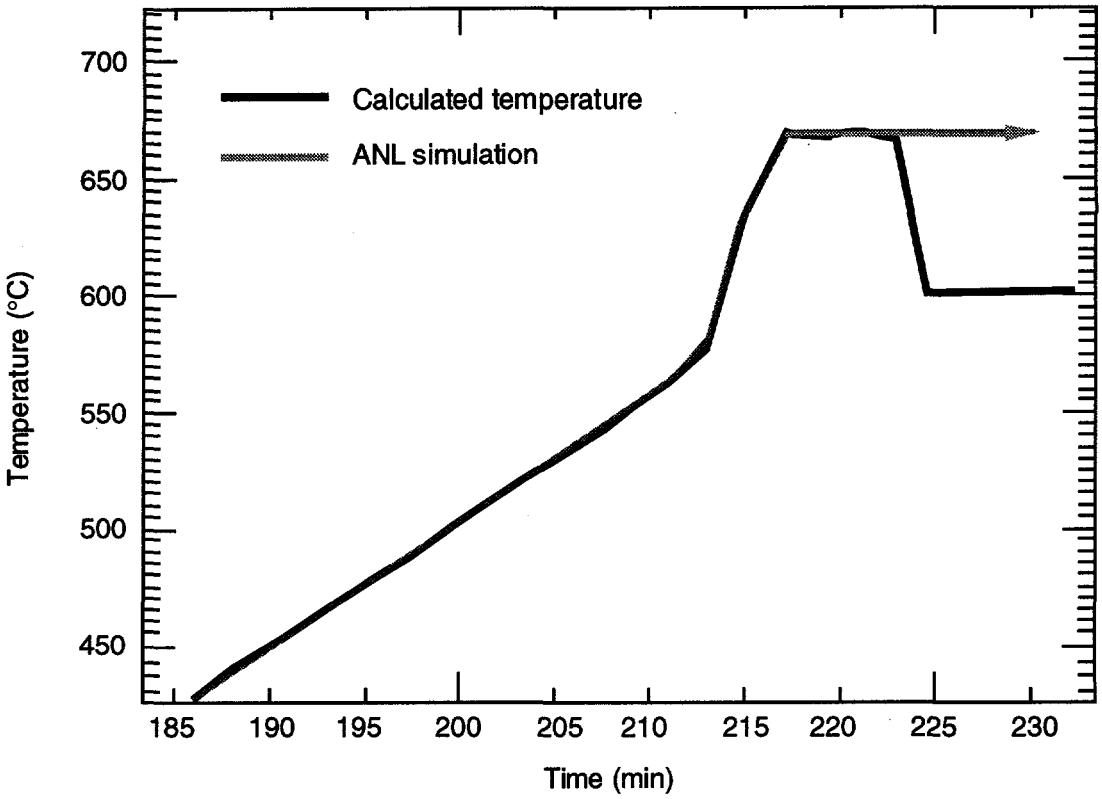


*Figure 44. Comparison of industry calculated severe accident temperature ramp with simulation used in ANL severe accident tube-rupture tests. In the ANL simulation, the temperature is held constant at 670°C after ≈217 min rather than following the subsequent drop shown in the calculated curve.*

## 4.5 High-Pressure Test Facility

Steam generator tubes are currently designed with a stress factor of 3 on normal operating condition loadings and/or a factor of 1.4 on postulated design basis accident conditions (e.g., main steamline break). As a part of the present experimental program on tube integrity, it is of interest to verify these design margins and to determine flow rates through subcritical throughwall cracks at high pressures. For this reason, a third tube-rupture and leak-rate test facility is being constructed to perform tests at pressures up to 52 MPa (7,500 psi) and flow rates up to 45.4 L/min (12 gal/min).

### 4.5.1 Facility Description and Status

As discussed in Section 4.6.1 ("Design Analysis of the Tube Failure Facility"), the critical lengths for throughwall cracks at pressures above the 21 Mpa (3,000 psi) capability of the blowdown facility (see Section 4.3) are rather short, and the corresponding leak rates are relatively small. Therefore, the required maximum flow rate for the high-pressure tube-rupture and leak-rate test facility is only ≈45 L/min (12 gal/min) in order to maintain flow through a subcritical leaking crack and drive it to instability. Ideally, one would like to be able to conduct these high-pressure tests at the nominal SG operating

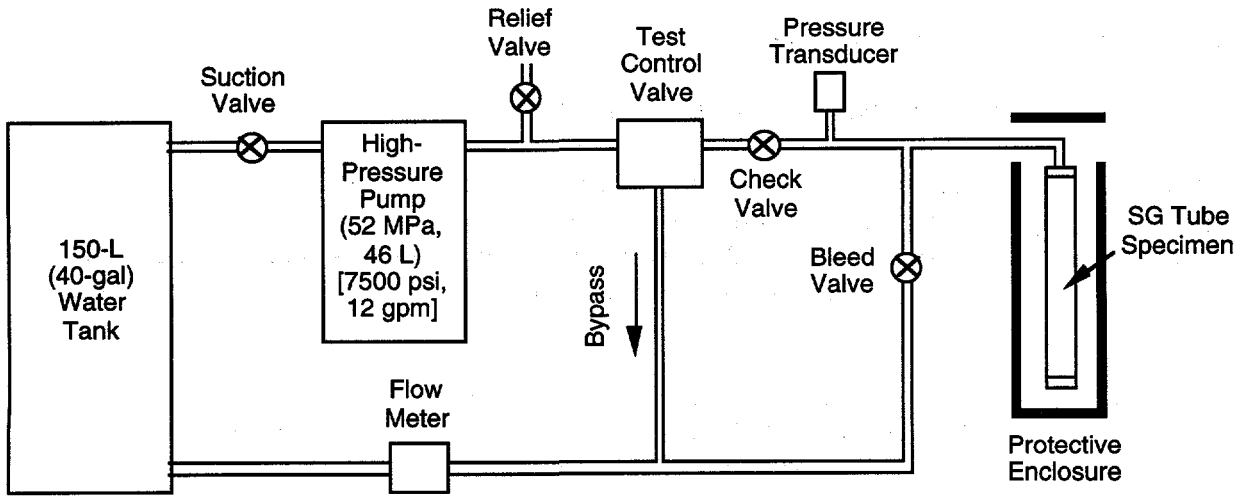


*Figure 45. Schematic diagram of high-pressure tube-rupture and leak-rate test facility.*

temperature of 300°C (572°F) with superheated water as the fluid. However, it was determined that the design and construction of such a facility was impractical, and it was instead decided to opt for room-temperature operation using water as the pressurizing fluid.

The design of the high-pressure test facility is shown schematically in Fig. 45. One of the two key components in the system is the high-pressure positive-displacement triplex pump used to supply water at pressures up to 42 Mpa (7,500 psi) and a fixed flow rate of 45.4 L/min (12 gal/min). The second key component is the test control valve used to apportion the flow from the pump either to the specimen or around the bypass loop. The water supply for the system is contained in a 150-L (40-gal) tank, and the specimen internal pressure is monitored by a pressure transducer.

The operation of the facility can be illustrated by considering a test on a specimen that initially contains a short nonthroughwall flaw. The test begins with the specimen at zero internal pressure and all of the flow from the pump diverted through the bypass loop. The specimen pressure is gradually ramped up by intermittently directing small amounts of pressurized water to the specimen. At some point, the preexisting flaw may "pop through" the wall without initially becoming unstable. The valve will automatically direct more of the flow through the specimen to maintain the desired specimen internal pressure while simultaneously maintaining flow through this subcritical leaking crack. The specimen internal pressure can then continue to be ramped upward with the test control valve until unstable rupture of the specimen occurs.

The high-pressure pump, test control valve, and 150-L (40-gal) water tank have been acquired as a skid-mounted "hydro-laser" unit that is used commercially for high-pressure cleaning and paint-removal operations. The remaining components have not yet been acquired. Progress on this facility has been delayed to divert effort to the construction and operation of the high-temperature severe accident test facility, which has been assigned higher priority.

## 4.6 Modeling of Crack Behavior

### 4.6.1 Design Analysis of the Tube Failure Facility

The tube failure facility is intended for the study of leakage and failure behavior under normal and design basis accident conditions. To help ensure that the facility has sufficient capacity, analytical models were used to estimate critical crack sizes, leak-before-burst behavior, and expected leak rates for axial and circumferential cracks of varying length and depth.

The critical pressures and crack sizes for unstable fracture (burst) of a thin-wall internally pressurized cylindrical shell with a throughwall axial crack can be estimated from the equation, originally proposed by Hahn et al.,[15]

$$p_{cr} = \frac{\bar{\sigma}t}{mR_m} = \frac{p_b}{m}, \qquad (1)$$

where

$$\bar{\sigma} = 0.5(\sigma_y + \sigma_u),$$

$$m = 0.614 + 0.481\lambda + 0.386\exp(-1.25\lambda),$$

$$\lambda = \left[12(1-\nu^2)\right]^{\frac{1}{4}} \frac{c}{\sqrt{R_m t}} = \frac{1.82c}{\sqrt{R_m t}},$$

$$p_b = \frac{\bar{\sigma}t}{R_m} = \text{burst pressure of a virgin tube},$$

$R_m$ and t are mean radius and wall thickness of the tube, respectively

2c = axial crack length, and

$\sigma_y$ and $\sigma_u$ are yield and ultimate tensile strength, respectively.

For partthrough axial cracks, the pressure required to rupture the remaining ligament can be calculated from an equation originally proposed by Kiefner et al.,[16]

$$p_{sc} = \frac{\bar{\sigma}t}{m_p R_m} = \frac{p_b}{m_p}, \qquad (2)$$

where

$$m_p = \frac{1 - \frac{a}{mt}}{1 - \frac{a}{t}}$$

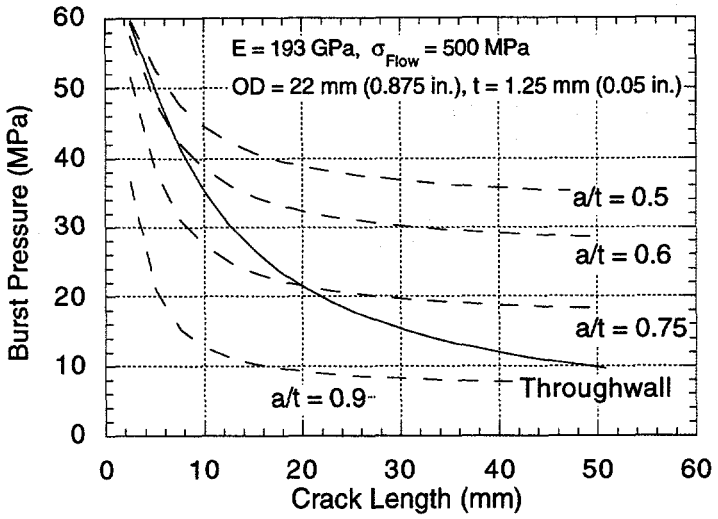


*Figure 46. Pressures for failure of axial cracks. failure loci that lie above curve for throughwall cracks correspond to unstable failures ("bursts"). Failure loci that lie below curve for throughwall cracks correspond to failure by stable leaks. Resulting throughwall cracks become unstable only after pressure increases above that required for instability of through wall crack.*

and

a = axial crack depth.

The pressures required to produce failure of a flawed tube were calculated for axial cracks of various dimensions in an internally pressurized tube with an OD of 22 mm (0.875 in.) and a wall thickness t of 1.3 mm (0.05 in.) and are plotted in Fig. 46 as a function of crack length for various crack depth to wall thickness (a/t) ratios. The assumed elastic modulus E of 193 GPa (28 x $10^3$ ksi) and yield stress σ(flow) of 502 MPa (72.85 ksi) correspond to the values for mill-annealed Alloy 600 at 288°C (550°F). Short, deep nonthrough wall cracks will first break the remaining ligament and go through the wall; a significant pressure increase beyond that necessary to drive them throughwall is required to make them grow in length. For example, a 12.7-mm (0.5-in.) crack with a/t = 0.9 (90% throughwall) will grow throughwall and begin to leak at ≈ 11 MPa (1.6 ksi). As the pressure is increased from 11 to 30 MPa (1.6 to 4.4 ksi), the crack will open more and leakage will increase, but the crack will not grow in length until the pressure reaches ≈30 MPa (4.4 ksi). At this pressure the crack can grow unstably in length, i.e., "burst." To make the tube "burst," the test system must be able to achieve a pressure of 30 MPa (4.4 ksi) with the crack leaking. The initial flow when the crack first goes through the wall (11 MPa or 1.6 ksi) will be ≈ 3.8 L/min (1 gal/min) (see below). The flow through a 12.7-mm

MPa or 1.6 ksi) will be ≈ 3.8 L/min (1 gal/min) (see below). The flow through a 12.7-mm (0.5-in.) crack immediately before instability (30 MPa or 4.4 ksi) is ≈19 L/min (5 gal/min). The total volume of flow that would have to be supplied depends upon the time required to increase the pressure from 11 to 30 MPa (1.6 to 4.4 ksi).

Shallower, longer cracks will actually "burst" without significant prior leakage because they will not break through and leak until the pressure is much higher than that required to cause a through wall crack of the same length to extend unstably. For example, a 25 mm (1 in.) crack with a/t = 0.5 will not leak until p ≈ 37 MPa (5.4 ksi). However, once the remaining ligament tears and the crack goes throughwall, the pressure is well above that required to extend a throughwall 25-mm (1-in.) crack, i.e., ≈18 MPa (2.6 ksi).

Under normal operating conditions, the pressure across the tube, $\Delta p_{no}$, is ≈ 9 MPa (1.3 ksi); under a main steamline break in which the secondary side has dropped to atmospheric pressure, the pressure across the tube, $\Delta p_{MSLB}$, is ≈17.7 MPa (2.56 ksi). These values are indicated in Fig. 46. Tubes must actually be capable of withstanding $3 \cdot \Delta p_{no} \approx 27$ MPa (3.9 ksi) and $1.4 \cdot \Delta p_{MSLB} \approx 25.2$ MPa (3.66 ksi) to meet ASME and NRC requirements for sufficient margin. The margin is lower for a main steamline break because it is such an unlikely event (≈$10^{-5}$/reactor year is the usual estimated occurrence frequency). The margin on the normal operating pressure governs the allowable flaw size, although the main steamline break would actually represent the highest pressure on the tube. An unflawed tube will burst at ≈ 65 MPa (9.4 ksi). Cracks < ≈15 mm (0.6 in.) long will never become unstable under any normal or design basis scenario. For cracks < ≈ 50 mm (2 in.) long, only deep cracks (>75% throughwall) would break through and leak under a main steamline break. Through wall cracks longer than ≈56 mm (2.2 in.) would be unstable, even under normal operating pressures.

To obtain estimates of the leak rate through a crack, the crack opening area (A) was calculated from an equation proposed by Kastner et al.[17] Equation 3 was derived by integrating the equation for elastic crack opening displacement corrected for plasticity by an Irwin-type correction factor (small scale yielding).

$$A = \frac{32}{3}\frac{K_1}{E\sqrt{2\pi}}\left[(c + r_{pl})^{3/2} - r_{pl}^{3/2}\right]\alpha(\lambda) \qquad (3)$$

where

$$r_{pl} = \frac{1}{2\pi}\left(\frac{K_1}{\bar{\sigma}}\right)^2,$$

$K_1$ = elastic stress intensity factor,

E = Young's modulus, and

$\alpha(\lambda) = 1 + 0.1\lambda + 0.16\lambda^2$.

Crack opening areas calculated from Eq. 3 are close to those calculated from elastic-plastic fracture mechanics equations as long as the bulk of the tube remains elastic at burst. The

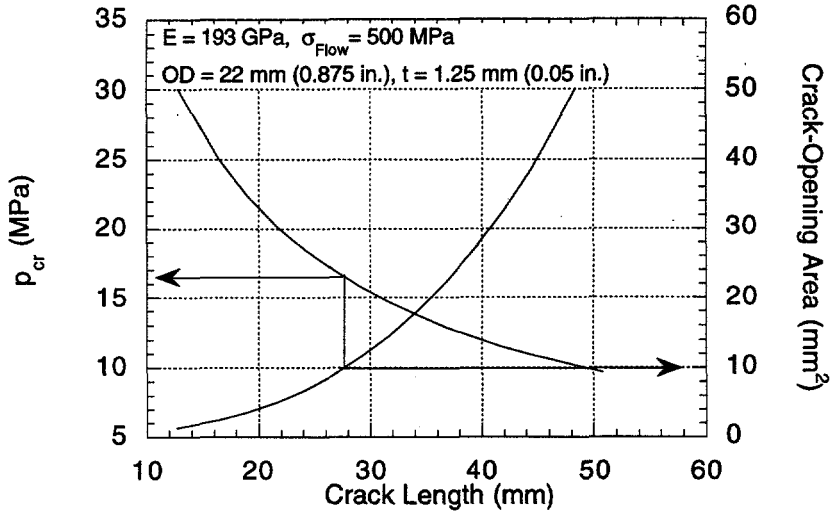


*Figure 47. Pressure for crack instability and crack opening area vs. crack length at the onset of instability for an axial throughwall crack.*

crack opening area and the pressure difference across the tube at the onset of instability are shown in Fig. 47 as a function of crack length.

For room–temperature, single–phase flows, the flow rate Q through the crack can be estimated as

$$Q = KA\sqrt{2\frac{\Delta p}{\rho}}, \tag{4}$$

where K is a nondimensional constant, A is the crack opening area, Δp is the pressure gradient, and ρ is the fluid density. A review of the literature[18] suggests that K ≈ 0.5 for cracks in tubing. Single–phase flow rates should bound the flow rates for the two–phase flows that will occur at higher temperatures. Two–phase flow calculations are complex, but only rough estimates are needed to estimate the required capacity of the test system. The simplest approximation is to take $\Delta p = \Delta p_{eff} \approx p - p_{sat}$, where $p_{sat}$ is the saturation pressure at the temperature of interest (at 288°C [550°F], $p_{sat}$ = 7.21 MPa [1.045 ksi]), rather than the full pressure drop. The estimated flow rate as a function of pressure for an axial crack at the onset of crack instability is shown in Fig. 48. If the test system pressure-vs.-flow characteristic lies above this curve, a burst test can be conducted in which not only the pressure that produces leakage but also that required to make the crack grow unstably can be determined. The flow rate at which the system characteristic intersects this pressure

The maximum flow through the crack and maximum pressure that the tube can withstand without the crack becoming unstable and growing rapidly are shown in Fig. 49

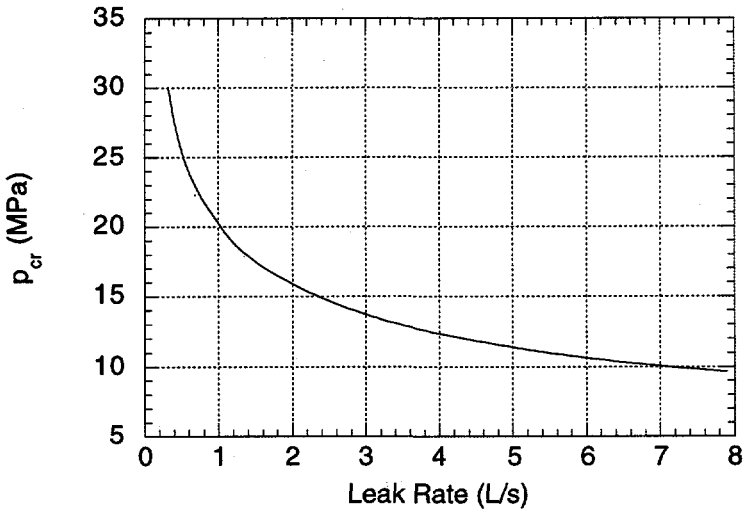


*Figure 48. Pressure and flow rate at onset of instability for axial crack vs. flow characteristic will determine the maximum crack length for which a test to instability can be run.*

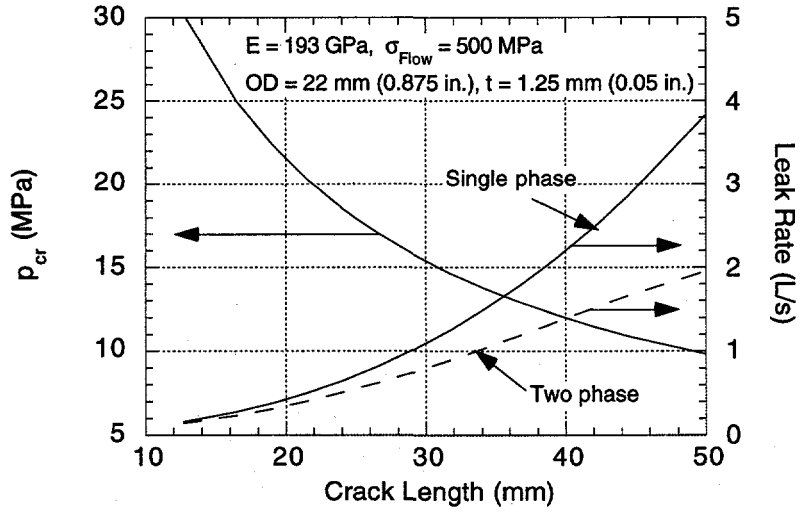


*Figure 49. Pressure at crack instability and associated leak rate versus crack length for axial crack.*

as a function of crack length. Once the crack becomes unstable, it is impossible to predict the leak area, and the resulting flow rates could be close to those for a double-ended rupture, i.e., ≈1720 and 2460 L/min (455 and 650 gal/min) for 19.1- and 22.2-mm (0.750- and 0.875-in.) OD tubing, respectively). Because cracks longer than ≈ 56 mm (2.2 in.) would be unstable under normal operating conditions, the maximum flow rate through any stable crack will be ≈ 300 L/min (80 gal/min) under single-phase flow.

For a given crack length and a pressure less than the critical pressure for crack instability $p_{cr}$, the flow through the crack will scale roughly like $Q_{max}\cdot(p/p_{cr})^{1.5}$, which can be used to estimate the total volume of flow G in a burst test before the crack becomes unstable:

$$G = \frac{Q_{max} t_R}{2.5(1-\alpha)}\left(1-\alpha^{2.5}\right), \tag{5}$$

where $\alpha = p_l/p_{cr}$, $p_l$ is the pressure at which the crack first begins to leak, and $t_R$ is the time required to increase the pressure from $p_l$ to $p_{cr}$, assuming that the pressure increases linearly with time. For a throughwall crack $p_l$, $\alpha = 0$.

### 4.6.2 Failure of Circumferential Cracks

The open literature contains many models and much experimental data on the rupture of SG tubing with axial flaws. Although the literature on the problem of circumferential cracks in tubing is more limited, much information is available on the failure of piping. However, piping is subjected primarily to bending loads and most of the available test data are for the case of large bending loads. Failure loads for tubing with circumferential cracks can be calculated by using the plastic limit load analyses described by Ranganath et al.,[19] which were based on earlier work by Kanninen et al.[20] If bending is negligible, i.e., the tube is free to deflect in the transverse direction, the failure pressure for a tube with a circumferential throughwall crack of angular length 2θ is

$$p_{cr} = \frac{2\bar{\sigma}t}{R_m}\left(1-\frac{\theta}{\pi}-\frac{2\beta}{\pi}\right), \tag{6a}$$

where

$$\beta = \sin^{-1}\left(\frac{\sin\theta}{2}\right). \tag{6b}$$

Limit load analyses have also been proposed for partthrough circumferential cracks. The analysis of Kurihara et al.[21] applies an empirical correction to account for the difference in stress level between the remaining ligament of the partthrough crack and the remainder of the pipe cross section. The pressure required to rupture the remaining ligament of a partthrough circumferential crack of depth a, for the free bending case, is given by the equation

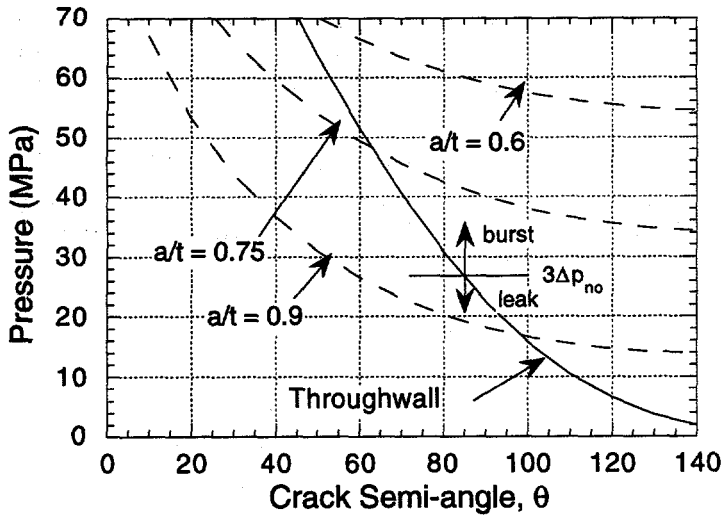


*Figure 50. Pressure above which circumferential crack becomes unstable vs. crack semi-angle for various crack depth-to-tubewall-thickness (a/t) ratios. Free-bending tube with an OD 22 mm (0.875 in.) and a wall thickness of 1.3 mm (0.05 in.) is assumed.*

$$\frac{p_{sc}}{p_b} = \frac{4\gamma}{\pi}\left[\frac{\pi}{2} + \frac{\theta\left(1-\frac{a}{t}-\gamma\right)}{2\gamma} - \beta\right], \tag{7a}$$

where

$$\beta = \sin^{-1}\left[\frac{\left(\gamma+\frac{a}{t}-1\right)\sin\theta}{2\gamma}\right], \text{ and} \tag{7b}$$

$$\gamma = 1-\left(\frac{a}{t}\right)^{\kappa}\left(\frac{\theta}{\pi}\right)^{\mu}. \tag{7c}$$

Based on comparisons with pipe tests, values for $\kappa$ and $\mu$ of 2.0 and 0.2, respectively, have been suggested.

Stability of circumferential cracks (free-bending) was also analyzed by using Eqs. 6a and 7a; the results are shown in Fig. 50. Because the axial stress in an internally pressurized tube is only one half as large as the circumferential stress, tubes containing only deep and rather long circumferential cracks will leak because of axial stresses before burst, even without an axial crack. Even a crack that subtends $2\theta = 90°$ and is 90% throughwall will not leak at $3{\cdot}\Delta p_{no}$.

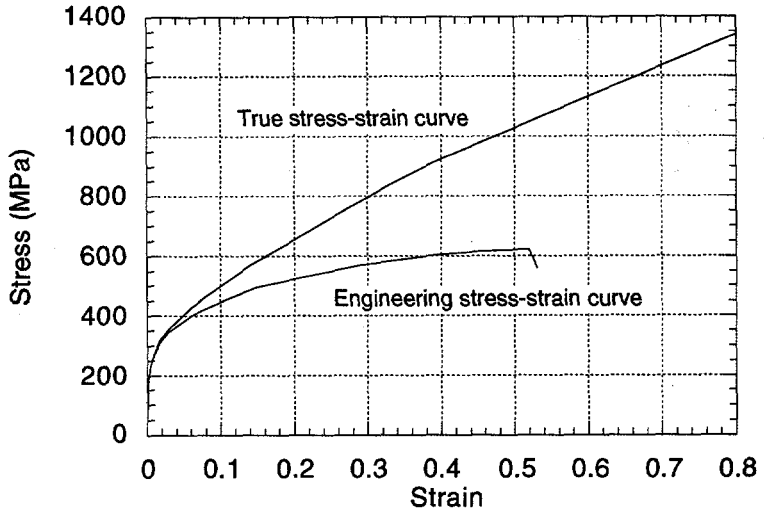


*Figure 51. Engineering and true stress-strain curves for Alloy 600 at 288°C.*

Free bending is a limiting failure mode for circumferentially cracked tubing. If the lateral deflection of the tube is completely restrained and the tube deforms only axially, another limiting failure occurs. In this case, for the throughwall crack,

$$p_{cr} = \frac{2\bar{\sigma}t}{R_m}\left(1-\frac{\theta}{\pi}\right). \qquad (7d)$$

It appears that, in most cases, sufficient lateral constraint is present (e.g., by tube support plates) so the failure pressures are much closer to those predicted by Eq. 7d than by the free bending case. Finite-element analyses are being conducted to verify these results and more accurately characterize the effects of lateral constraint on the failure pressure as well as the crack opening area.

4.6.2.1 Effects of lateral constraint on the burst pressure of a circumferentially cracked tube.

Elastoplastic finite-element analyses are being conducted to determine the effects of a lateral constraint on the burst pressure of a tube with a single throughwall circumferential crack. The stress-strain curves of the material are shown in Fig. 51. Because the analyses included the effects of finite deformation, the true stress-strain curve was used. Initially, two tubes with 180 and 240° throughwall circumferential cracks were analyzed. A typical finite-element model and displaced shape for the free-bending case are shown in Figs. 52 a and b. Note that the beam bends almost like a rigid body about a hinge at the cracked section. Fig. 53a shows the variations of the free-end displacements and the maximum rotation with normalized burst pressure for 180 and a 240° circumferential throughwall cracks. The displacement and rotation curves fall on top of each other, confirming that the displacement is of the rigid-body-rotation type. Both cracked tubes reach maximum

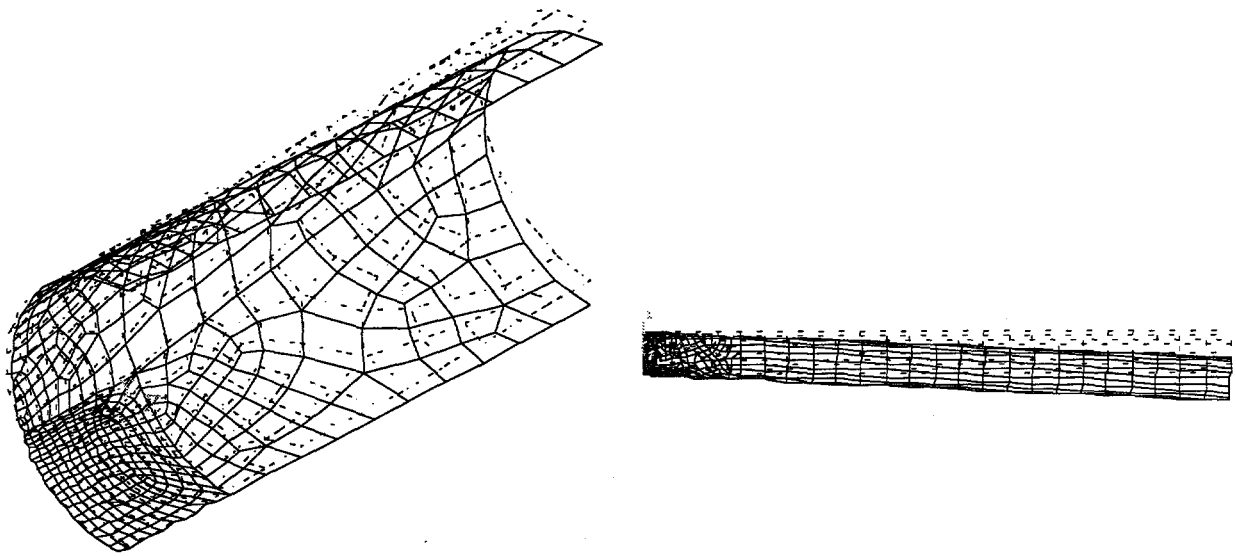

(a) (b)

*Figure 52. Typical (a) near-tip finite-element model for a tube with a throughwall circumferential crack and (b) displaced shape of the tube for the free-bending case.*

pressures at a rotation of ≈8°. This finding is in agreement with the experimental observation of Hernalsteen[22] that tubes appear to fail at a fixed rotation of the cracked section. Fig. 53b shows available burst pressure data reported by Cochet and Flesch[23] and data predicted by the free-bending simple beam model (Eq. 6a) and finite-element analysis. The simple model underpredicts the test burst pressures and the finite-element results slightly.

Figure 54 shows the variations of the maximum rotation and the constraining force at the support plate with normalized burst pressure for a 0.66-m (26-in.) -long tube that contained a 240° throughwall circumferential crack and was supported at its end. After an initial relatively shallow slope, both curves rise steeply with pressure, beyond a normalized burst pressure of 0.5, which is the point at which significant yielding begins to occur throughout the tube. In contrast to the free-bending case, the pressure does not level off but keeps increasing with rotation. Thus, it appears that the final instability point is very likely determined by the toughness limit of the material.

4.6.2.2 A simple beam model for the burst of a supported tube with a circumferential crack.

Consider a tube (Fig. 55) of radius R, wall thickness t, and length L, with a throughwall circumferential crack of angular length 2θ subjected to internal pressure p and ignore all

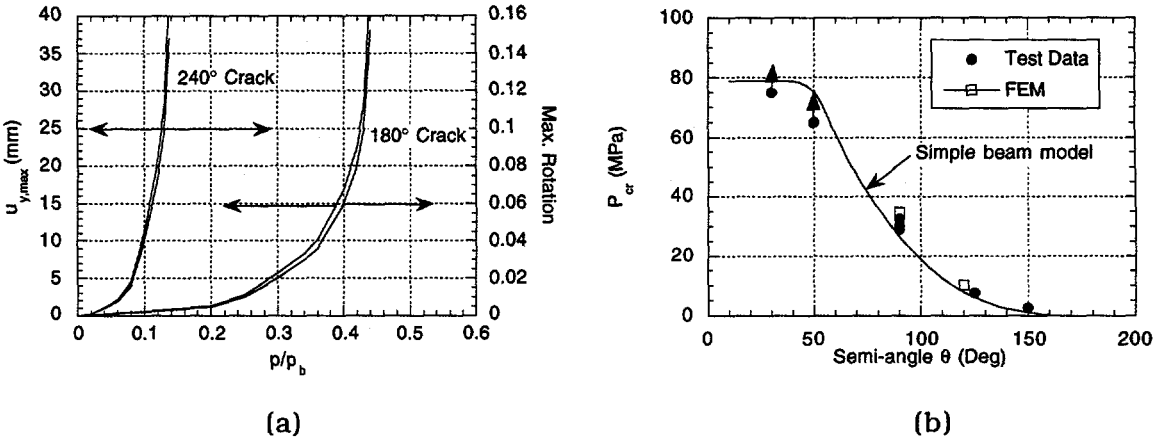


*Figure 53. (a) Variation of free-end displacements and maximum rotations with normalized burst pressure for tubes with 240 and 180° throughwall circumferential cracks; (b) Experimental burst pressure data and burst pressures predicted by simplified beam model and FEM. Arrows indicate tests discontinued prior to burst.*

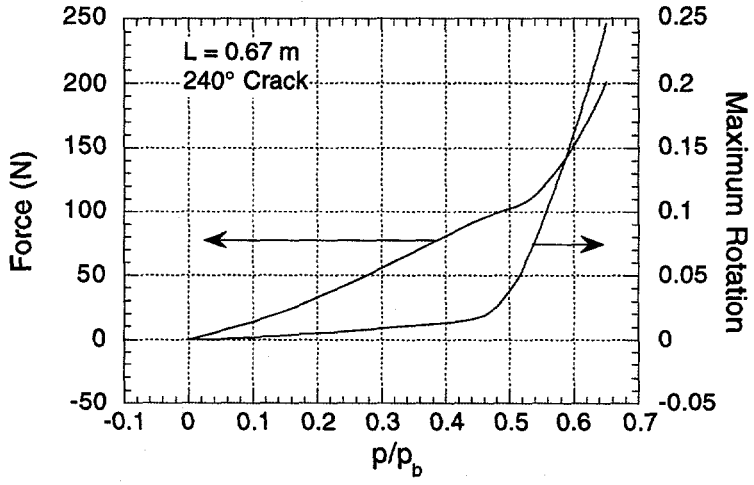


*Figure 54. Variation of maximum rotation and constraint force with normalized burst pressure for a 0.67 m (26 in.) long tube that contains a 240° throughwall circumferential crack and is supported transversely at its end.*

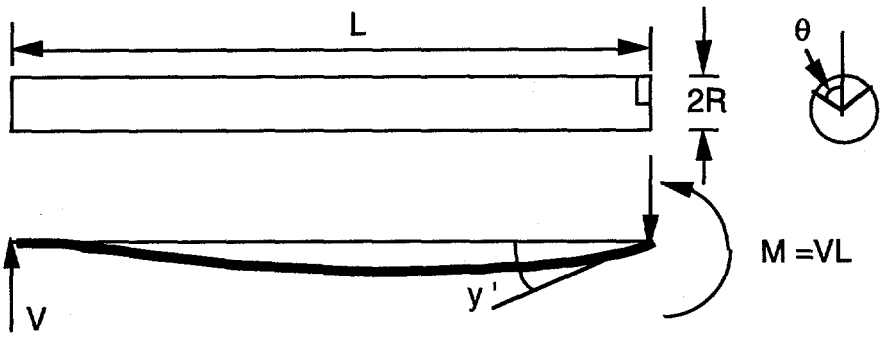


*Figure 55. Idealized model for analysis*

hoop stress effects on plastic collapse. Using symmetry, consider only half of the tube, from $\alpha = 0$ to $\alpha = \pi$, with the crack extending from $\alpha = 0$ to $\alpha = \theta$. A vertical restraining force V acts at each support and results in an externally applied bending moment $M = VL$ at the section that contains the crack. The bending rotation at the section that contains the crack is given by

$$y' = \frac{VL^2}{3EI} = \frac{VL^2}{3\pi ER^3 t}. \tag{8}$$

In general, the cross section of the tube that contains the crack will undergo an axial strain $\varepsilon_o$ and a curvature $\kappa$, so that the axial strain at any location is given by

$$\varepsilon_z = \varepsilon_o + \kappa R \cos \alpha .$$

Two cases may arise.

Case 1 $\varepsilon_o > \kappa R$

In this case, there is no negative yielding in the cracked section. If the section experiences tensile yielding from $\alpha = \alpha_t$ to $\alpha = \theta$, the equilibrium of axial forces gives

$$\sigma_y Rt\,(\pi - \theta) - E\kappa R^2 t[(\pi - \alpha_t)\cos\alpha_t + \sin\alpha_t] = 1/2 p\pi R^2,$$

where E is the Young's modulus and $\sigma_y$ is the flow stress. At collapse, $\alpha_t = \pi$, and the critical pressure as a fraction of the unflawed burst pressure is

$$\frac{p_{cr}}{p_b} = \frac{2}{\pi}(\pi - \theta). \tag{9}$$

The bending moment at the cracked section at collapse is given by

$$M = VL = 2\sigma_y R^2 t \sin\theta, \tag{10a}$$

which is independent of L. From Eq. 8, the slope y' at the cracked section is

$$y' = \frac{2\sigma_y L}{3\pi ER}\sin\theta . \qquad (10b)$$

Note that, in this case, the slope at collapse increases linearly with length L.

Case 2 $\varepsilon_o < \kappa R$

In this case, there will be both tensile and compressive yielding at the cracked section. The location of the neutral axis is given by

$$\alpha_n = \cos^{-1}[-\varepsilon_o/\kappa R].$$

As before, axial force equilibrium at collapse gives

$$\frac{p_{cr}}{p_b} = \frac{2}{\pi}(2\alpha_n - \theta - \pi). \qquad (11)$$

The bending moment at the cracked section is given by

$$M = VL = 2\sigma_y R^2 t\,(\sin\theta - 2\sin\alpha_n), \qquad (12)$$

which on solving for $\alpha_n$ gives

$$\alpha_n = \sin^{-1}\left[\frac{1}{2}\sin\theta - \frac{VL}{4\sigma_y R^2 t}\right], \qquad (13a)$$

which, on applying Eq. 8, gives

$$\alpha_n = \sin^{-1}\left[\frac{1}{2}\sin\theta - \frac{3\pi ER}{4\sigma_y L}y'\right]. \qquad (13b)$$

Note that as $L \to \infty$, Eqs. 11 and 13b give the burst pressure for the free-bending case. If we make the additional assumption that, for a given crack geometry, y' at collapse is a constant $y'_c$, independent of L, then, because $\alpha_n \le \pi$, a critical length $L_{cr}$ can be defined as a constant for a given crack geometry as follows:

$$L_{cr} = \frac{3\pi ER}{2\sigma_y \sin\theta}y_c', \qquad (14)$$

and Eq. 13b can be rewritten as

$$\alpha_n = \sin^{-1}\left[\frac{1}{2}\left(1 - \frac{L_{cr}}{L}\right)\sin\theta\right]. \qquad (13c)$$

Thus, we conclude that,

If $L < L_{cr}$ , Case 1 is controlling, and

If $L > L_{cr}$ , Case 2 is controlling.

To solve for the collapse pressure from Eqs. 11 and 13b, we need a value of $y_c'$. One option for obtaining this value is to first measure the reactive force V at collapse experimentally and then use Eq. 8 to compute $y_c'$. In Fig. 56a, the burst pressure is plotted as a function of the length of the tube L for various values of the parameter $y'_c$. Note that the burst pressure remains constant for $L < L_{cr}$ and drops rapidly with increasing L for $L > L_{cr}$. The variations of the reactive force V and the value of y' at collapse with length L are plotted in Fig. 56b for the cases of $y'_c = 0.03$ and 0.04. The reactive force V decreases with L while the value of y' at collapse first increases with L (Case 1) and then remains constant at $y'_c$ (Case 2).

Although the values of the support reactions at rupture are comparable to those calculated by the FEM, the values of the rotation are significantly smaller because the model assumes that the tube away from the section that contains the crack remains elastic. The model will be modified in the future to include the effects of plastic deformation in the whole tube.

### 4.6.3 Severe Accident Test Analyses

During design basis accidents, the temperature of the SG tubing is <350°C (662°F). In this temperature range, creep effects are negligible in Alloy 600. However, in severe accidents, much higher temperatures are possible. At these higher temperatures, plastic deformation is likely to be much more extensive than at normal reactor operating temperatures and creep effects may no longer be negligible. The behavior of flawed SG tubing during severe accidents has recently been considered in two reports[11,12] Both analyses assume that failure of flawed SG tubing in severe accidents can be described in terms of a model in which failure is characterized by a flow stress, which is a function of temperature. In contrast, the failure of unflawed tubing and other components, such as the surge line nozzle, is described in terms of creep damage failure. As an alternative to the flow stress models, a simplified model that includes creep effects in the failure of flawed tubing has been developed.

Two time/temperature histories have been considered in our initial calculations. One is based on the INEL analysis.[11] In this analysis, the temperature rises fairly rapidly to ≈800°C. Then, because the cladding is almost completely oxidized, the rate of temperature increase drops sharply. Shortly after this drop in the heatup rate, the INEL analysis predicts failure of the surge line nozzle and depressurization of the system. Because of the uncertainties associated with the time to failure of the nozzle, the calculations for the tubing have ignored the predicted depressurization. Thus, the test specimens were subjected to a temperature ramp of 3.75°C/min (6.75°F/min) from 300 to 550°C (572 to 1022°F), followed by 7.5°C/min (13.5°F/min) up to 800°C (1472°F) and then 1.75°C/min (3.15°F/min) to failure.

The second time/temperature history is based on an industry analysis.[12] In this case, the tubing temperature also rises rapidly, but the predicted peak temperature is only 940K

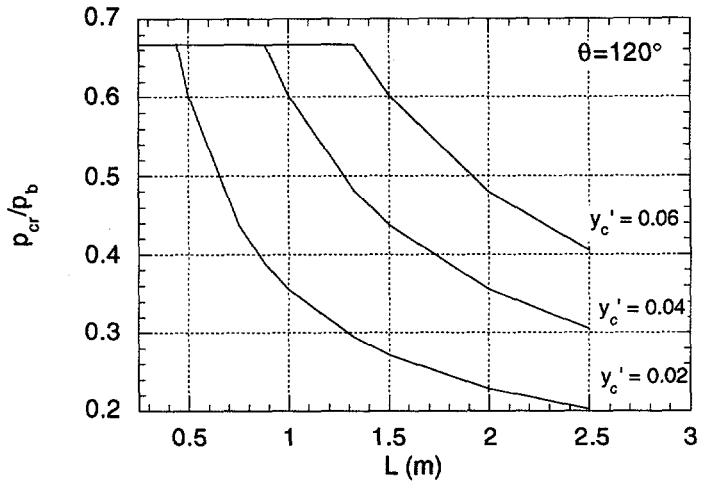


(a)

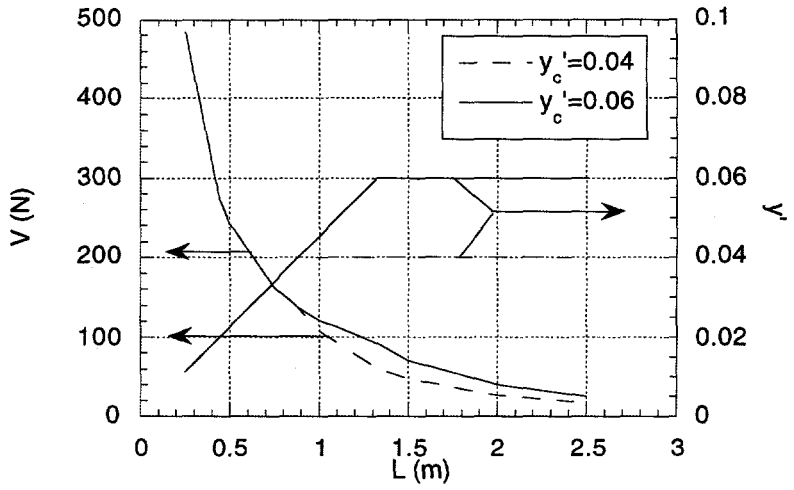


(b)

*Figure 56. Variation of (a) calculated rupture pressure with length of tube for various values of critical slope $y_c'$ and (b) calculated support force and maximum rotation at rupture with tube length.*

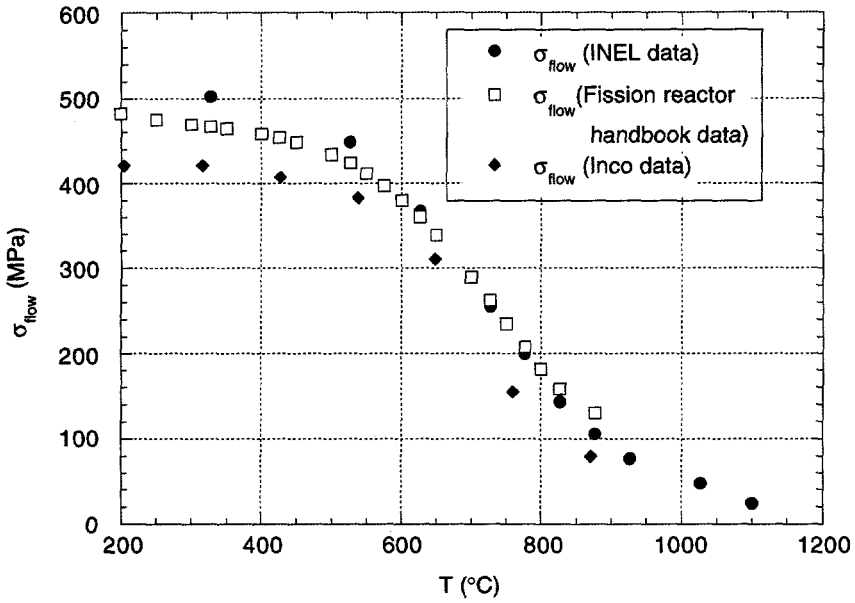


*Figure 57. Flow stress curves of Alloy 600 as a function of temperature.*

(667°C or 1233°F). Although both the INEL and the industry analysis predict a marked decease in heatup of the tubes after oxidation of the cladding is completed, in Ref. 11, the temperature still increases at a significant rate of ≈ 2°C/min (3.6°F/min), whereas in Ref. 12, it is predicted to be virtually constant at 940 K (667°C or 1233°F). Reference 12 also predicts system depressurization due to failure of the surge line shortly after the tubing reaches 940 K (667°C or 1233°F). The two histories are shown in Figs. 43 and 44.

4.6.3.1 Flow stress model

In the flow stress model, it is assumed that, at a constant hoop stress σ, rupture occurs at a temperature T whenever the following rupture equation is satisfied, independent of temperature history:

$$\sigma = \frac{\overline{\sigma(T)}}{m_p}, \qquad (15)$$

where $\overline{\sigma(T)}$ is the flow stress, which is a function of temperature, and $m_p$ is a hoop stress magnification factor that accounts for the crack. The flow stress (i.e., average of yield and ultimate tensile strengths) was computed from the tensile test data provided by INEL[24] and is shown in Fig. 57. The magnification factors that correspond to the following three models were used to analyze the severe accident tests:

(1) Kiefner model[16]

$$m_p = \frac{1-\frac{a}{mt}}{1-\frac{a}{t}}, \tag{16a}$$

(2) PNNL model[25]

$$m_p = \left[1-\frac{a}{t}+\frac{a}{t}\exp(-0.41\lambda)\right]^{-1}, \tag{16b}$$

(3) EDF model[26]

$$m_p = \left[1-\frac{\frac{c}{t}\frac{a}{t}}{1+\frac{c}{t}}\right]^{-1} \tag{16c}$$

Tables 4-6 show experimentally observed and predicted burst temperatures that were obtained from the three models. The predicted failure temperatures for the unflawed tubes ($m_p$ =1) are close to the experimentally observed values, which indicates that the flow stress values that were used are reasonable. However, the failure temperatures of the flawed tubes that were predicted by the flow stress models are less than the experimentally observed failure temperatures in all cases, but particularly so for the shorter and deeper cracks.

All of the test specimens, except the one with the 6.4-mm (0.25-in.)- long, 80%-deep crack, showed extensive plastic deformation (a "fish mouth" crack opening with plastic tearing at the crack tips) and would almost certainly have experienced unstable fracture if the specimens had not depressurized rapidly after ligament rupture. The specimen with the 6.4-mm (0.25–in.)- long, 80% throughwall crack did not show extensive plastic deformation and would not have experienced unstable fracture even if the specimen had not depressurized. Both the Kiefner and the EDF models predict that this crack would leak before rupture, and both agree with the experimental observation. The PNNL model does not distinguish between unstable fracture and ligament rupture and empirically correlates unstable fracture with crack size. Thus, although the PNNL model appears to predict the failure temperature for the specimen with the 6.4-mm (0.25–in.) crack better than the other two models, it is only so because it predicts unstable fracture rather than ligament rupture. The other two models also predict higher temperatures for unstable fracture of the specimen with the short throughwall crack than those shown in Tables 4 and 6.

4.6.3.2 Creep rupture model

To develop a creep rupture model, we used a linear damage rule,

$$\int_0^{t_R} \frac{dt}{t_f(T,\sigma)} = 1, \tag{17}$$

*Table 4. Predicted (by Kiefner equation using INEL flow stress) and observed temperature at rupture for steam generator tubes of two diameters following the INEL ramp of Fig. 43.*

| Crack Length, mm (in) | | a/t[a] | Temperature (°C) 19.1-mm (0.750-in.) diam Predicted | Temperature (°C) 19.1-mm (0.750-in.) diam Observed | Temperature (°C) 22.2-mm (0.875-in.) diam Predicted | Temperature (°C) 22.2-mm (0.875-in.) diam Observed |
|---|---|---|---|---|---|---|
| Unflawed | | Unflawed | 835 | 823 | 834 | 835 |
| 6.4 | (0.25) | 0.8 | 671 | 798 | 693 | 803 |
| 25.4 | (1.0) | 0.65 | 670 | 758 | 676 | 773 |
| 50.8 | (2.0) | 0.5 | 731 | 783 | 733 | 808 |
| 50.8 | (2.0) | 0.25 | 797 | 808 | 797 | 825 |

[a] a/t = flaw depth/tube wall thickness.

*Table 5. Predicted (by PNNL equation using INEL flow stress) and observed temperature at rupture for steam generator tubes of two diameters following the INEL ramp of Fig. 43.*

| Crack Length, mm (in) | | a/t[a] | Temperature (°C) 19.1-mm (0.750-in.) diam Predicted | Temperature (°C) 19.1-mm (0.750-in.) diam Observed | Temperature (°C) 22.2-mm (0.875-in.) diam Predicted | Temperature (°C) 22.2-mm (0.875-in.) diam Observed |
|---|---|---|---|---|---|---|
| Unflawed | | Unflawed | 835 | 823 | 834 | 835 |
| 6.4 | (0.25) | 0.8 | 746 | 798 | 758 | 803 |
| 25.4 | (1.0) | 0.65 | 643 | 758 | 656 | 773 |
| 50.8 | (2.0) | 0.5 | 718 | 783 | 717 | 808 |
| 50.8 | (2.0) | 0.25 | 792 | 808 | 791 | 825 |

[a] a/t = flaw depth/tube wall thickness.

*Table 6. Predicted (by French (EDF) equation using INEL flow stress) and observed temperature at rupture for steam generator tubes of two diameters following the INEL ramp of Fig. 43.*

| Crack Length, mm (in) | | a/t[a] | Temperature (°C) 19.1-mm (0.750-in.) diam Predicted | Temperature (°C) 19.1-mm (0.750-in.) diam Observed | Temperature (°C) 22.2-mm (0.875-in.) diam Predicted | Temperature (°C) 22.2-mm (0.875-in.) diam Observed |
|---|---|---|---|---|---|---|
| Unflawed | | Unflawed | 835 | 823 | 834 | 835 |
| 6.4 | (0.25) | 0.8 | 662 | 798 | 678 | 803 |
| 25.4 | (1.0) | 0.65 | 660 | 758 | 664 | 773 |
| 50.8 | (2.0) | 0.5 | 726 | 783 | 726 | 808 |
| 50.8 | (2.0) | 0.25 | 794 | 808 | 793 | 825 |

[a] a/t = flaw depth/tube wall thickness.

*Table 7. Predicted (by creep rupture equation) and observed temperature at rupture for steam generator tubes of two diameters following the INEL ramp of Fig. 43. The first and second predicted temperatures correspond to those using Larson-Miller parameters provided by INEL and Cofie, respectively.*

| Crack Length, mm (in) | a/t[a] | Temperature (°C) 19.1-mm (0.750-in.) diam | | Temperature (°C) 22.2-mm (0.875-in.) diam | |
|---|---|---|---|---|---|
| | | Predicted | Observed | Predicted | Observed |
| Unflawed | Unflawed | 837, 854 | 823 | 837, 853 | 835 |
| 6.4 (0.25) | 0.8 | 723, 748 | 798 | 738, 762 | 803 |
| 25.4 (1.0) | 0.65 | 722, 747 | 758 | 726, 751 | 773 |
| 50.8 (2.0) | 0.5 | 767, 790 | 783 | 768, 791 | 808 |
| 50.8 (2.0) | 0.25 | 811, 823 | 808 | 811, 823 | 825 |

[a] a/t = flaw depth/tube wall thickness.

where $t_R$ is the time to rupture for the specimen, $t_f$ is the time to creep rupture at stress, $\sigma$ is the stress, and T is temperature (function of time). The creep failure model can be extended to flawed tubing by assuming that the stress magnification factors for throughwall and partthrough cracks given by Eqs. 16a–16c are applicable also to the case of creep. Such an analogy can be shown to be valid for certain classes of creep and plasticity problems.[27] It is not strictly valid for the problem considered here, but the expectation is that it will provide a reasonable approximation and can be validated by the test program. The time to creep rupture was determined with the following LMPs [using ksi, R (Rankine), and h as the units for stress, temperature, and time, respectively], which were obtained from INEL[24] and Cofie[12]:

$$LMP(INEL) = 36.196 - 8.9433*LOG_{10}(S) \quad (18a)$$

$$= T[LOG_{10}(t_f) + 13] \times 10^{-3} \quad (18b)$$

$$LMP(COFIE) = 40.3 - 4*LOG_e(S) \quad (18c)$$

$$= T[LOG_{10}(t_f) + 15] \times 10^{-3}. \quad (18d)$$

The parameters provided by Cofie generally give a longer rupture life than the INEL parameters. The predicted failure temperatures, computed with the Kiefner magnification factor (Eq. 16a), are presented with experimental results in Table 7. Although the failure temperatures are still under-predicted, they are much closer to those observed in the experiments than those predicted by the flow stress models. In particular, they are quite close for the longer cracks.

Detailed finite-element analyses are planned to shed some light on the effects of stress redistribution and creep on the ligament stress distribution. Pre- and posttest measurements of crack depth are also being planned to improve the predicted burst temperatures.

# 5 Development of Methodology and Technical Assessments for Current and Emerging Regulatory Issues (O. K. Chopra, D. R. Diercks, and W. J. Shack)

The objective of this task is to use the data, results, correlations and modeling assembled in work under the first three objectives to provide technical assessments and evaluations of current and emerging regulatory issues related to steam generator tube integrity. These include items such as confirmatory research on existing and new models, the evaluation of tube repair methods, and input and assessment for the new rule and regulatory guide on steam generator tube integrity.

The NRC is developing a "performance-based" rule and regulatory guide related to steam generator tube integrity. Evaluations and assessments are necessary to determine (a) if the proposed criteria provide adequate levels of integrity, (b) if the criteria can be met, and (c) what combinations of inspection requirements (POD, sizing accuracy), sampling plans and expansion rules will lead to meeting the criteria. The NRC will need to evaluate specific industry proposed implementations of the performance based criteria. This will require the use of a comprehensive validated model that integrates all important aspects of integrity evaluations starting from inservice inspection results and ending with a total leak rate at the end of an operating cycle under various assumed conditions. Further, the probabilities of single and multiple tube ruptures under various reactor coolant conditions need to be quantified.

Cracking and failure of tubes repaired by sleeving is an emerging issue. The long term serviceability of tubes repaired by sleeving needs to be assessed. Key variables that strongly affect serviceability are the material condition, the operating environment, and the level of residual stress remaining in the tube after sleeving. The industry is currently developing various *in situ* repair methods for tubes cracked in service as alternatives to sleeving or plugging. The continued serviceability of the repaired tubes needs to be established and the extent to which the repair may have affected the material properties needs to be assessed. Criteria for the qualification and acceptance of any tube repair method (sleeving included) are needed.

Present activities under this task are concentrating on the compilation of data and evaluation of steam generator tube repair techniques and qualifications. The principal repair techniques under evaluation include sleeving and other methods of direct tube repair e.g., electroplating, weldment additions, and autogeneous remelt process. The current effort is focused on collecting information on the various sleeve designs and their qualification. The test methods to qualify the installation processes and to verify that the sleeved tubes have acceptable resistance to SCC are being evaluated. Process and material variables that may be relevant to qualification testing are being defined.

## References


1. Voltage-Based Interim Plugging Criteria for Steam Generator Tubes, U.S. Nuclear Regulatory Commission Report NUREG-1477 (Draft Report for Comment), June 1993.

2. D. Dobbeni, D. Degreve, J. P. Roussseaux, and M. Zavadsky, NDE of Sleeved Tubes: Belgian Approach, EPRI 14th Steam Generator Workshop, Seattle, Aug. 7-9, 1995.

3. H. Houserman, R. Warlick, and R. Vollmer, Using Satellite Technology to Improve SG Eddy Current Inspections, *Nucl. Eng. Int.*, Vol. 37, No. 456, July 1992, pp. 37-38.

4. D. L. Atherton, D. D. Mackintosh, S. P. Sullivan, J. M. S. Dubois and T. R. Schmidt, Remote-Field Eddy Current Signal Representation, *Mater. Eval.*, July, 1993, pp. 782-789.

5. C. V. Dodd and J. R. Pate, Advancement in Eddy-Current Test Technology for Steam Generator Tube Inspection, in *Twentieth Water Reactor Safety Information Meeting, NUREG/CP-0126*, Vol. 3, March 1993, pp. 267-276.

6. S. J. Norton and J. R. Bowler, Theory of Eddy Current Inversion, *J. Appl. Phys.*, Vol. 73, No. 2, Jan. 15, 1993.

7. J. M. Mann, L. W. Schmerr and J. C. Moulder, Neural Network Inversion of Uniform-Field Eddy Current Data, *Mater. Eval.*, Jan. 1991, pp. 34-39.

8. K. Satake, M. Tanaka, N. Shimizu, Y. Araki, and K. Morimoto, Three-Dimensional Analysis on Eddy Current Testing for S/G Tubes, *IEEE Transactions on Magnetics*, Vol. 28, No. 2, March 1992, pp. 1466-1468.

9. T. Stepinski and N. Maszi, Conjugate Spectrum Filters for Eddy Current Signal Processing, *Mater. Eval.*, July 1993, pp. 839-844.

10. J. L. Rose, K. M. Rajana, and F. T. Carr, "Ultrasonic guided wave Inspection Concepts for Steam Generator Tubing," *Mater. Eval.*, Feb. 1994, pp. 307-311.

11. P. G. Ellison, L. W. Ward, C. Dobbe. S. A. Chavez, C. L. Atwood, C. L. Smith, L. M. Wolfram, J. L. Jones, L. N. Haney, and W. J. Reece, *The Risk Significance of Induced Steam Generator Tube Rupture*, INEL-95/0641, Rev. 1 (Draft), Lockheed Martin Idaho Technologies, Inc., Idaho National Engineering Laboratory, December 1995.

12. E. L. Fuller, M. A. Kenton, M. Epstein, R. E. Henry, and N. G. Cofie, *Risks from Severe Accidents Involving Steam generator Tube Leaks or Ruptures*, EPRI TR-106194 (Draft), Electric Power Research Institute, Palo Alto, CA, January 1996.

13. J. R. Pate and C. V. Dodd, Computer programs for Eddy-Current Defect Studies, NUREG/CR-5553, Oak Ridge National Laboratory, 1990.

14. R. A. Clark and R. L. Burr, Corrosion, Vol. 36, July 1980, pp. 382-383.

15. G. T. Hahn, M. Sarrate, and A.R. Rosenfield, Criteria for crack extension in cylindrical pressure vessels, *Int. J. Fracture Mech.*, Vol. 5, No. 3, 1969.

16. J. F. Kiefner, W. A. Maxey, R. J. Eiber, and A. R. Duffy, Failure stress levels of flaws in pressurized cylinders, in *Progress in Flaw Growth and Fracture Toughness Testing*,, Kaufman, J. G., ed., National Symposium on Fracture Mechanics (6th: 1972: Philadelphia), American Society for Testing and Materials, ASTM Special Technical Publication 536, Philadelphia 1973.

17. W. Kastner, E. Röhrich, W. Schmitt, and R. Steinbuch, Critical crack sizes in ductile piping, *Int. J. Pressure Vessels & Piping*, Vol. 9, 1981.

18. E. Gillot, B. Cochet, P. Richard, and C. F. Faidy, Validation of Leak Before Break Analysis for Steam Generator Tubes, SMIRT-9, Vol. D, Lausanne, 1987.

19. S. Ranganath and H. S. Mehta, Engineering Methods for the Assessment of Ductile Fracture Margin in Nuclear Power Plant Piping, Elastic Plastic Fracture Second Symposium, Vol. 2, Fracture Resistance Curves and Engineering Applications, American Society for Testing and Materials, ASTM Special Technical Publication 803, Philadelphia 1973.

20. M. F. Kanninen, A. Zahoor, G. M. Wilkowski, I. Abou–Sayed, C. Marschall, D. Broek, S. Sampath, C. Rhee, and J. Ahmad, Instability Predictions for Circumferentially Cracked Type 304 Stainless Steel Pipes under Dynamic Loading, EPRI NP–2347 (Vol. 1: Summary; Vol. 2: Appendices), Electric Power Research Institute, Palo Alto, CA, April 1982.

21. R. Kurihara, S. Ueda, and D. Sturm, Estimation of the Ductile Unstable Fracture of Pipe with a Circumferential Surface Crack subjected to Bending, *Nucl. Eng. and Design*, Vol. 106, 1988.

22. P. Hernalsteen, Structural and Leakage Integrity of Tubes Affected by Circumferential Cracking, pp. 233-257 in Proc. CNRA/CSNI Workshop on Steam Generator Tube Integrity, NUREG/CP-0154, NEA/CNRA/R(96)1 (February 1997).

23. B. Cochet and B. Flesch, Application of the leak before break concept to steam generator tubes, SMiRT–9, Vol. D, Lausanne, 1987.

24. L. A. Stickler, J. L. Rempe, S. A. Chavez, G. L. Thinnes, S. D. Snow, R. J. Witt, M. L. Corradini, and J. A. Cos, *Calculations to Estimate the Margin to Failure in the TMI-2 Vessel*, NUREG/CR-6196, EG&G Idaho, Inc., March 1994.

25. R. J. Kurtz, R. A. Clark, L. R. Bradley, W. M. Bowen, P. G. Doctor, R. H. Ferris, and F. A. Simonen, *Steam Generator Tube Integrity Program/Steam Generator Group Project, Final Project Summary Report*, NUREG/CR–5117, PNNL, Richland, WA, May 1990.

26. B. Flesch and B. Cochet, Crack stability criteria in steam generator tubes, *Int. Cong. on Pressure Vessel Technology*, Beijing, Sept. 1988.

27. I. Finnie and W. R. Heller, *Creep of engineering materials, New* York, McGraw-Hill, 1959.

## Appendix: ORNL Computer Codes

| Program Name | Brief Description | Reference |
|---|---|---|
| ABBORAR | Defect impedance change for boreside coil | A-1 |
| ABENCAR | Defect impedance change for encircling coil | A-1 |
| AIRCO | Computes the air inductance of a coil | A-2 |
| AIRMAG | Computes the magnetic field of an air coil | A-2 |
| APUFIT | Fits readings from a pulsed instrument | A-3 |
| APULG | Takes readings from a pulsed instrument | A-3 |
| BIGFIT | Fits computed or experimental readings | A-4,A-5 |
| BIGRDG | Makes experimental readings and stores data | A-4,A-5 |
| BODEDF | Makes a Bode difference plot | A-6 |
| BODEPL | Makes an absolute Bode plot | A-6 |
| CIR.DAT | Data file for ORNL boreside/encircling coils | A-7 |
| CLADT | Calculates impedance for a clad conductor | A-2 |
| CONDTF | Measures conductivity (through transmission) | A-4,A-8 |
| DATGEN | Generates multiple property data file | A-4 |
| DBDSF | Defect sensitivity factor for differential boreside | A-1 |
| DBDSFPLT | Generates a contour plot from DBDSF data | A-1 |
| DEFBOR | Absolute boreside coil | A-1 |
| DEFBORDF | Differential boreside coil | A-1 |
| DEFBORDG | Differential boreside coil | A-1 |
| DEFENC | Absolute encircling coil | A-1 |
| DEFENCDF | Differential encircling coil | A-1 |
| DEFPLA | Defect in a plate | A-1 |
| DEFRDG | Makes readings on the impedance analyzer | A-6 |
| DEFBORAR | Defect impedance change, averaged over depth | A-1 |
| DEFENCAR | Defect impedance change, averaged over depth | A-1 |
| DFPLARY | Defect impedance change, averaged over depth | A-1 |
| DFPLVOL | Defect impedance change, averaged over volume | A-1 |
| DFRFPARY | Defect voltage change, averaged over depth | A-1 |
| DFRFPLA | Defect voltage change, single value of r | A-1 |
| DFRFRSTP | Defect voltage change, step in r direction | A-1 |
| DIFBOR | Differential boreside coil | A-1 |
| FINDFIT | Fits multiple frequency data, saves best | |
| FITANA | Fitting program for the impedance analyzer | A-6 |
| GETKY | Utility to get the value of typed key | |
| INVDEF | Inversion program for a defect in a plate | A-1,A-9 |
| INVPLA | Inversion program for a defect in a plate | A-1,A-9 |
| MAGSCN | Calculates magnetic field at different points | |
| MULDEF | Multilayer defect program for the reflection probe | |
| MULIMP | Multilayer defect program for the coil impedance | A-4 |
| MULPUL | Multilayer program for pulsed calculation | |
| MULRFD | General multilayer design program for reflection probe | A-4 |
| MULTIC | Multilayer, reflection probe, conductivity changes | A-10 |
| MULTID | Multilayer, reflection probe, defects | A-10 |
| MULTIT | Multilayer, reflection probe, thickness changes | A-10 |
| NORIMP | Measures normalized impedance | A-6 |
| PAN.DAT | ORNL pancake coil data file | |
| PCAVVSCN | Average defect (over volume) for pancake coil | A-1 |
| PCAVZSCN | Average defect (over depth) for pancake coil | A-1 |

| | | |
|---|---|---|
| PCBLDF | Builds a magnitude and phase lookup file | A-1 |
| PCDSF | Calculates DSF for a PC | A-1 |
| PCDSFPLT | Generates a contour plot of the magnitude of DSF | A-1 |
| PCGRAPH | Plots two sets of data on same graph | A-1 |
| PCINV | Inverts scan of PC data | A-1 |
| PCRTSCAN | Converts raw voltage readings to impedance change | A-1 |
| PERMCON | Permeability from through transmission readings | |
| PHNWRK | Calculates voltage for calibrator network | A-5 |
| PULFIT | Fits pulse data to properties | A-3 |
| PULRDG | Makes readings on pulsed EC instrument | A-3 |
| RDGANA | Makes readings on Impedance analyzer | A-6 |
| REF.DAT | Data file for ORNL reflection probes | A-4 |
| RESFIT | Fits resistivity to readings | |
| RFAVZSCN | Defect voltage, average over depth | A-1 |
| RFBLDF | Builds a lookup file of magnitude and Phase of DSF | A-1 |
| RFCLAD | Magnitude and phase for reflection probe, clad conductor | A-10 |
| RFDSF | Magnitude and phase of DSF a for lattice of points | A-1 |
| RFDSFL | Magnitude and phase of DSF a for lattice of points | A-1 |
| RFDSFPLT | Generates a contour plot of magnitude of DSF | A-1 |
| RFGRAPH | Plots two sets of data on same graph, rf probe | A-1 |
| RFINV | Inverts scan of defect using reflection coil data | A-1 |
| SUBMLRF | Subroutines for reflection coil | A-10 |
| SUBTUB | General subroutines | |
| TICOIL | Calculates RLC for low-temperature drift reflection coil | A-10 |

*Programs with a date listed after 4/23/87 have been written on the PC-AT. Those with an earlier date will need to be modified. Most of the programs are written in Ryan McFarland Fortran, but will run on Microsoft and NDP Fortran with only slight modifications. The programs that read from an instrument or send data to a controller use IEEE-488 bus, which will have to be configured to your particular board. Some of the programs also use Graphmatic and Printmatic routines.

## References for Appendix


A-1. J. R. Pate and C. V. Dodd, Computer Programs For Eddy-Current Defect Studies, NUREG CR/ORNL TM, 1990.

A-2. W. A. Simpson, C. V. Dodd, J. W. Luquire, and W. G. Spoeri, Computer Programs for Some Eddy-Current Problems - 1970, ORNL-TM-3295, June 1971.

A-3. C. V. Dodd, et al., Pulsed Eddy Current Inspection of Thin- Walled Stainless Steel Tubing, ORNL-6408, Martin Marietta Energy Systems, Oak Ridge National Laboratory, Oak Ridge, Tenn., Sept. 1987.

A-4. W. E. Deeds, C. V. Dodd, and G. W. Scott, Computer-Aided Design of Multifrequency Eddy-Current Tests for Layered Conductors with Multiple Property Variations, ORNL/TM-6858, Oct. 1979.

A-5. C. V. Dodd and L. D. Chitwood, Three-Frequency Eddy-Current Instrument, ORNL/TM-10663, Martin Marietta Energy Systems, Oak Ridge National Laboratory, Oak Ridge, Tenn., May 1988.

A-6. C. V. Dodd, L. M. Whitaker, and W. E. Deeds, An Eddy-Current Laboratory Test System Using Commercial Equipment, ORNL-6366, Martin Marietta Energy Systems, Oak Ridge National Laboratory, Oak Ridge, Tenn., April 1987.

A-7. W. E. Deeds, and C. V. Dodd, Multiple Property Variations in Coaxial Cylindrical Conductors Determined with Multiple-Frequency Eddy Currents, NUREG/CR-0967; NUREG/TM-335, Martin Marietta Energy Systems, Oak Ridge National Laboratory, Nov. 1979.

A-8. C. V. Dodd, and W. E. Deeds, Absolute Eddy-Current Measurement of Electrical Conductivity, pp. 387-394 in Rev. Prog. Quant. Nondstr. Eval., (Proc. AF/DARPA Rev. Progr. Quant. NDE, 1981) Vol. 1, eds. D. O. Thompson, and D. E. Chimenti, Plenum, New York, 1982.

A-9. C. V. Dodd, C. D. Cox, and W. E. Deeds, Experimental Verification of Eddy-Current Flaw Theory, pp. 359-64 in Review of Progress in Quantitative Nondestructive Evaluation, Vol. 4A, first half of proceedings of 11th Annual Review of Progress in Quantitative Nondestructive Evaluation, D. O. Thompson and D. E. Chimenti, eds., Plenum, New York, 1985.

A-10. C. V. Dodd, C. C. Cheng, W. A. Simpson, D. A. Deeds, and J. H. Smith, The Analysis of Reflection Type Coils for Eddy-Current Testing, ORNL-TM-4107, April 1973.

NRC FORM 335 (2–89) NRCM 1102, 3201, 3202

U. S. NUCLEAR REGULATORY COMMISSION

# BIBLIOGRAPHIC DATA SHEET

*(See instructions on the reverse)*

1. REPORT NUMBER *(Assigned by NRC. Add Vol., Supp., Rev., and Addendum Numbers, if any.)*
NUREG/CR-6511, Vol. 1
ANL-96/17

2. TITLE AND SUBTITLE
Steam Generator Tube Integrity Program:
Semiannual Report August 1995—March 1996

3. DATE REPORT PUBLISHED
MONTH: April
YEAR: 1997

4. FIN OR GRANT NUMBER
W6487

5. AUTHOR(S)
D. R. Diercks, S. Bakhtiari, O. K. Chopra, K. E. Kasza, D. S. Kupperman
S. Majumdar, J. Y. Park, and W. J. Shack

6. TYPE OF REPORT
Technical; Semiannual

7. PERIOD COVERED *(Inclusive Dates)*
August 1995—March 1996

8. PERFORMING ORGANIZATION – NAME AND ADDRESS *(If NRC, provide Division, Office or Region, U.S. Nuclear Regulatory Commission, and mailing address; if contractor, provide name and mailing address.)*

Argonne National Laboratory
9700 South Cass Avenue
Argonne, IL 60439

9. SPONSORING ORGANIZATION – NAME AND ADDRESS *(If NRC, type "Same as above": if contractor, provide NRC Division, Office or Region, U.S. Nuclear Regulatory Commission, and mailing address.)*

Division of Engineering Technology
Office of Nuclear Regulatory Research
U. S. Nuclear Regulatory Commission
Washington, DC 20555-0001

10. SUPPLEMENTARY NOTES
J. Muscara, NRC Project Manager

11. ABSTRACT (200 words or less)

This report summarizes work performed by Argonne National Laboratory on the Steam Generator Tube Integrity Program from the inception of that program in August 1995 through March 1996. The program is divided into five tasks, namely (1) Assessment of Inspection Reliability, (2) Research on ISI (in-service-inspection) Technology, (3) Research on Degradation Modes and Integrity, (4) Development of Methodology and Technical Requirements for Current and Emerging Regulatory Issues, and (5) Program Management. Under Task 1, progress is reported on the preparation of and evaluation of nondestructive evaluation (NDE) techniques for inspecting a mock-up steam generator for round-robin testing, the development of better ways to correlate burst pressure and leak rate with eddy current (EC) signals, the inspection of sleeved tubes, workshop and training activities, and the evaluation of emerging NDE technology. Under Task 2, results are reported on closed-form solutions and finite element electromagnetic modeling of EC probe response for various probe designs and flaw characteristics. Under Task 3, facilities are being designed and built for the production of cracked tubes under aggressive and near-prototypical conditions and for the testing of flawed and unflawed tubes under normal operating, accident, and severe accident conditions. In addition, crack behavior and stability are being modeled to provide guidance on test facility design, to develop an improved understanding of the expected rupture behavior of tubes with circumferential cracks, and to predict the behavior of flawed and unflawed tubes under severe accident conditions. Task 4 is concerned with the cracking and failure of tubes that have been repaired by sleeving, and with a review of literature on this subject.

12. KEY WORDS/DESCRIPTORS *(List words or phrases that will assist researchers in locating this report.)*
Steam Generator
Tubes
Stress Corrosion Cracking
Eddy Current Testing
Nondestructive Evaluation
Inservice Inspection
Pressure Testing
Tube Burst
Leak Rate
Alloy 600, Incoloy 600

13. AVAILABILITY STATEMENT
Unlimited

14. SECURITY CLASSIFICATION
*(This Page)*
Unclassified
*(This Report)*
Unclassified

15. NUMBER OF PAGES

16. PRICE

NRC FORM 335 (2–89)